CHAPTER ONE

INTRODUCTION

1.1 Background to the Study

The gravity method involves measuring the gravitational attraction exerted by the earth at a measurement station on the surface. It is a relatively cheap, non-invasive, non-destructive remote sensing method. It is a force that acts at a distance. Hence, it is passive, that is, no energy need to be put into the ground in order to acquire data, thus, the method is well suited to a populated setting. The strength of the gravitational field is directly proportional to the mass and therefore the density of subsurface materials. The small portable instrument used also permits walking traverses. Measurements of gravity provide information about densities of underlying rocks. The primary objective of studying detailed gravity data is to provide a better understanding of the subsurface geology. There is a wide range in density among rock types, and therefore geologists can make inferences about the distribution of strata. The success of this method depends on the different earth materials having different bulk densities (mass) that produce variations in the measured gravitational field. These variations can then be interpreted by a variety of analytical and computer methods to determine the depth, geometry and density that cause the gravity field variations. The most commonly used processed data are known as Bouguer gravity anomalies, measured in mGal. The interpretation of Bouguer gravity anomalies ranges from manually inspecting the grid or profiles for variations in the gravitational field to more complex methods that involve separating the gravity anomaly due to an object of interest from some sort of regional gravity field. Structures and bodies of geologic interest can be inferred from interpretation of the Bouguer gravity anomalies.

The Anambra Basin has been identified as one of the major in-land sedimentary basins in Nigeria (Nwajide, 2006; 2013). It evolved from the Abakaliki Basin in the Post

Santonian period (Murat, 1972). Previous work on the petroleum potentials of the Anambra Basin are well documented (Ndefo *et al.,* 1987; Onuoha, 2005, Nwajide, 2005; Onwuemesi and Egboka, 2007; Odoh *et al.,* 2009; and Ogala, 2011) and geophysics (Onuoha, 1986; Onwuemesi, 1995; Onwuemesi, 1997; Onuoha and Ekine, 1999; Odoh and Onwuemesi, 2007; Ekine and Onuoha, 2008 and Ekine and Onuoha, 2010).

Ajakaiye and Burke (1973) used four published gravity networks to compile a Bouguer gravity map which covered about 40 % of the area of Nigeria. In their work, they stated that the Niger Delta is very close to isostatic equilibrium and overlies the oceanic crust. They further observed that the Benue Trough extends below the Quaternary sediments of the Chad Basin. The work also recognized rocks of the Basement complex in the Jos plateau with the intruding Jurassic granites. Adighije (1981a) made a gravity study of the lower Benue Trough, which included the Anambra Basin. He established a maximum sediment thickness of 4,250 m and the average densities of the sedimentary rocks in the area as Albian shales (2.65 gcm^{-3}), Cenomanian sandstone (2.48 gcm^{-3}), Turonian-Senonian sandstone (2.45 gcm^{-3}),Turonian-Senonian shale (2.53 gcm^{-3}), Maastrichtian – Tertiary sandstone (2.30 gcm^{-3}). Adighije (1981b) extended his interpretation of the gravity data to the entire Benue Trough, in which case he reviewed the evolution of the trough from the perspective of gravity data.

In the interpretation of the aeromagnetic data in the Nkalagu area, Onyewuchi *et al., (*2012) gave an average sedimentary thickness to be 3.574 km, which they suggested to be favourable for hydrocarbon generation. Onwuemesi (1997) determined the sedimentary thickness in the basin, using aeromagnetic data, to range from 0.9 km – 5.6 km, depth to Curie temperature isotherm varied between 16 and 30 km below the mean sea level, while the geothermal gradient associated with it ranged between 20 and 35 ^{0}C/Km. Onuoha and Ekine (1999) studied the geothermal gradient of the Anambra Basin using data from deep exploration wells and estimated the geothermal gradient and heat flow values as 25 to 49 ±1

^{0}C/km and 48 to 76 ±3 mW/m^2. They further suggested that the geothermal gradient is related to basin hydrodynamics with higher geothermal gradients and heat flow existing in areas of low hydraulic head distribution. Agagu and Ekweozor (1982) was of the view that the geothermal gradient within the basin is lithologically controlled, hence, it varies between 9.2 and 24 ^{0}C/km in the Ajali and Mamu Formations, while it ranges between 29.4 to 70 ^{0}C/km in shaly sections. The high temperature gradient in the shales was attributed to lack of convection currents in the impermeable shales and possibly due to overpressure which is common in the reduction of thermal conductivity (Agagu and Ekweozor, 1982). The above geothermal gradient is similar to the records from Niger Delta (Evamy *et al.,* 1978). Onuba *et al.,* (2011) evaluated aeromagnetic data in the Okigwe area of the Anambra Basin and determined sediment thickness in the area to be 2.0 to 4.99 km.

The actual status of the Anambra and Afikpo Basins has been a subject of controversy. Murat (1972) stated that the uplift of the early Cretaceous sediments in the Abakaliki area led to an opening of new depocentres at the western and southeastern parts of the Abakaliki area. This implies that the both areas were originally part of the southern Benue Trough but later separated due to tectonic activities. While the western part is regarded as the Anambra Basin, the southeastern part is the Afikpo Basin (Afikpo Syncline). His view was supported by whiteman (1982). Conversely, Akande and Erdtmann (1998) and Obaje *et al.* (1999) were of the view that the Anambra Basin was an integral part of the southern Benue Trough on the ground that it was formed from the compressional history/ stage of the trough. Nwajide (2013) disagrees to an extent with the above authors. He was of the view that the Anambra basin is a distinct basin overlying the Benue Trough at the southern end and is in turn overlain in the southern end by the Niger Delta. He also considered the Afikpo Basin as part of the Anambra Basin considering the fact that they are both result of the same Santonian thermo-tectonic event; there is really no physical separation or barrier between the two areas

and there does not appear to be any tectonic definition of that area into a depression separate from the area to the northwest.

An intensive Search for hydrocarbon within the Anambra Basin dated back to the 1950s, with the drilling of an oil well at Ihuo, northwest of Owerri. Since then, the basin has not been as beneficial to Nigerians as the Niger Delta basin. Nwajide (2005) identified potential source rocks in the basin as the Awgu Shales, Nkporo Shales and the shale members of the Mamu Formation, while the potential reservoir units are the sandstone members of the Nkporo unit and the structural features such as the anticlines, faults and unconformities which occur in the area. Geochemical analysis of some potential source rocks in the basin has shown that it has Type II and Type III kerogenes, which suggests more gas prone (Nwajide, 2005; Ojo *et al.,* 2009). Okeke *et al.,* (2014) established a Type IV kerogen and the absence of $nC_1 – nC_{11}$ alkanes, on the shale samples of the Nsukka Formation on the southern part of the basin, at the Okigwe area. A 2D seismic data was generated in the basin by Shell D'Arcy in the 1940s (Nwajide, 2005), which led to the drilling of the first test well in 1951. Onuoha and Ekine (1990) used a time – dependent geothermal gradient model to suggest that there is a progressive trend of over maturation towards the deeper formations. According to Onuoha (2005), the Maastrichtian to Palaeocene sediments in the southwestern portion of the basin should be major targets for liquid hydrocarbon, while Senonian and older sediments should yield gas, whereas the northern part of the basin may not be very prospective as they are occupied by Coniacian to Recent sediments. He further stated that hydrocarbon migration seems to have been influenced by the movement of circulating meteoric waters.

1.2 Statement of the Problem

Considering the series of work done so far in the Anambra Basin, little have been done in recent times in evaluating structure of the Anambra Basin and its hydrocarbon potentials from the perspective of gravity data. Basin evolution and geodynamics have been the concentration of the previous gravity works in the study area. None tried to link the interpretation to hydrocarbon search in the Anambra Basin. The work of Ajakaiye and Burke (1973) was on a national scale. They considered the Anambra Basin as part of the Benue Trough and could not give detail information about the basin nor its hydrocarbon potentials. The 2D seismic survey carried out by Shell D'Arcy in the 1940s (Nwajide, 2005) was not made for public consumption and could not enhance the understanding of the hydrocarbon potentials of the basin. The present work has tried to address this.

The actual status of the Anambra and Afikpo Basins has been a subject of controversy. Previous models on their status (whiteman, 1982; Akande and Erdtmann, 1998; Obaje *et al.*, 1999 and Nwajide, 2013) are all based on field relationships, which cannot independently define the status of these basins without geophysical models. Hence, there is need to review their relationship using gravity data. Adighije (1981a) made a gravity study of the lower Benue Trough, including the Anambra and Afikpo Basins, in which he determined the densities of some rock types within the study area and sediment thickness. However, no models were generated to explain the relationship of the Anambra and Afikpo Basins with their parent Benue Trough. He could not determine the status of these basins or their relationship with each other. No information was given by the author to enhance the understanding of this basin from the gravity data, hence the need for the present work.

Heat plays a vital role in the sediment maturation, hydrocarbon generation and migration. Onwuemesi (1997) made a curie depth isotherm and geothermal gradient study of the Anambra Basin using aeromagnetic data, however, the study was not in any way linked to

hydrocarbon study in the basin. Onuoha and Ekine (1999) as well studied the geothermal gradient of the Anambra Basin using data from deep exploration wells, but could not correlate their result with the availability of hydrocarbon in the study area. Consequently, there is need to correlate the geothermal gradient in the basin with hydrocarbon occurrence in other to understand the effect of heat flow in hydrocarbon generation and distribution within the study area.

Nwajide (2005) opined that the potential reservoir units in the Anambra Basin are the sandstone members of the Nkporo Group and the structural features such as the anticlines, faults and unconformities which occur in the area. Conversely, Onuoha (2005) was of the view that the reservoir ranges from sediments of the Cretaceous age to Tertiary Paleocene age. This disagreement has been identified as a gap and was also investigated. Time has been invested in the present work solving the set of identified problems, which has enhanced the understanding of the status of the Anambra Basin and its petroleum potentials.

1.3 Aim and Objectives of the Present Work.

The aim of the present work is to interpret gravity anomalies and re-evaluate the hydrocarbon potentials of Anambra Basin, southeastern Nigeria. The specific objectives include:

1. To produce a residual gravity map of Anambra basin.
2. To delineate areas of gravity highs and lows as revealed by density contrasts caused by different rock types.
3. To determine sediment thickness in the basin.
4. To generate geologic models of causative bodies.
5. To infer basin boundaries from gravity models.

6. To correlate the residual gravity data with existing well data in other to infer hydrocarbon availability from gravity data.
7. To correlate gravity data with geothermal gradient data in other to infer a possible relationship between them.

1.4 Scope of Study

The focus of this study is on the Anambra Basin of Nigeria with emphasis on analysis of gravity, well and elevation data sets within the basin. The scope of the research includes processing, qualitative and quantitative interpretation of gravity data, as well as cross correlation of gravity data with well and elevation data. The relationship between gravity values, impact of geothermal gradient and elevation on availability of hydrocarbon within the basin were discussed.

1.5 Significance of the Study

At the end of this work, it is expected that answers would be provided to all the identified gaps. The actual status of the Anambra and Afikpo Basins would be defined. This will in turn redefine the geology of the study area and form a major contribution to knowledge. Specific areas with potential reservoirs would be identified, major hydrocarbon bearing formations would be defined and a standard reconnaissance tool for hydrocarbon exploration in the area on the grounds of gravity data would be generated. This would boost the economic viability of the area as both indigenous and foreign investors would be attracted, which would encourage employment opportunities, raise standard of living of the indigenes, lead to aggressive grassroot development, and advancement in the economy of both the state and the federal governments. With the high rate of decline in the hydrocarbon reserve of the Niger Delta region overtime, the Anambra Basin would be a good substitute,

with the contributions of the present work. This would as well encourage mentorship as the proliferation of oil industries in the area would provide opportunity for the young or intending scholars to engage in internship programmes with them, carry out further researches with state of art equipment and as well create multiple rooms for collaboration between the university community and the industries.

CHAPTER TWO

LITERATURE REVIEW

2.1 Geology of the Anambra Basin

Anambra Basin is bounded on the east by the Abakaliki Anticlinorium and on a south-westerly direction by the Benin hinge-line, while the southern extreme is marked by the upper limits of the Eocene growth faults of the Niger Delta (Murat, 1972). The basin is about 300 km long in a northeast - southwest direction, extending between the Onitsha environs in Anambra State to the Loko area in Benue State of Nigeria. Its south-western tip is about 160 km wide, while the north-eastern extreme is about 48 km wide (Fig. 2.1) (Whiteman, 1982).

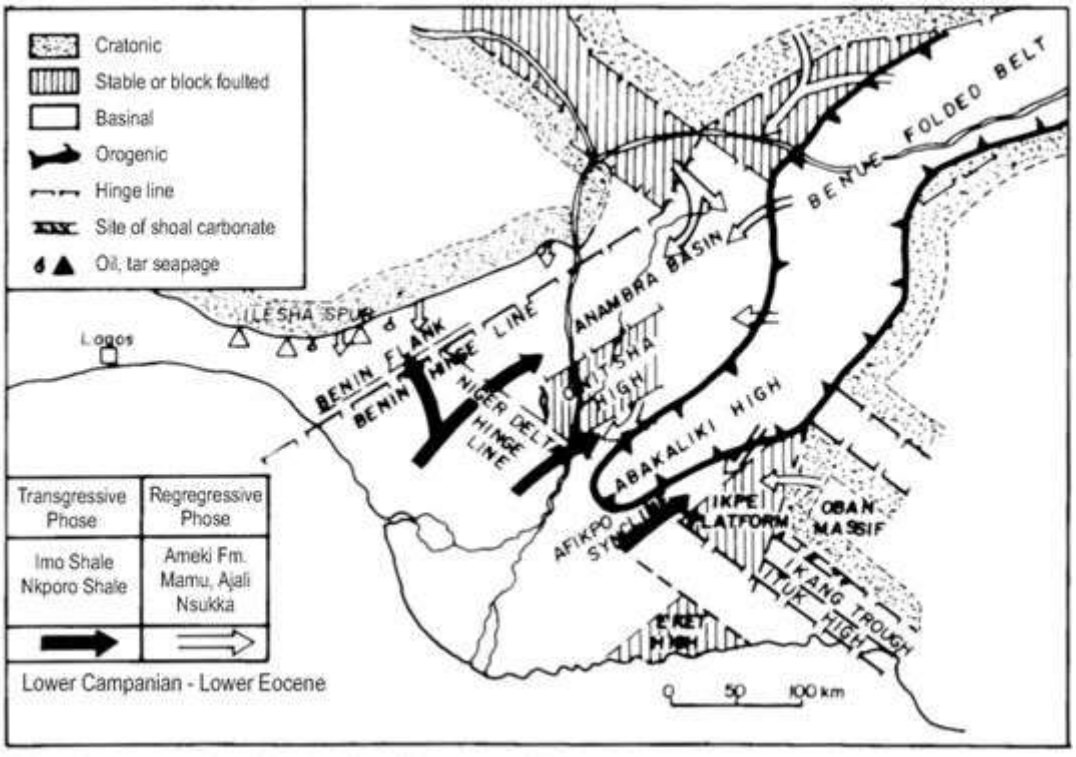

Fig. 2.1: Tectonic map of Southern Nigeria (adapted from Murat, 1970).

Geological works published in the area include but not restricted to that of Reyment, 1965; Murat, 1972; Adeleye, 1975; Peters, 1978; Whiteman, 1982; Hoque and Nwajide, 1984; Agagu *et al.*, 1985; Akande *et al.*, 1998; Adeigbe and Salufu, 2009. Sedimentation in the

Anambra Basin commenced with the Campanian-Maastrichtian marine and paralic shales of the Nkporo group, overlain by the coal measures (Nwajide, 2005). In the Paleocene, the marine shales of the Imo Formation were deposited, overlain by the tidal Nanka Sandstone of the Ameki Group (Eocene). The Enugu and the Nkporo Shales (Nkporo Group) represent the brackish marsh and fossiliferous pro-delta facies of the Late Campanian-Early Maastrichtian depositional cycle (Reijers and Nwajide, 1998). According to Obaje (2009), deposition of the sediments of the Nkporo/Enugu Formations reflects a funnel-shaped shallow marine setting that graded into channelled low-energy marshes. The coal-bearing Mamu Formation and the Ajali Sandstone accumulated during this epoch of overall regression of the Nkporo cycle. The Ajali Sandstone marks the height of the regression at a time when the coastline was still concave. The converging littoral drift cells governed the sedimentation and are reflected in the tidal sand waves which are characteristic for the Ajali Sandstone (Nwajide, 2013). The type locality of the Nkporo Shale is at the nkporo community in Abia state, while that of Enugu Shale is at Enugu, near the Onitsha-Road Flyover (Reyment, 1965). The Mamu Formation is well exposed at the Miliken Hills in Enugu, with well-preserved sections along the road cuts from the King Petrol Station up the Miliken Hills and at the left bank of River Ekulu near the bridge to Onyeama mine. The Nsukka Formation and the Imo Shale contain significant amount of organic matter and may be a potential source for the hydrocarbons in the northern part of the Niger Delta (Reijers and Nwajide, 1998). In the Anambra Basin, they are only locally expected to reach maturity levels for hydrocarbon expulsion. Geological evidences show that after the formation of the Anambra Basin in the Santonian, the sediments that accumulated in the basin have not suffered any significant deformation (Odoh *et al.*, 2009).

2.2 Historical Overview of the Gravity Method

The first reported test of airborne gravity measurements occurred in the 1950's (Lundberg, 1957) based on the principle of gradiometry. However, Lundberg's test was received with general scepticism in the exploration industry (Hammer, 1983). On the successful use of a gravity meter aboard submarines and ships in the 1950s, the Air Force Cambridge Research Center initiated program extends the method to an airborne style. The first test was performed in 1958 by the U.S. Air Force, using a LaCoste and Romberg gimbal-supported sea gravimeter (S5), with navigation data provided by a Doppler system on the aircraft and a camera tracking range on the ground (Thompson and LaCoste, 1960). This was followed by another test by Fairchild Aerial Surveys (Nettleton et al., 1960) using the same LaCoste and Romberg gravimeter instrument, but the aircraft was equipped with a mapping camera for positioning and a radar altimeter and hypsometer to determine the altitude.

The main problems for airborne gravimetry at the time were the navigation of the aircraft, including velocity, elevation and space positioning, the Eotvos effect, in-flight accelerations of the aircraft, and the lack of a gravimeter able to work in a dynamic environment (Thompson and LaCoste, 1960). However, it appeared that a relatively low accuracy of about 10 mGal could be obtained using existing navigation systems, complemented by accurate ground control techniques, such as optical and radar tracking ranges. Furthermore, experience with large aircraft at high altitudes indicated that smooth flight conditions could be obtained, thus reducing large accelerations. The Eotvos effect, which is directly related to the aircraft velocity, was considered to be a major problem for gravity measurements in an aircraft. However, with proper flight programming, accurate Eotvos corrections could be made. As mentioned above, the gravimeters used in the first tests were modified sea gravimeters using a gimbal suspension to handle horizontal accelerations. This system had been developed and tested by LaCoste and Romberg for use at sea. Later, these systems were replaced by

stabilized platform systems (Fig. 2.2), which performed much better (LaCoste, 1967).

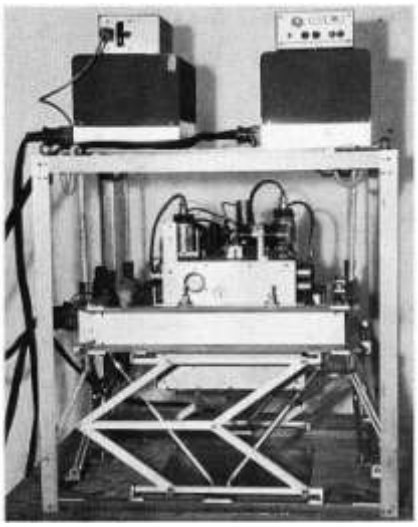

Fig. 2.2: Stabilized platform gravity meter (LaCoste *et al.*, 1967).

The tests in the beginning of the 1960s were performed with gravity meters installed in fixed-wing aircraft.

The first successful measurement of gravity from a helicopter was performed in 1965 by the U.S. Naval Oceanographic Office, using a gimbal-suspended LaCoste - Romberg Sea Gravimeter (Gumert and Cobb, 1970; Gumert, 1998). A more thorough test followed in 1966, providing gravity data with accuracies of about 3 mGal, leading to the development of a complete helicopter gravity measuring system (Gumert and Cobb, 1970). The instrumentation consisted of a LaCoste and Romberg stable-platform gravity meter, a laser altimeter, a camera and a HIRAN navigation system. The advantages of a helicopter over fixed-wing aircraft are the better terrain-following capability, the increased spatial resolution resulting from flying at lower altitude and lower speed and the fact that a helicopter is less affected by turbulent conditions than most other types of aircraft (Lee *et al.*, 2006). Its only disadvantage may be a somewhat smaller range.

Despite improvements in scalar gravity system design, and the development of high resolution radar altimeters for vertical acceleration determination in the eighties (Brozena,

1984), airborne gravimetry did not become fully operational until the introduction of Global Positioning System (GPS). The use of carrier phase measurements and Differential GPS (DGPS) opened new ways to resolve navigational problems (Brozena *et al.*,1989; Schwarz *et al.,* 1989; Kleusberg *et al.*,1990). The impact of the new positioning technology led to two important developments in airborne gravimetry (Schwarz and Li, 1997). The first one was the perfection of existing scalar gravimeter systems, which could be used, on the one hand, for geophysical exploration and, on the other hand, for large regional surveys as required by geodesy. The second development was the combination of GPS with inertial measuring units (IMU) for sensor stabilization and gravity vector determination.

One of the first large-scale airborne gravity surveys was the campaign over Greenland in 1991 and 1992, performed by the U.S. Naval Research Laboratory (NRL) in cooperation with the Danish National Survey and Cadastre (KMS), which proved the suitability of airborne gravimetry for gravity field mapping (Brozena, 1992; Brozena and Peters, 1994; Forsberg and Kenyon, 1994). Other examples of wide-area surveys are the gravity survey of Switzerland, a joint project between the Swiss Federal Institute of Technology and LaCoste and Romberg Gravity Meters Inc. in 1992 (Klingel´ *et al.*, 1995), the AGMASCO project over the Skagerrak (1996) and the Azores (1997) conducted by a joint program of various European institutes (Forsberg *et al.,* 1997; Hehl *et al*.,1997) and the gravity surveys over the West Antarctic ice sheet (1991-1997) flown by the Lamont-Doherty Earth Observatory in collaboration with the Institute for Geophysics of the University of Texas (Bell *et al*., 1999). Recent major projects are the nationwide geoid and regional surveys of Malaysia (2002-2003), Mongolia (2004-2005) and Ethiopia (2006-2007) performed by DNSC (Olesen and Forsberg, 2007b), and the survey of Taiwan (Hwang *et al*., 2007). The reported accuracies of these campaigns were 1.5-2 mGal at 5-6 km spatial resolution.

The use of a Strap down Inertial Navigation System (SINS) for airborne gravimetry was

pioneered at the University of Calgary (Schwarz *et al.,* 1991), where development and testing continued until the beginning of this decade. The advantage of such a system is its smaller size and relatively low costs. Results of the first airborne test in 1995, using a Honeywell LASEREF III inertial system, showed that relative gravity can be obtained with an accuracy of 2-3 mGal at a half-wavelength resolution of 5 km (Wei and Schwarz, 1998). A side-by-side comparison of a strapdown INS system with a LaCoste and Romberg stable platform gravimeter, described by Glennie and Schwarz (1999), demonstrated that both systems performed equally well in terms of RMS errors, but the LCR system showed a better long-term stability. Later, Bruton *et al.* (2002) showed that with the same SINS system, the strapdown approach can yield accuracies of 1.5 mGal at a half-wavelength of 2 km and 2.5 mGal at a half-wavelength of 1.4 km, demonstrating the potential of this approach for high-resolution applications. The SINS approach also allows for the determination of the gravity vector, but in that case, the system requirements are more stringent (Schwarz *et al.*,1991 and Jekeli, 1994). Nevertheless, Jekeli and Kwon (1999) obtained the full gravity vector at an accuracy level of 7-8 mGal for the horizontal component and 3 mGal for the vertical component, using the same data as Wei and Schwarz (1998).

2.3 Principle of Airborne Gravimetry

Gravimeters are highly sensitive accelerometers. If an accelerometer is put stationary on the Earth's surface and it is level (i.e. the sensitive axis coincides with the direction of the gravity vector), the magnitude of gravity can be determined directly. However, the situation becomes much more complex when the accelerometer is moving, since an accelerometer cannot distinguish between kinematic and gravitational accelerations and because the instrument is not easily kept level. Thus, in airborne gravimetry, the solution of the following two problems is fundamental (Schwarz and Li, 1997):

1. Sensor orientation or stabilization under aircraft dynamics.
2. Separation of gravitational and non-gravitational acceleration.

There are a number of possible ways to solve the first problem. The use of a damped two-axes platform system, such as the LaCoste & Romberg Air-Sea gravimeter, is the most established method for altitude stabilization. The platform is mechanically stabilized by using gyros and accelerometers in a feedback loop. The damping period of the platform is typically chosen at 4 minutes for airborne applications. This means that horizontal accelerations with a longer period, as in long turns, are regarded by the system as changes of the vertical. In theory, the effect of horizontal accelerations is completely eliminated by using a Schuler-tuned platform with a damping period of 84.4 minutes (Schuler period). However, such a long period requires extremely accurate gyros and accelerometers that have virtually no errors or drifts within this time range (Meyer *et al.,* 2003). Example of systems that use a Schuler-tuned three-axes inertial platform are the GT-1A gravimeter, developed by Joint Stock Company Gravimetric Technologies in the Russian Federation and made available for commercial use by Canadian Micro Gravity Pty Ltd (Gabell *et al.,* 2004) and the Airborne Inertially Referenced Gravimeter (AIRGrav) developed by Sander Geophysics Limited (Sander *et al.,* 2004).

An alternative to a stabilized platform system is a Strapdown Inertial Navigation System (SINS) that consists of three orthogonal accelerometers and a set of three gyroscopes. In that case the mechanical stabilization is replaced by computing the rotation matrix between the body frame and the local-level frame. The separation of gravitational and inertial acceleration is possible by computing the difference between the specific force measured by an accelerometer and the output of a system that provides the inertial acceleration. This process is also known as motion compensation.

Since the introduction of GPS, all airborne systems use carrier phase DGPS positioning to

determine aircraft motion. However, a laser-altimeter or radar-altimeter can also be used if only the vertical aircraft acceleration is required. The following classification is generally used for airborne gravimetry (Schwarz and Li, 1997; Wei, 1999):

- Scalar gravimetry
- Vector gravimetry
- Gravity gradiometry

In scalar gravimetry the magnitude of the gravity (disturbance) vector is determined. This can be implemented using a stable platform system or by using a strapdown system. The latter case is often referred to as Strapdown INS Scalar Gravimetry (SISG), in which case only the vertical component of the gravity vector is of interest. An alternative concept is to use a triad of three orthogonal accelerometers to obtain the magnitude of gravity from the difference between the specific force vector and the aircraft acceleration vector. Because the absolute orientation of the accelerometers with respect to the local vertical is not needed in this case, this approach is called Rotation Invariant Scalar Gravimetry (RISG). This approach was first explored by Czompo (1994) and later compared with SISG by Wei and Schwarz (1997).

In vector gravimetry all three components of the gravity vector are determined. This can only be done with systems that make use of inertial technology, that is SINS and inertial platform systems. The horizontal components are generally of much poorer accuracy than the vertical component due to attitude errors caused by gyro drifts (Bruton, 2000). Good results for the estimation of the full gravity vector have been obtained by Jekeli and Kwon (1999).

In airborne gravity gradiometry, the second derivatives of the gravity potential are observed. In the last decade, several operational gradiometer systems capable of rapidly measuring all components of the gravity gradient tensor have been developed (Alberts, 2009). Examples are the FALCON gravity gradiometer of BHP Billiton (Lee, 2001) and the Air-

FTG gradiometer system operated by Bell Geospace (Murphy, 2004). The standard gradiometer concept is based on a design that uses opposing pairs of accelerometers on a rotating disk. The input axes of the accelerometer pair point in opposite directions so that the common mode acceleration is cancelled out when their signals are summed. As a result, gradiometer systems are much less sensitive to GPS positioning errors and results can be obtained with higher accuracy and resolution compared to scalar and vector gravimetry. This technique is therefore particularly interesting for the mining and oil industry. For an overview of the characteristics of gravity gradiometry, see Bell *et al.,* (1997).

2.4 Basic Principles of Gravity Surveying

The basis of the gravity survey method is Newton's Law of Gravitation, which states that the force of attraction F between two masses m_1 and m_2, whose dimensions are small with respect to the distance r between them, is given by

$$F = G\frac{m_1 m_2}{r^2} \quad \text{.....(2.1)}$$

where G is the Gravitational Constant $\left(6.67\times10^{-11} m^3 kg^{-1} s^{-2}\right)$

Consider the gravitational attraction of a spherical, non-rotating, homogeneous Earth of mass M and radius R on a small mass m on its surface. It is relatively simple to show that the mass of a sphere acts as though it were concentrated at the centre of the sphere and by substitution in equation (1)

$$F = \frac{Mm}{R^2} = mg \quad \text{.....(2.2)}$$

Force is related to mass by acceleration and the term

$$g = \frac{GM}{R^2} \quad \text{.....(2.3)}$$

is known as the gravitational acceleration or, simply, *gravity*. The weight of the mass is given by *mg*. On such an Earth, gravity would be constant. However, the Earth's ellipsoidal shape, rotation, irregular surface relief and internal mass distribution cause gravity to vary over its surface.

The gravitational field is most usefully defined in terms of the *gravitational potential*

$$U = \frac{GM}{R} \quad \text{.....(2.4)}$$

Whereas the gravitational acceleration *g* is a vector quantity, having magnitude and direction (vertically downwards), the gravitational potential *U* is a scalar, having magnitude only. The first derivative of *U* in any direction gives the component of gravity in that direction. Consequently, a potential field approach provides computational

2.3.1 Earth's Properties that Affect the Gravity Measurements.

(A) Earth Rotates: Earth is not round but bulges at equator and is flattened at poles, with equatorial radius of 21 kilometers greater than at poles.

(B) Earth's mass is not symmetrical about the equatorial plane: Earth is "pear-shaped". The equator isn't perfectly spherical but only varies by a few meters. The regular surface which most nearly approximates the surface of the actual Earth is a surface called the geoid. The geoid surface is everywhere perpendicular to a plumb bob. The geoid corresponds to mean sea level. In land covered areas, the geoid is the surface that would be determined by the level to which water would rise in narrow canals cut through the continents. Since g depends on distance from centre of Earth (radius), g varies with latitude. International Gravity Formula can be used to determine g at particular latitude:

g = 9.780318 (1 + .0053024 sin2 - 0.0000059 $\sin 2^2$) units are m/sec2. Calculated value for g "corrected" for latitude is called the theoretical gravity and abbreviated g_t.

2.3.2 Methods of Actual Measurement of Gravity: Actual value of gravity can be measured using the following methods:

1. The Simple Pendulum: This can be done by applying the formular

$$g = \frac{4\pi^2 L}{T^2} \quad \text{.....(2.5)}$$

(Where L is length of pendulum and T is period). Accuracy = 1.5 mgal.)

2. Experimentally by measuring acceleration of object dropped at Earth's surface (i.e. Free Fall). Accuracy = 0.1 mgal. The measuring apparatus is not portable (although one of the latest models available is said to be portable because it weighs less than one ton).

3. Use of Gravity Meter (or Gravimeter): This is the most common method of measuring gravity from place to place. Accuracy = .01 mGal.

2.5 The Gravity Meter (Gravimeter)

For the past 50 years the vast majority of gravity measurements have been made using meters with unstable (*astatic*) spring systems, and this seems likely to remain the case for the foreseeable future. Gravity surveys are complicated by the fact that such meters measure gravity differences, not absolute field strengths.

2.5.1 Astatic (Unstable) Spring Systems: Astatic systems use *zero-length* main springs, in which tension is proportional to actual length. Examples include the Worden and LaCoste Romberg gravity meters. With the geometry shown in Figure 2.3 and for one particular

Fig. 2.3: The Worden and LaCoste - Romberg gravity meters (Mariita, 2007)

value of gravity field, the spring will support the balance arm in any position. In stronger fields, a much weaker auxiliary spring can be used to support the increase in weight, which will be equal to the product of the total mass and the increase in gravity field. The zero-length spring *backs off* a constant weight so that the measuring spring can respond to small changes in gravity field.

The Worden and Sodin gravimeters have two auxiliary springs (Figure 2.4), one for fine and one for coarse adjustments, attached to balance arms of more complicated design. LaCoste meters have no auxiliary springs and measurements are made by adjusting the point of support of the main spring.

Because spring systems are mechanical, they are subject to drift. Short period drift is largely due to temperature changes that affect the elastic constants of the springs despite the compensation devices that are usually included. There is also longer term extensional *creep* of springs under continual tension. Repeated readings at base stations are required to monitor drift and to allow the necessary corrections to be calculated (Lowrie, 2007).

Fig. 2.4: 'Manual' gravity meters. From left to right, LaCoste 'G' (geodetic),Worden 'Student' and Sodin. (After Milsom, 2003)

Although gravity meters remained essentially unchanged for almost 50 years, major moves were made in the last decade of the twentieth century towards automating readings and reducing the need for skilled operators. The LaCoste G and D meters were fitted with electronic readouts and the Scintrex CG-3 pioneered automated tilt correction and reading. The basic LaCoste meter was then completely redesigned as the fully automatic Graviton-EG, in which actual levelling, rather than merely the levelling correction, is automated. Inevitably, data loggers have also been added and can be directly downloaded to laptop PCs. The Graviton-EG, the CG-3 and its successor, the CG-5 Autograv, are also sufficiently rugged to be transported in the field without additional protective cases. However, despite the advantages of the newer models, the longevity (and, to some extent, the high cost) of gravity meters ensures that the less sophisticated versions will be around for many years to come.

2.5.2 Setting up A Gravity Meter

Gravity meters are normally read on concave dishes supported by three short stubs to which longer legs can be attached. The stubs are usually used alone, pressed firmly but not too deeply into the ground. The under surface of the dish must not touch the ground since a fourth support point allows 'rocking' back and forth. Thick grass under the dish may have to be removed before a reading can be taken. Extension legs may also be used but readings will then take longer, the dish itself may have to be levelled (some incorporate a bull's-eye bubble) and the height above ground will have to be measured. The meters themselves rest on three adjustable, screw-threaded feet and are levelled using two horizontal spirit-levels, initially by being moved around the dish until both level bubbles are 'floating'. The temptation to hurry this stage and use the foot screws almost immediately should be resisted. Usually one of the levels (probably the cross-level, at right angles to the plane of movement of the balance arm) is set parallel to a line joining two of the feet. Adjustments to the third foot then scarcely affect this level. The quickest method of levelling is to centre the cross-level bubble, using one or both of the two foot screws that control it, and then use the third screw to set the long-level. Some meters can rotate in their casings and level bubbles and feet may become misaligned, but levelling is very much easier if any such slippage is corrected. Experienced observers often use two screws simultaneously but the ability to do this efficiently comes only with practice.

Once a meter is level, a reading can be obtained. With most gravity meters, this is done by rotating a calibrated dial to bring a pointer linked to the spring system to a fixed point on a graduated scale. Because the alignment is rather subjective if the pointer is viewed directly through an eyepiece, all readings in a single loop should be made by the same observer. The subjective element is then eliminated when the base reading is subtracted. Subjectivity is much reduced when instruments are fitted with electronic repeaters. It is vital

that the level bubbles are checked whilst the dial is being adjusted, and especially immediately after a supposedly satisfactory reading has been taken. Natural surfaces subside slowly under the weight of observers, off-levelling the meter. On snow or ice, the levels have to be adjusted almost continuously as the dish melts its way down, unless it is insulated from the surface by being placed on a small piece of plywood. All mechanical measuring systems suffer from whiplash and two readings will differ, even if taken within seconds of each other, if the final adjustments are made by opposite rotations of the reading dial. The only remedy is total consistency in the direction of the final adjustment.

Earthquakes can make the pointer swing slowly from side to side across the field of view and survey work must be stopped until the disturbance is over. Fortunately, this effect is rare in most parts of the world, although very large earthquakes can affect gravity meters at distances of more than 10,000 kms. Severe continuous vibration, as from nearby machinery or the roots of trees moved by the wind, can make reading difficult and may even displace the reading point.

2.6 Gravity Corrections / Reductions

Gravity readings are taking on land, ocean or in the air, within the areas of interest. These readings are generally influenced by other factors aside the density of the rocks. Such factors include latitude, elevation, topography, tidal forces, and bouguer plates. Thus, gravity difference between two stations (i.e. bouguer gravity anomaly Δg) is partly due to other factors other than the attraction of unknown anomalous mass. It is the effect of these factors that we correct for in order to have only the anomalous value from the rock bodies alone.

2.6.1 Latitude Correction – Gravity increases with latitude. This is brought about by the shape of the earth and its rotation. The centripetal acceleration generated by the Earth's

rotation has a negative radial component that consequently causes gravity to decrease from the poles to the equator. Thus, gravity values increase from the equator to the poles. Also, the spheroidal shape of the earth causes the points near the equator to be farther away from the centre of mass of the Earth than those at the poles, causing gravity to increase from the equator to the poles. The variation in gravity due to latitude occurs in the North-South direction. Hence, the corrections made in this regard are either added or subtracted depending on whether the base station is in higher or lower latitude.

Clairaut's formula relates gravity to latitude on the reference spheroid in an equation form as follows:

$$G_{\phi} = g_0(1 + k_1 \sin^2 \phi - k_2 \sin^2 \phi) \ldots\ldots\ldots\ldots\ldots\ldots\ldots\ldots (2.6)$$ (Kearey et al., 2002)

Where:

G_{ϕ} = The predicted value of gravity at latitude ϕ

g_0 = The value of gravity at the equator

k_1 & k_2 = constants dependent on the shape and speed of rotation of the earth.

Their numerical values according to Gravity formular 1967 are:

g_0 = 9780318gu

k_1 = 0.0053024

k_2 = 0.0000059

Since gravity increases towards the poles, the correction for stations closer to the poles than the base station must be subtracted from the measured gravity.

2.6.2 Terrain (or Topographic) Correction: This correction tries to take care of the effect of surface irregularities or undulations in the vicinity of the station. The presence of hills and

valleys affect the gravity readings. To carryout terrain correction (Δg_T) for a hill adjacent to a gravity station, the hill is divided into a number of vertical prisms and the contribution of each vertical element to the vertical acceleration at the point of observation is calculated. The terrain correction is calculated using the formular.

$$\Delta g_T = G\rho\phi\left\{\left(\sqrt{r_1^2 + h^2} - r_1\right) - \left(\sqrt{r_2^2 + h^2} - r_2\right)\right\} \quad \text{.....(2.7)} \quad \text{(Lowrie, 2007)}$$

Where:

G = Universal gravitational constant

ρ = Density of the hill

ϕ = Angle subtended at the observation point

r_1 = Inner radius of the prism

r_2 = Outer radius of the prism

h = Height of the prism

2.6.3 Bouguer Plate Correction: This correction takes care of the effect of layer of rock whose thickness corresponds to the thickness of the elevation difference between the measurement and reference levels. The correction is made by extension of the calculation for the terrain correction. The bouguer plate correction (Δg_{BP}) is negative if the station is above sea-level but positive if it is below sea-level. It is calculated using the formula,

$$\Delta g_{BP} = 2\pi G\delta h \text{.....} \text{.....} \text{.....} \text{.....} \text{.....} \text{.....} (2.8) \text{ (Lowrie, 2007)}$$

Where:

G = Universal gravitation

δ = Density of the rock

h = Thickness of the layer.

The bouguer plate correction is subtracted from the measured gravity value if the gravity station is above sea-level, but added if the gravity station is below sea-level.

Two assumptions are made in deriving the bouguer correction; first is that the slab is of uniform density and secondly, that it is of infinite horizontal extent. Neither is really valid (Telford *et al.,* 1990). However, to modify the first assumption, the interpreter must be conversant with the geology of the area as to the rock type and its density. The number two assumption is ratified by terrain correction.

2.6.4 Free-air Correction: This correction tries to specifically take care of the variation in elevation alone between the measurement station and the datum level, without putting into consideration the rock mass existing within that same height or thickness. Thus, free –air correction pays no attention to the density of the rock materials between the measurement elevation and the reference ellipsoid. Its principle is based on the fact that gravitational acceleration varies inversely with distance from the centre of the earth. The free-air correction is added to the field reading if the measurement station is above the datum plane and subtracted when below. The free air correction is always of opposite sense to the Bouguer plate correction.

2.6.5 Combined Elevation Correction: Sometimes free-air and bouguer plate corrections are combined and carried out once as a single correction, and it is then called elevation correction. When this is done, the calculated value of the elevation correction is added to the measured gravity reading if the gravity station is above the sea level and subtracted if it is below.

2.6.6 Eotvos Correction: This correction is applicable to measurements taken while in motion, such as in a ship or aircraft. This is because a ship or aircraft in motion generates a centripetal acceleration which either reinforces or opposes gravity, depending on the direction of motion. It is calculated with the following equation.

$$EC = 75.03V \sin\alpha \cos\phi + 0.04154V^2 gu \quad \text{.....(2.9)}$$ (Kearey *et al.,* 2002)

Where:

EC = Eotvos Correction

V = Speed of vehicle

α = The heading

ϕ = latitude of the observation

2.6.7 Low Pass Filtering: Airborne gravity measurements are made in a very dynamic environment, resulting in extremely large noise in the data. Typically, noise-to-signal ratios of 1000 or more can be observed (Schwarz and Li, 1997). Extracting the gravity signal from measurements contaminated by such strong noise is one of the major challenges in airborne gravimetry. The largest contribution consists of high frequency noise, caused by the effect of aircraft vibrations on the gravimeter system and the amplification of GPS system noise when computing accelerations. To reduce these effects, a filtering technique can be applied to the airborne gravity data. Because in the low-frequency part of the spectrum the noise level is below the level of the gravity signal, the most commonly used filters are low-pass filters, although some alternative model-based approaches have been proposed (Hammada and Schwarz, 1997). When a low-pass filter is used, the filter passes low-frequency signals, but attenuates any signal above the cut-off frequency.

In general, there are two classes of low-pass filters namely (A) finite impulse response (FIR) and (B) infinite impulse response (IIR) filters. The impulse response of a filter is the output

sequence from the filter when a unit impulse is applied as its input. The term IIR, however, is not very accurate, since the actual impulse responses of nearly all IIR filters virtually reduce to zero in a finite time. Therefore, the terms non-recursive and recursive filters are often used instead. Both types of low-pass filters have been used for airborne gravity data processing. The FIR filter for instance has been used by the University of Calgary (Wei and Schwarz, 1998) for the processing of SINS data and by Brozena and Peters (1988), who combined it with a resistor-capacitor (RC) filter to sharpen the frequency roll-off. An example of an IIR filter is the Butterworth filter, which has been used by Forsberg *et al.,* (1999) and Meyer *et al.,* (2003). An advantage of using a low-pass filter is its easy implementation. However, even though both signal and noise are attenuated in the high-frequency band, some noise will remain in the pass-band, reducing the accuracy of the gravity data. The accuracy may be improved by using a larger filter length, but this reduces the resolution of the data.

Instead of low-pass filtering, a few model-based approaches have been used, mainly applied to SINS data. One example is Kalman filtering with a shaping filter as the stochastic model for the gravity disturbance (Eisfeller and Spietz, 1989; Hammada and Schwarz, 1997). Another approach is based on the wave filtering concept, where a deterministic model filtering is used that approximates the gravity disturbance by a simple function or a ramp (Salychev *et al.,* 1994). Hammada and Schwarz (1997) compared the model-based filtering approaches with low-pass filtering, and concluded that a low-pass filter performs systematically better.

2.7 Gravity Data Processing

2.7.1 Filtering: The term filtering can be applied to any of the various techniques that attempt to separate anomalies on the basis of their wavelength and/or trend (Blakely, 1995). The term separate is a good intuitive one because the idea is construct an image (anomaly

map) and then use filtering to separate anomalies of interest to the interpreter from other interfering anomalies (such as regional and local anomalies). In fact, fitting a low order polynomial surface (3rd order is used often) to a grid to approximate the regional is a common practice. Then subtracting the values representing this surface from the original grid values creates a residual grid that represents the local anomalies. In gravity studies, the familiar concepts of high pass, low pass, and bandpass filters are applied in either the frequency or spatial domains. Directional filters are also used to select anomalies based on their trend. In addition, a number of specialized techniques have been developed for the enhancement of maps of anomalies based on the physics of the gravity and magnetic fields and are discussed below. The various approaches to filtering can be sophisticated mathematically, but the choice of filter parameters or design of the convolution operator always involves a degree of subjectivity. It is useful to remember that the basic steps in enhancing a map of gravity anomalies in order to emphasize features in the Earth's crust are:

1) **First Remove a Conservative Regional Trend from the Data:** The choice of regional is usually not critical but may greatly help in interpretations. Because the goal is to remove long wavelength anomalies, this step consists of applying a gentle high pass filter. Over most continental areas, Bouguer anomaly values are large negative numbers, thus the usual practice of padding the edges of a grid with zeros prior to applying a Fourier transform and filtering will create large edge effects. One way to avoid this effect is to first remove the mean in the data and gridding an area larger than the image to be displayed. However in areas where large regional anomalies are present, it may be best to fit a low order polynomial surface to the gridded values, and then continue the processing with the residual values with respect to this surface.

2) Application of Specialized Filters: One can then apply additional filters as needed to remove unwanted wavelengths or trends. In addition to the usual wavelength filters, a variety of specialized filters have been developed for gravity data that include:

Upward Continuation - A process (low pass filter) by which a map simulating the result if the survey had been conducted on a plane at a higher elevation is constructed. This process is based on the physical fact that the further the observation is from the body causing the anomaly, the broader the anomaly. It is mathematically stable because it involves extracting long wavelength anomalies from short wavelength ones.

Downward Continuation - A high pass filter by which a map simulating the result if the survey had been conducted on a plane at a lower elevation is constructed. In theory, this process enhances anomalies due to relatively shallow sources. However, care should be taken when applying this process to anything but very clean, densely-sampled data sets, because of the potential for amplifying noise due to mathematical instability.

Vertical Derivatives - In this technique, the vertical rate of change of the gravity or magnetic field is estimated (usually the 1st or 2nd derivative). This is a specialized high pass filter, but the units of the resulting image are not milligals or nanoteslas and they cannot be modelled without special manipulations of the modelling software. As in the case of downward continuation, care should be taken when applying this process to anything but very clean data sets because of the potential for amplifying noise. This process has some similarities to non-directional edge enhancement techniques used in the analysis of remote sensing images.

Strike Filtering - This technique is directly analogous to the directional filters used in the analysis of remote sensing images. In gravity processing, the goal is to remove the effects of some linear trend with a particular azimuth. For example in much of the central U.S., the ancient processes that formed the Earth's crust created a northeast trending structural fabric that is reflected in gravity and magnetic maps in the area and can obscure other anomalies

(Alberts, 2009). Thus, one might want to apply a strike-reject filter which deletes linear anomalies whose trends (azimuths) range from $N30^0E$ to $N60^0E$.

Horizontal Gradients - In this technique, faults and other abrupt geologic discontinuities (edges) are detected based on the high horizontal gradients that they produce. Simple differential equations are usually employed to calculate the gradients along the rows and columns of the grid. A linear maximum in the gradient is interpreted as a discontinuity such as a fault. These features are easy to extract graphically to be used as an overlay on the original gravity or magnetic map or on products such as Landsat images.

2.7.2 Computer Modelling of Gravity Data

In most applications of gravity techniques, the data processing and qualitative interpretation of maps is followed by a quantitative interpretation in which a profile (or grid) of anomaly values is modelled by constructing an earth model whose calculated gravitational effect closely approximates the observed profile (or grid). Modelling of profiles of anomaly values has become common place and is now a routine part of any investigation of the subsurface. In its simplest form, the process of constructing an earth model is one of trial and error iteration in which one's knowledge of the local geology, data from drill holes, and other data such as seismic surveys are valuable constraints in the process. As the modelling proceeds, one must make choices concerning density and geometry of the bodies of rock that make up the model. In the absence of any constraints (which is rare), the process is subject to considerable ambiguity since there will be many subsurface structural configurations which can fit the observed data. With some constraints, one can usually feel that the process has yielded a very useful interpretation of the subsurface. However, ambiguities will always remain just as they do in all other geophysical techniques aimed at studying the structure of the subsurface.

There are countless published articles on possible mathematical approaches to the modelling. However, for the two dimensional case (i.e. the modelling of profiles drawn perpendicular the structural grain in the area of interest) a very flexible and easy approach is used almost universally. This technique is based on the work of Talwani *et al.,* (1959), and Cady (1980), although many groups have written their own versions of this software with increasingly effective graphical interfaces and output. The original computer program was published by Talwani *et al.*, (1959), and Cady (1980) was among the first to introduce an approximation (called $2^1/_2$ D) that allows for a certain degree of three dimensionality. In the original formulation, the earth model was composed of bodies of polygonal cross section that extended to infinity in and out of the plane of the profile of gravity readings. In the $2^1/_2$ D formulation, the bodies can be assigned finite strike-lengths in both directions. Today, anyone can have a $2^1/_2$ D modelling running on their PC.

The use of three dimensional approaches is not as common as it should be because of the complexity of constructing and manipulating the earth model. However, there are many 3-D approaches available (Blakely, 1995). As discussed above, a full 3-D calculation of the gravitational attraction of the topography using a modern digital terrain model should be a better way to calculate Bouguer and terrain corrections as well as construct earth models. This type of approach will be employed more often in the future as the computer software needed becomes more readily available.

CHAPTER THREE

MATERIAL AND METHOD

3.1 Data Availability and Description

3.1.1 Gravity Data

Gravity data as used in this work was collected both by air survey and on land along major, minor roads and footpath across Anambra, Enugu, and Ebonyi states (between 2008 and 2011), which covers sheets 286, 287,288, 300, 301, 302, 311, 312, and 313 of the Geologic Survey Agency of Nigeria, with sampling interval of 2 kms. The survey was tied to IGSN'71(International Gravity Survey Network) (Morelli *et al.,* 1971) through the Primary Gravity Network of Nigeria (PGNN) (Osazuwa, 1985). Total number of data points per state is Anambra (725), Ebonyi (501), Enugu (866). Area coverage per state is Anambra (4,844 km^2), Ebonyi (5,530 km^2), Enugu (7,000 km^2). Station density per state is Anambra (1/6.7 km^2), Ebonyi (1/11 km^2), Enugu (1/1 km^2). Number of second order base stations established per state is Anambra (28), Ebonyi (27), Enugu (28). The Fugro Gravity Survey was flown at a line spacing of 4 km with a sensor elevation of 570 m. A.S.L. Flight direction was 0^o-180^o. Final Bouguer gravity grid was calculated from the Free-Air using a Bouguer density of 2.67 gm/cm^3. The Bouguer gravity grid was generated using a minimum curvature algorithm at a grid cell size of 1,000 m (one-quarter of the line-spacing).

3.1.2 Elevation Data (Shuttle Radar Topographic Mission Map)

During the field survey for gravity data acquisition, elevations at different locations were measured alongside using Wallace & Tiernan Barometric Altimeter, while the coordinates were also measured using Garmin Csx 76 global positioning system (GPS). These data sets were keyed into the Oasis Montaj software to produce the Shuttle Radar Topographic Mission Map (STRM) which was used in the present work.

3.1.3 Well Data

The wells location map as presented by Onuoha (2005) was adopted as a type of well data in this work and was correlated with the gravity data as part of the interpretations for hydrocarbon potentials of the basin. Another form of well data in this work, otherwise called borehole data, is a lithologic log data from some of the drilled oil wells in the basin and was adopted from the works of Nwajide (2013).

3.1.4 Geothermal Gradient / Heat Flow Data

The geothermal gradient / heat flow data that as used in this work was adopted from onuoha and Ekine (1999). The data was generated from bottom hole temperatures (BHT) using well logs supplied by the exploration department of ELF Petroleum Nigeria limited (EPNL).

3.2 Methodology

3.2.1 Gravity Data Acquisition

The field equipment applied in data acquisition include Lacoste & Romberg, G-512 Gravimeter (#0.01mGal), Wallace & Tiernan Barometric Altimeter (#1m), American Paulin System MDM-5 (#0.5m), Sling Psychrometer – measurement of Air Temperature, and Garmin Csx 76 GPS (#1m). The Gravimeter was calibrated using Northern Nigeria Calibration Line (Jos – Ilela) 376.72 mGal (Osazuwa, 1992), while the Relative humidity used in correcting the barometric readings was determined from the Psychrometer chart. The measured gravitational acceleration g_z of the Earth was derived from the gravity potential function $\phi(x, y, z)$. The gradient of the potential function $\phi(x, y, z)$produced the gravitational acceleration vector thus:

$$\nabla\phi(x,y,z)=\frac{\partial\phi_i}{\partial x}+\frac{\partial\phi_j}{\partial y}+\frac{\partial\phi_k}{\partial z}=\overline{F}\text{ ----------(3.1)}$$

Where $\overline{F}$ = force field vector.

Taking the curl vector of the force, we have:

$$\nabla\overline{F}=\nabla\left(\overline{F}_{1i}+\overline{F}_{2j}+\overline{F}_{3k}\right)\text{----------(3.2)}$$

Equation (11) can be written as:

$$Curl\overline{F}=\begin{vmatrix} i & j & k \\ F_1 & F_2 & F_3 \\ \frac{\partial}{\partial x} & \frac{\partial}{\partial y} & \frac{\partial}{\partial z} \end{vmatrix}\text{----------(3.3)}$$

If $\nabla\overline{F}=0$, it means that vector field $\overline{F}$ is irrotational and conservative, and that the work done by the vector field is independent of the part taken but only depends on the beginning and end point positions.

Then:

$$\overline{F}=-\nabla\phi\text{----------(3.4)}$$

The negative sign implies that the force field vector is an attractive force between two masses. The Newton's law of attraction between two masses m_1 and m_2 due to force vector $\overline{F}$ is given by:

$$\overline{F}=-\frac{Gm_1m_2\hat{r}}{r^2}\text{----------(3.5)}$$

Where:

m_1 and m_2 are the masses of the two bodies

G = gravitational constant $(6.67259\times10^{-11} m^3 Kg^{-1} S^{-2})$

$\hat{r}$ = unit vector in the direction of force field

If m_1 is the mass of the Earth having mass M_e, we have that:

$$\bar{F} = -\frac{GM_e m_2 \hat{r}}{r^2} \text{ ----------} \quad (3.6)$$

If m_2 is allowed to move due to the influence of the force field, it would move with an acceleration g.

Recall that:

$$\bar{F} = m_2 \bar{g} \text{ ----------} \quad (3.7)$$

Hence,

$$m_2 \bar{g} = -\frac{GM_e m_2 \hat{r}}{r^2} \text{ ----------} \quad (3.8)$$

$$\bar{g} = -\frac{GM_e \hat{r}}{r^2} \text{ ----------} \quad (3.9)$$

If $m_2 = 1$

Then the gravitational acceleration is equal to the force. Thus:

$$\bar{g} = \bar{F} \text{ ----------} \quad (3.10)$$

The work done in bringing a unit mass from infinity (centre of the Earth) up to the surface of the Earth is the gravitational Potential $\phi_{(x,y,z)}$.

Recall that $work(\phi) = Force \times Distance$

$$\therefore \quad d\phi = -\frac{GM_e}{r^2} dr \text{ ---------- (3.11)}$$

$$\int d\phi = -GM_e \int_{\infty}^{R} \frac{dr}{r^2} \text{ ---------- (3.12)}$$

$$\phi = \frac{GM_e}{R} \text{ ---------- (3.13}a\text{)}$$

In x, z plane,

Note that $R = \left(x^2 + z^2\right)^{\frac{1}{2}}$ ---------- (3.13b)

$$\therefore \phi_{(x,z)} = \frac{GM_e}{\left(x^2 + z^2\right)^{\frac{1}{2}}} \text{ ---------- (3.14)}$$

Equation (23) was differentiated with respect to z to obtain the vertical gravity field g_z which was used in Geophysical data gathering, processing and interpretation.

Hence,

$$g_z = -\frac{d\phi_{(x,z)}}{dz} \text{ ---------- (3.15)}$$

For the measurement Profile in the direction of x-axis on the xz plane, then:

$$g_x = -\frac{d\phi_{(x,z)}}{dz} = \frac{GM_e z}{\left(x^2 + z^2\right)^{\frac{3}{2}}} \text{----------(3.16)}$$

Aero gravity data gathering was used to obtain the vertical gravity fields in Anambra Basin of Nigeria. A follow-up ground gravity data acquisition was also made to increase the data density.

3.2.2 Determination of Bouguer Gravity Anomaly: A discrepancy between the corrected, measured and the theoretical gravity is called a gravity anomaly (Lines and Newrick, 2004). The most common types are the Bouguer anomaly and Free air anomaly. After all necessary corrections such as: Latitude correction (g_ϕ), The free-Air correction (g_{FA}), The elevation correction (Ec), The Bouguer correction (B), And the Terrain correction (T), the Bouguer gravity anomaly was calculated using the formular:

$$\Delta g_B = g_m + (\Delta g_{FA} - \Delta g_{BP} + \Delta g_T + \Delta g_{tide}) - g_n \text{.....(3.17)}$$ (Lowrie, 2007)

Where:

Δg_B = Bouguer gravity anomaly

g_m = Measured gravity data

Δg_{FA} = Free air correction

Δg_{BP} = Bouguer plate correction

Δg_T = Terrain correction

Δg_{tide} = Tidal correction

g_n = Normal or theoretical gravity

After all the corrections outlined in equation (3.17), the vertical gravity data distribution were then assembled and contoured for processing and interpretation.

3.2.3 Separation of Residual and Regional Anomalies.

This was done using the idea of fitting a linear or polynomial function onto data taken on a vector plane.

For A Data Obtained on a 1D Vector Plane.

The equation of a linear function on a ID vector plane is given by:

$$Y_i = (mx_i + c) + e_i \quad \text{.....(3.18)}$$ Unwin, 1978

Where:

Y_i = Response variable (i.e. Regional gravity reading)

x_i = Predictor variable (i.e. Measurement distance)

c = Constant

e_i = Residual

$$\therefore \quad e_i = Y_i - (mx_i + c) \quad \text{.....(3.19)}$$

Using Least square criterion, we want to find the combination of m and c that in relationship to the observed values minimises the sum of squares of the residuals.

Let S = sum of the squares of the residuals e_i

Hence,

$$S = \sum_{i=1}^{N} e_i^2$$

$$\Rightarrow S = \sum_{i=1}^{N} e_i^2 = \sum_{i=1}^{N} [Y_i - (mx_i + c)]^2 \quad \text{.....(3.20)}$$

The condition on which S is minimized is that the partial derivatives of S (i.e. sum of the squares of the residuals) with respect to the constants m and c are equal to zero;

i.e.

$$\frac{\partial S}{\partial m} = \frac{\partial S}{\partial c} = 0 \qquad \text{Unwin, 1978}$$

To obtain the constants *m* and *c*, we differentiate equation 29 with respect to *m* and *c* and equate to zero.

Hence

$$\left.\begin{aligned} \frac{\partial S}{\partial m} &= 2\sum_{i=1}^{N}\left[Y_i - \left(mx_i + c\right)\right].\left(-x_i\right) = 0 \\ \frac{\partial S}{\partial c} &= 2\sum_{i=1}^{N}\left[Y_i - \left(mx_i + c\right)\right].\left(-1\right) = 0 \end{aligned}\right\} \quad \text{.....(3.21)}$$

Dividing through by 2, Equation (30) can be modified as

$$\left.\begin{aligned} \frac{\partial S}{\partial m} &= \sum_{i=1}^{N}\left[Y_i - \left(mx_i + c\right)\right].\left(-x_i\right) = 0 \\ \frac{\partial S}{\partial c} &= \sum_{i=1}^{N}2\left[Y_i - \left(mx_i + c\right)\right].\left(-1\right) = 0 \end{aligned}\right\} \quad \text{.....(3.22)}$$

Opening the bracket in equation (31) we have

$$\left.\begin{aligned} &\sum_{i=1}^{N}\left[-Y_i x_i - \left(-mx_i^2 - cx_i\right)\right] = 0 \\ &\sum_{i=1}^{N}\left[-Y_i - \left(-mx_i - c\right)\right] = 0 \end{aligned}\right\} \quad \text{.....(3.23)}$$

$\Rightarrow$

$$\left.\begin{aligned} &-\sum_{i=1}^{N}Y_i x_i + m\sum_{i=1}^{N}x_i^2 + c\sum_{i=1}^{N}x_i = 0 \\ &-\sum_{i=1}^{N}Y_i + m\sum_{i=1}^{N}x_i + Nc = 0 \end{aligned}\right\}$$

.....(3.24)

Rearranging equation 33 by taking the negative signs to the right,

$$\left.\begin{aligned} m\sum_{i=1}^{N} x_i^2 + c\sum_{i=1}^{N} x_i &= \sum_{i=1}^{N} Y_i x_i \\ m\sum_{i=1}^{N} x_i + Nc &= \sum_{i=1}^{N} Y_i \end{aligned}\right\} \quad \text{.....(3.25)}$$

Putting equation (34) in matrix form we have

$$\begin{bmatrix} \sum_{i=1}^{N} x_i^{\,2} & \sum_{i=1}^{N} x_i \\ \sum_{i=1}^{N} x_i & N \end{bmatrix} \bullet \begin{bmatrix} m \\ c \end{bmatrix} = \begin{bmatrix} \sum_{i=1}^{N} Y_i x_i \\ \sum_{i=1}^{N} Y_i \end{bmatrix} \text{.....(3.26)}$$

This is equivalent to

$$AX = B.$$

Where

$$A = \begin{bmatrix} \sum_{i=1}^{N} x_i^{\,2} & \sum_{i=1}^{N} x_i \\ \sum_{i=1}^{N} x_i & N \end{bmatrix}, \qquad X = \begin{bmatrix} m \\ c \end{bmatrix} \qquad \text{and} \qquad B = \begin{bmatrix} \sum_{i=1}^{N} Y_i x_i \\ \sum_{i=1}^{N} Y_i \end{bmatrix}$$

Thus our matrix equation (35) becomes

$$AX = B \text{.....(3.27)}$$

To find X, we will first find the inverse of A (i.e. A^{-1}) given as

$$A^{-1} = \frac{1}{|A|} \bullet adjA \text{.....(3.28)}$$

Where: $adjA =$ Adjoined of A and

$|A| =$ Determinant of A

Recall that given any 2X2 matrix 'C' defined as

$$C = \begin{bmatrix} a & b \\ c & d \end{bmatrix},$$

The inverse of C

$$C^{-1} = \frac{1}{|C|}\begin{bmatrix} d & -b \\ -c & a \end{bmatrix}$$

Since A is a 2x2 matrix,

$$A^{-1} = \frac{1}{|A|}\begin{bmatrix} N & -\sum_{i=1}^{N} x_i \\ -\sum_{i=1}^{N} x_i & \sum_{i=1}^{N} x_i^2 \end{bmatrix} \ldots\ldots\ldots\ldots\ldots\ldots\ldots\ldots (3.29)$$

Where:

$|A|$ is the determinant of A.

Pre-multiplying the equation (36) above by A^{-1}

$$\Rightarrow \quad A^{-1}AX = A^{-1}B$$

$$\Rightarrow \quad IX = A^{-1}B \ldots\ldots\ldots\ldots\ldots\ldots\ldots\ldots (3.30)$$

Where I is an Identity matrix. Recall that when you multiply a matrix by its inverse, you would get that matrix.

$$\Rightarrow \quad X = A^{-1}B \ldots\ldots\ldots\ldots\ldots\ldots\ldots\ldots (3.31)$$

A multiplication of Identity matrix with any matrix would give you that matrix.

Substituting for X, A^{-1} and B in equation (3.32)

$$\Rightarrow \qquad \begin{bmatrix} m \\ c \end{bmatrix} = \frac{1}{|A|} \begin{bmatrix} N & -\sum_{i=1}^{N} x_i \\ -\sum_{i=1}^{N} x_i & \sum_{i=1}^{N} x_i^2 \end{bmatrix} \begin{bmatrix} \sum_{i=1}^{N} Y_i x_i \\ \sum_{i=1}^{N} Y_i \end{bmatrix} \text{.....} (3.33)$$

Determinant of A is given as

$$|A| = \begin{vmatrix} \sum_{i=1}^{N} x_i^{\,2} & \sum_{i=1}^{N} x_i \\ \sum_{i=1}^{N} x_i & N \end{vmatrix} = N \sum_{i=1}^{N} x_i^{\,2} - \left(\sum_{i=1}^{N} x_i \right)^2$$

$$\therefore \qquad |A| = N \sum_{i=1}^{N} x_i^{\,2} - \left(\sum_{i=1}^{N} x_i \right)^2 \text{.....} (3.34)$$

Substituting for $|A|$ in equation (3.33)

$$\Rightarrow \qquad \begin{bmatrix} m \\ c \end{bmatrix} = \frac{1}{N \sum_{i=1}^{N} x_i^{\,2} - \left(\sum_{i=1}^{N} x_i \right)^2} \begin{bmatrix} N & -\sum_{i=1}^{N} x_i \\ -\sum_{i=1}^{N} x_i & \sum_{i=1}^{N} x_i^2 \end{bmatrix} \begin{bmatrix} \sum_{i=1}^{N} Y_i x_i \\ \sum_{i=1}^{N} Y_i \end{bmatrix} \text{.....} (3.35)$$

$$\begin{bmatrix} m \\ c \end{bmatrix} = \begin{bmatrix} \frac{N}{N\sum_{i=1}^{N} x_i^{\,2} - \left(\sum_{i=1}^{N} x_i\right)^2} & \frac{-\sum_{i=1}^{N} x_i}{N\sum_{i=1}^{N} x_i^{\,2} - \left(\sum_{i=1}^{N} x_i\right)^2} \\ \frac{-\sum_{i=1}^{N} x_i}{N\sum_{i=1}^{N} x_i^{\,2} - \left(\sum_{i=1}^{N} x_i\right)^2} & \frac{\sum_{i=1}^{N} x_i^2}{N\sum_{i=1}^{N} x_i^{\,2} - \left(\sum_{i=1}^{N} x_i\right)^2} \end{bmatrix} \begin{bmatrix} \sum_{i=1}^{N} Y_i x_i \\ \sum_{i=1}^{N} Y_i \end{bmatrix} \quad ..(3.36)$$

By multiplication of matrices, equation 3.36 becomes

$$\begin{bmatrix} m \\ c \end{bmatrix} = \begin{bmatrix} \frac{N\sum_{i=1}^{N} Y_i x_i}{N\sum_{i=1}^{N} x_i^{\,2} - \left(\sum_{i=1}^{N} x_i\right)^2} + \frac{-\sum_{i=1}^{N} x_i \sum_{i=1}^{N} Y_i}{N\sum_{i=1}^{N} x_i^{\,2} - \left(\sum_{i=1}^{N} x_i\right)^2} \\ \frac{-\sum_{i=1}^{N} x_i \sum_{i=1}^{N} Y_i x_i}{N\sum_{i=1}^{N} x_i^{\,2} - \left(\sum_{i=1}^{N} x_i\right)^2} + \frac{\sum_{i=1}^{N} x_i^2 \sum_{i=1}^{N} Y_i}{N\sum_{i=1}^{N} x_i^{\,2} - \left(\sum_{i=1}^{N} x_i\right)^2} \end{bmatrix}$$

$$\begin{bmatrix} m \\ c \end{bmatrix} = \begin{bmatrix} \frac{N\sum_{i=1}^{N} Y_i x_i - \sum_{i=1}^{N} x_i \sum_{i=1}^{N} Y_i}{N\sum_{i=1}^{N} x_i^{\,2} - \left(\sum_{i=1}^{N} x_i\right)^2} \\ \frac{\sum_{i=1}^{N} x_i^2 \sum_{i=1}^{N} Y_i - \sum_{i=1}^{N} x_i \sum_{i=1}^{N} Y_i x_i}{N\sum_{i=1}^{N} x_i^{\,2} - \left(\sum_{i=1}^{N} x_i\right)^2} \end{bmatrix} \quad .....(3.37)$$

By equality of two matrices,

$$m = \frac{N\sum_{i=1}^{N} Y_i x_i - \sum_{i=1}^{N} x_i \sum_{i=1}^{N} Y_i}{N\sum_{i=1}^{N} x_i^{\,2} - \left(\sum_{i=1}^{N} x_i\right)^2} \quad \ldots\ldots\ldots (3.38)$$

$$c = \frac{\sum_{i=1}^{N} x_i^2 \sum_{i=1}^{N} Y_i - \sum_{i=1}^{N} x_i \sum_{i=1}^{N} Y_i x_i}{N\sum_{i=1}^{N} x_i^{\,2} - \left(\sum_{i=1}^{N} x_i\right)^2} \quad \ldots\ldots\ldots (3.39)$$

For Data Obtained on 2D Vector Plane

The equation of the response variable Y_{ij} becomes

$$Y_{ij} = (ax_i + by_j + c) + e_{ij} \ldots\ldots\ldots\ldots\ldots\ldots\ldots\ldots (3.40)$$ Unwin, 1978

Where:

Y_{ij} = Response variable (Regional gravity reading)

x_i = Predictor variable in the direction of unit vector *i* (i.e. Measurement point in x-direction)

y_j = Predictor variable in the direction of unit vector *j* (i.e. Measurement point in y-direction)

$a, b \text{ and } c$ = Constants.

e_{ij} = Residuals

$$\therefore \quad e_{ij} = Y_{ij} - (ax_i + by_j + c) \ldots\ldots\ldots\ldots\ldots\ldots\ldots\ldots\ldots\ldots (3.41)$$

Let S = sum of the squares of the residuals, e_{ij}

Hence,

$$S = \sum_{\substack{i=1 \\ j=1}}^{N} e_{ij}^2 \text{.....(3.42)}$$

$$\Rightarrow S = \sum_{\substack{i=1 \\ j=1}}^{N} e_{ij}^2 = \sum_{\substack{i=1 \\ j=1}}^{N} \left[Y_{ij} - \left(ax_i + by_j + c \right) \right]^2 \text{.....(3.43)}$$

The condition on which S is minimized is that the partial derivatives of S (i.e. sum of the squares of the residuals) with respect to the constants a , b and c are equal to zero;

i.e.

$$\frac{\partial S}{\partial a} = \frac{\partial S}{\partial b} = \frac{\partial S}{\partial c} = 0 \text{.....(3.44)}$$ Unwin, 1978

Differentiating equation 3.44 with respect to *a*, *b* and *c* and equate to zero,

$$\left.\begin{aligned} \frac{\partial S}{\partial a} &= 2\sum_{\substack{i=1 \\ j=1}}^{N} \left[Y_{ij} - \left(ax_i + by_j + c \right) \right] \left(- x_i \right) = 0 \\ \frac{\partial S}{\partial b} &= 2\sum_{\substack{i=1 \\ j=1}}^{N} \left[Y_{ij} - \left(ax_i + by_i + c \right) \right] \left(- y_j \right) = 0 \\ \frac{\partial S}{\partial c} &= 2\sum_{\substack{i=1 \\ j=1}}^{N} \left[Y_{ij} - \left(ax_i + by_j + c \right) \right] \left(-1 \right) = 0 \end{aligned}\right\} \text{.....(3.45)}$$

Dividing through by 2

$$\left.\begin{aligned}
&\sum_{\substack{i=1\\j=1}}^{N}\left[Y_{ij}-\left(ax_i+by_j+c\right)\right]\left(-x_i\right)=0\\
&\sum_{\substack{i=1\\j=1}}^{N}\left[Y_{ij}-\left(ax_i+by_i+c\right)\right]\left(-y_j\right)=0\\
&\sum_{\substack{i=1\\j=1}}^{N}\left[Y_{ij}-\left(ax_i+by_j+c\right)\right]\left(-1\right)=0
\end{aligned}\right\} \qquad \text{.....(3.46)}$$

Opening the brackets,

$$\left.\begin{aligned}
&\sum_{\substack{i=1\\j=1}}^{N}\left[-Y_{ij}x_i-\left(-ax_i^2-bx_iy_j-cx_i\right)\right]=0\\
&\sum_{\substack{i=1\\j=1}}^{N}\left[-Y_{ij}y_j-\left(-ax_iy_j-by_j^2-cy_j\right)\right]=0\\
&\sum_{\substack{i=1\\j=1}}^{N}\left[-Y_{ij}-\left(-ax_i-by_j-c\right)\right]=0
\end{aligned}\right\} \qquad \text{.....(3.47)}$$

Opening further, equation 55 becomes

$$\left.\begin{aligned} -\sum_{\substack{i=1\\j=1}}^{N} Y_{ij}x_i + a\sum_{i=1}^{N} x_i^2 + b\sum_{\substack{i=1\\j=1}}^{N} x_i y_j + c\sum_{i=1}^{N} x_i = 0 \\ -\sum_{\substack{i=1\\j=1}}^{N} Y_{ij}y_j + a\sum_{\substack{i=1\\j=1}}^{N} x_i y_j + b\sum_{j=1}^{N} y_j^2 + c\sum_{j=1}^{N} y_j = 0 \\ -\sum_{\substack{i=1\\j=1}}^{N} Y_{ij} + a\sum_{i=1}^{N} x_i + b\sum_{\substack{i=1\\j=1}}^{N} y_j x_i + Nc = 0 \end{aligned}\right\} \quad \text{.....(3.48)}$$

Taking the negative quantities to the right hand side of the equation,

$$\left.\begin{aligned} a\sum_{i=1}^{N} x_i^2 + b\sum_{\substack{i=1\\j=1}}^{N} x_i y_j + c\sum_{i=1}^{N} x_i = \sum_{\substack{i=1\\j=1}}^{N} Y_{ij}x_i \\ a\sum_{i=1}^{N} x_i y_j + b\sum_{j=1}^{N} y_j^2 + c\sum_{j=1}^{N} y_j = \sum_{\substack{i=1\\j=1}}^{N} Y_{ij}y_j \\ a\sum_{i=1}^{N} x_i + b\sum_{j=1}^{N} y_j + Nc = \sum_{j=1}^{N} Y_j \end{aligned}\right\} \quad \text{.....(3.49)}$$

This can be further put in matrix form (Davis, 2014) as shown in equation 3.49.

$$\begin{bmatrix} \sum_{i=1}^{N} x_i^2 & \sum_{\substack{i=1\\j=1}}^{N} x_i y_j & \sum_{i=1}^{N} x_i \\ \sum_{\substack{i=1\\j=1}}^{N} x_i y_j & \sum_{j=1}^{N} y_j^2 & \sum_{j=1}^{N} y_j \\ \sum_{i=1}^{N} x_i & \sum_{j=1}^{N} y_j & N \end{bmatrix} \begin{bmatrix} a \\ b \\ c \end{bmatrix} = \begin{bmatrix} \sum_{\substack{i=1\\j=1}}^{N} Y_{ij}x_i \\ \sum_{\substack{i=1\\j=1}}^{N} Y_{ij}y_j \\ \sum_{\substack{i=1\\j=1}}^{N} Y_{ij} \end{bmatrix} \text{.....(3.50)}$$

Equation 3.50 is equivalent to the matrix equation:

$$D\ E\ =\ F$$

Where:

$$D=\begin{bmatrix} \sum_{i=1}^{N} x_i^2 & \sum_{\substack{i=1\\j=1}}^{N} x_i y_j & \sum_{i=1}^{N} x_i \\ \sum_{\substack{i=1\\j=1}}^{N} x_i y_j & \sum_{j=1}^{N} y_j^2 & \sum_{j=1}^{N} y_j \\ \sum_{i=1}^{N} x_i & \sum_{j=1}^{N} y_j & N \end{bmatrix}, \qquad E=\begin{bmatrix} a \\ b \\ c \end{bmatrix} \quad \text{and}$$

$$F=\begin{bmatrix} \sum_{\substack{i=1\\j=1}}^{N} Y_{ij} x_i \\ \sum_{\substack{i=1\\j=1}}^{N} Y_{ij} y_j \\ \sum_{\substack{i=1\\j=1}}^{N} Y_{ij} \end{bmatrix}$$

Hence, our matrix equation becomes

$$DE = F \qquad (3.51)$$

To get E, we need to first of all get the inverse of D (i.e. D^{-1}) and pre-multiply equation 3.51 by the D^{-1}.

Hence,

$$D^{-1} = \frac{1}{|D|} \bullet adjD \qquad (3.52)$$

Where:

$adjD$ is the Adjoined of D

$|D|$ is the determinant of D

To get the determinant of D

$$|D| = \begin{vmatrix} \sum_{i=1}^{N} x_i^2 & \sum_{\substack{i=1 \\ j=1}}^{N} x_i y_j & \sum_{i=1}^{N} x_i \\ \sum_{\substack{i=1 \\ j=1}}^{N} x_i y_j & \sum_{j=1}^{N} y_j^2 & \sum_{j=1}^{N} y_j \\ \sum_{i=1}^{N} x_i & \sum_{j=1}^{N} y_j & N \end{vmatrix}$$

$$\therefore |D| = \sum_{i=1}^{N} x_i^2 \left(N \sum_{j=1}^{N} y_j^2 - \sum_{j=1}^{N} y_j \sum_{j=1}^{N} y_j \right) - \sum_{\substack{i=1 \\ j=1}}^{N} x_i y_j \left(N \sum_{\substack{i=1 \\ j=1}}^{N} x_i y_j - \sum_{i=1}^{N} x_i \sum_{j=1}^{N} y_j \right) + \sum_{i=1}^{N} x_i \left(\sum_{\substack{i=1 \\ j=1}}^{N} x_i y_j \sum_{j=1}^{N} y_j - \sum_{i=1}^{N} x_i \sum_{j=1}^{N} y_j^2 \right) \quad \text{.....(3.53)}$$

To determine $adjD$ we first determine the cofactors of the element of D,

Let the matrix D (equation 3.51) be represented as

$$D = \begin{bmatrix} d_{11} & d_{12} & d_{13} \\ d_{21} & d_{22} & d_{23} \\ d_{31} & d_{32} & d_{33} \end{bmatrix}$$

And let c_{ij} be the cofactors of the elements of D, such that c_{11} is a cofactor of d_{11} and so on.

Hence, by the definition of cofactors of an element of a matrix,

$$C_{11} = \left(N \sum_{j=1}^{N} y_j^2 - \sum_{j=1}^{N} y_j \sum_{j=1}^{N} y_j \right)$$

$$C_{12} = -\left(N\sum_{\substack{i=1\\j=1}}^{N} x_i y_j - \sum_{i=1}^{N} x_i \sum_{j=1}^{N} y_j \right)$$

$$C_{13} = \left(\sum_{\substack{i=1\\j=1}}^{N} x_i y_j \sum_{j=1}^{N} y_j - \sum_{j=1}^{N} x_i \sum_{j=1}^{N} y_j^2 \right)$$

$$C_{21} = -\left(N\sum_{\substack{i=1\\j=1}}^{N} x_i y_j - \sum_{j=1}^{N} y_j \sum_{i=1}^{N} x_i \right)$$

$$C_{22} = \left(N\sum_{i=1}^{N} x_i^2 - \sum_{i=1}^{N} x_i \sum_{i=1}^{N} x_i \right)$$

$$C_{23} = -\left(\sum_{i=1}^{N} x_i^2 \sum_{j=1}^{N} y_j - \sum_{i=1}^{N} x_i \sum_{\substack{i=1\\j=1}}^{N} x_i y_j \right)$$

$$C_{31} = \left(\sum_{\substack{i=1\\j=1}}^{N} x_i y_j \sum_{j=1}^{N} y_j - \sum_{j=1}^{N} y_j^2 \sum_{i=1}^{N} x_i \right)$$

$$C_{32} = -\left(\sum_{i=1}^{N} x_i^2 \sum_{j=1}^{N} y_j - \sum_{\substack{i=1\\j=1}}^{N} x_i y_j \sum_{i=1}^{N} x_i \right)$$

$$C_{33} = \left(\sum_{i=1}^{N} x_i^2 \sum_{j=1}^{N} y_j^2 - \sum_{\substack{i=1\\j=1}}^{N} x_i y_j \sum_{\substack{i=1\\j=1}}^{N} x_i y_j \right)$$

Let C be the matrix of the cofactors of the elements of D. Thus,

$$C = \begin{bmatrix} C_{11} & C_{12} & C_{13} \\ C_{21} & C_{22} & C_{23} \\ C_{31} & C_{32} & C_{33} \end{bmatrix} \ldots\ldots\ldots\ldots\ldots\ldots\ldots\ldots\ldots\ldots\ldots\ldots(3.54)$$

By the definition of the adjoined of a matrix,

$$adjD = C^T \ldots\ldots\ldots\ldots\ldots\ldots\ldots\ldots\ldots\ldots\ldots\ldots(3.55)$$

Where C^T is the transpose of C.

$\Rightarrow$

$$adjD = C^T = \begin{bmatrix} C_{11} & C_{21} & C_{31} \\ C_{12} & C_{22} & C_{32} \\ C_{13} & C_{23} & C_{33} \end{bmatrix} \ldots\ldots\ldots\ldots\ldots\ldots(3.56)$$

Substituting equation 64 into equation 60,

$\Rightarrow$

$$D^{-1} = \frac{\begin{bmatrix} C_{11} & C_{21} & C_{31} \\ C_{12} & C_{22} & C_{32} \\ C_{13} & C_{23} & C_{33} \end{bmatrix}}{|D|} \ldots\ldots\ldots\ldots\ldots\ldots\ldots\ldots(3.57)$$

$\Rightarrow$

$$D^{-1} = \frac{1}{|D|} \begin{bmatrix} C_{11} & C_{21} & C_{31} \\ C_{12} & C_{22} & C_{32} \\ C_{13} & C_{23} & C_{33} \end{bmatrix} \ldots\ldots\ldots\ldots\ldots\ldots\ldots\ldots(3.58)$$

$$\therefore \quad D^{-1} = \begin{bmatrix} \frac{C_{11}}{|D|} & \frac{C_{21}}{|D|} & \frac{C_{31}}{|D|} \\ \frac{C_{12}}{|D|} & \frac{C_{22}}{|D|} & \frac{C_{32}}{|D|} \\ \frac{C_{13}}{|D|} & \frac{C_{23}}{|D|} & \frac{C_{33}}{|D|} \end{bmatrix} \ldots\ldots\ldots\ldots\ldots\ldots\ldots\ldots(3.59)$$

Pre-multiplying equation 3.51 with D^{-1}

$$D^{-1}DE = D^{-1}F \qquad (3.60)$$

$$\Rightarrow \quad IE = D^{-1}F \qquad (3.61)$$

Where $I =$ identity matrix.

$$\Rightarrow \quad E = D^{-1}F \qquad (3.62)$$

Substituting for E, D^{-1} and F in equation 3.62

$$\Rightarrow \quad \begin{bmatrix} a \\ b \\ c \end{bmatrix} = \begin{bmatrix} \frac{C_{11}}{|D|} & \frac{C_{21}}{|D|} & \frac{C_{31}}{|D|} \\ \frac{C_{12}}{|D|} & \frac{C_{22}}{|D|} & \frac{C_{32}}{|D|} \\ \frac{C_{13}}{|D|} & \frac{C_{23}}{|D|} & \frac{C_{33}}{|D|} \end{bmatrix} \begin{bmatrix} \sum_{\substack{i=1 \\ j=1}}^{N} Y_{ij} x_i \\ \sum_{\substack{i=1 \\ j=1}}^{N} Y_{ij} y_j \\ \sum_{\substack{i=1 \\ j=1}}^{N} Y_{ij} \end{bmatrix} \qquad (3.63)$$

Let $F_{11} = \sum_{\substack{i=1 \\ j=1}}^{N} Y_{ij} x_i$,

$F_{21} = \sum_{\substack{i=1 \\ j=1}}^{N} Y_{ij} y_j$ and

$F_{31} = \sum_{\substack{i=1 \\ j=1}}^{N} Y_{ij}$

$$\Rightarrow \quad \begin{bmatrix} a \\ b \\ c \end{bmatrix} = \begin{bmatrix} \frac{C_{11}}{|D|} & \frac{C_{21}}{|D|} & \frac{C_{31}}{|D|} \\ \frac{C_{12}}{|D|} & \frac{C_{22}}{|D|} & \frac{C_{32}}{|D|} \\ \frac{C_{13}}{|D|} & \frac{C_{23}}{|D|} & \frac{C_{33}}{|D|} \end{bmatrix} \begin{bmatrix} F_{11} \\ F_{21} \\ F_{31} \end{bmatrix} \ldots\ldots\ldots\ldots\ldots\ldots\ldots\ldots (3.64)$$

$$\Rightarrow \quad \begin{bmatrix} a \\ b \\ c \end{bmatrix} = \begin{bmatrix} \frac{C_{11}F_{11}}{|D|} + \frac{C_{21}F_{21}}{|D|} + \frac{C_{31}F_{31}}{|D|} \\ \frac{C_{12}F_{11}}{|D|} + \frac{C_{22}F_{21}}{|D|} + \frac{C_{32}F_{31}}{|D|} \\ \frac{C_{13}F_{11}}{|D|} + \frac{C_{23}F_{21}}{|D|} + \frac{C_{33}F_{31}}{|D|} \end{bmatrix}$$ (By multiplication of matrices)

$$\Rightarrow$$

$$\begin{bmatrix} a \\ b \\ c \end{bmatrix} = \begin{bmatrix} \frac{C_{11}F_{11} + C_{21}F_{21} + C_{31}F_{31}}{|D|} \\ \frac{C_{12}F_{11} + C_{22}F_{21} + C_{32}F_{31}}{|D|} \\ \frac{C_{13}F_{11} + C_{23}F_{21} + C_{33}F_{31}}{|D|} \end{bmatrix} \ldots\ldots\ldots\ldots\ldots\ldots\ldots\ldots (3.65)$$

By equality of matrices,

$$a = \frac{C_{11}F_{11} + C_{21}F_{21} + C_{31}F_{31}}{|D|} \ldots\ldots\ldots\ldots\ldots\ldots\ldots\ldots\ldots\ldots (3.66)$$

$$b = \frac{C_{12}F_{11} + C_{22}F_{21} + C_{32}F_{31}}{|D|} \ldots\ldots\ldots\ldots\ldots\ldots\ldots\ldots\ldots\ldots (3.67)$$

$$c = \frac{C_{13}F_{11} + C_{23}F_{21} + C_{33}F_{31}}{|D|} \ldots\ldots\ldots\ldots\ldots\ldots\ldots\ldots\ldots\ldots (3.68)$$

Substituting for C_{11}, F_{11}, C_{21}, F_{21}, C_{31} and F_{31} in equation 3.66,

$$a = \frac{\left(N\sum_{j=1}^{N} y_j^2 - \sum_{j=1}^{N} y_j \sum_{j=1}^{N} y_j\right)\sum_{\substack{i=1\\j=1}}^{N} Y_{ij}x_i - \left(N\sum_{\substack{i=1\\j=1}}^{N} x_i y_j - \sum_{j=1}^{N} y_j \sum_{i=1}^{N} x_i\right)\sum_{\substack{i=1\\j=1}}^{N} Y_{ij}y_j + \left(\sum_{\substack{i=1\\j=1}}^{N} x_i y_j \sum_{j=1}^{N} y_j - \sum_{j=1}^{N} y_j^2 \sum_{i=1}^{N} x_i\right)\sum_{\substack{i=1\\j=1}}^{N} Y_{ij}}{|D|} \quad ....(3.69)$$

Substituting for the determinant $|D|$ of equation (3.53) in equation (3.69),

$$\therefore a = \frac{\left(N\sum_{j=1}^{N} y_j^2 - \sum_{j=1}^{N} y_j \sum_{j=1}^{N} y_j\right)\sum_{\substack{i=1\\j=1}}^{N} Y_{ij}x_i - \left(N\sum_{\substack{i=1\\j=1}}^{N} x_i y_j - \sum_{j=1}^{N} y_j \sum_{i=1}^{N} x_i\right)\sum_{\substack{i=1\\j=1}}^{N} Y_{ij}y_j + \left(\sum_{\substack{i=1\\j=1}}^{N} x_i y_j \sum_{j=1}^{N} y_j - \sum_{j=1}^{N} y_j^2 \sum_{i=1}^{N} x_i\right)\sum_{\substack{i=1\\j=1}}^{N} Y_{ij}}{\sum_{i=1}^{N} x_i^2\left(N\sum_{j=1}^{N} y_j^2 - \sum_{j=1}^{N} y_j \sum_{j=1}^{N} y_j\right) - \sum_{\substack{i=1\\j=1}}^{N} x_i y_j\left(N\sum_{\substack{i=1\\j=1}}^{N} x_i y_j - \sum_{i=1}^{N} x_i \sum_{j=1}^{N} y_j\right) + \sum_{i=1}^{N} x_i\left(\sum_{\substack{i=1\\j=1}}^{N} x_i y_j \sum_{j=1}^{N} y_j - \sum_{i=1}^{N} x_i \sum_{j=1}^{N} y_j^2\right)} \quad ....(3.70)$$

Substituting for C_{12}, F_{11}, C_{22}, F_{21}, C_{32} and F_{31} in equation 3.67,

$$b = \frac{-\left(N\sum_{\substack{i=1\\j=1}}^{N} x_i y_j - \sum_{i=1}^{N} x_i \sum_{j=1}^{N} y_j\right)\sum_{\substack{i=1\\j=1}}^{N} Y_{ij}x_i + \left(N\sum_{i=1}^{N} x_i^2 - \sum_{i=1}^{N} x_i \sum_{i=1}^{N} x_i\right)\sum_{\substack{i=1\\j=1}}^{N} Y_{ij}y_j - \left(\sum_{i=1}^{N} x_i^2 \sum_{j=1}^{N} y_j - \sum_{\substack{i=1\\j=1}}^{N} x_i y_j \sum_{i=1}^{N} x_i\right)\sum_{\substack{i=1\\j=1}}^{N} Y_{ij}}{|D|} \quad ....(3.71)$$

Substituting for the determinant $|D|$ in equation (3.71),

$$\therefore b = \frac{-\left(N\sum_{\substack{i=1\\j=1}}^{N} x_i y_j - \sum_{i=1}^{N} x_i \sum_{j=1}^{N} y_j\right)\sum_{\substack{i=1\\j=1}}^{N} Y_{ij}x_i + \left(N\sum_{i=1}^{N} x_i^2 - \sum_{i=1}^{N} x_i \sum_{i=1}^{N} x_i\right)\sum_{\substack{i=1\\j=1}}^{N} Y_{ij}y_j - \left(\sum_{i=1}^{N} x_i^2 \sum_{j=1}^{N} y_j - \sum_{\substack{i=1\\j=1}}^{N} x_i y_j \sum_{i=1}^{N} x_i\right)\sum_{\substack{i=1\\j=1}}^{N} Y_{ij}}{\sum_{i=1}^{N} x_i^2\left(N\sum_{j=1}^{N} y_j^2 - \sum_{j=1}^{N} y_j \sum_{j=1}^{N} y_j\right) - \sum_{\substack{i=1\\j=1}}^{N} x_i y_j\left(N\sum_{\substack{i=1\\j=1}}^{N} x_i y_j - \sum_{i=1}^{N} x_i \sum_{j=1}^{N} y_j\right) + \sum_{i=1}^{N} x_i\left(\sum_{\substack{i=1\\j=1}}^{N} x_i y_j \sum_{j=1}^{N} y_j - \sum_{i=1}^{N} x_i \sum_{j=1}^{N} y_j^2\right)} \quad ....(3.72)$$

Substituting for C_{13}, F_{11}, C_{23}, F_{21}, C_{33} and F_{31} in equation 3.68,

$$c = \frac{\left(\sum_{i=1}^{N}\sum_{j=1}^{N} x_i y_j \sum_{j=1}^{N} y_j - \sum_{j=1}^{N} x_i \sum_{j=1}^{N} y_j^2\right)\sum_{i=1}^{N}\sum_{j=1}^{N} Y_{ij} x_i - \left(\sum_{i=1}^{N} x_i^2 \sum_{j=1}^{N} y_j - \sum_{i=1}^{N} x_i \sum_{\substack{i=1\\ j=1}}^{N} x_i y_j\right)\sum_{i=1}^{N}\sum_{j=1}^{N} Y_{ij} y_j + \left(\sum_{i=1}^{N} x_i^2 \sum_{j=1}^{N} y_j^2 - \sum_{\substack{i=1\\ j=1}}^{N} x_i y_j \sum_{\substack{i=1\\ j=1}}^{N} x_i y_j\right)\sum_{i=1}^{N}\sum_{j=1}^{N} Y_{ij}}{|D|} \quad .....(3.73)$$

Substituting for the determinant $|D|$ in equation 3.73,

$$\therefore c = \frac{\left(\sum_{i=1}^{N}\sum_{j=1}^{N} x_i y_j \sum_{j=1}^{N} y_j - \sum_{j=1}^{N} x_i \sum_{j=1}^{N} y_j^2\right)\sum_{i=1}^{N}\sum_{j=1}^{N} Y_{ij} x_i - \left(\sum_{i=1}^{N} x_i^2 \sum_{j=1}^{N} y_j - \sum_{i=1}^{N} x_i \sum_{\substack{i=1\\ j=1}}^{N} x_i y_j\right)\sum_{i=1}^{N}\sum_{j=1}^{N} Y_{ij} y_j + \left(\sum_{i=1}^{N} x_i^2 \sum_{j=1}^{N} y_j^2 - \sum_{\substack{i=1\\ j=1}}^{N} x_i y_j \sum_{\substack{i=1\\ j=1}}^{N} x_i y_j\right)\sum_{i=1}^{N}\sum_{j=1}^{N} Y_{ij}}{\sum_{i=1}^{N} x_i^2\left(N\sum_{j=1}^{N} y_j^2 - \sum_{j=1}^{N} y_j \sum_{j=1}^{N} y_j\right) - \sum_{\substack{i=1\\ j=1}}^{N} x_i y_j\left(N\sum_{\substack{i=1\\ j=1}}^{N} x_i y_j - \sum_{i=1}^{N} x_i \sum_{j=1}^{N} y_j\right) + \sum_{i=1}^{N} x_i\left(\sum_{\substack{i=1\\ j=1}}^{N} x_i y_j \sum_{j=1}^{N} y_j - \sum_{i=1}^{N} x_i \sum_{j=1}^{N} y_j^2\right)}. \quad .....(3.74)$$

Equations 3.70, 3.72 and 3.74 were used to derive the constants a, b, and c. After the derivations of the constants, they were further substituted into equation 3.41 to enable us calculate the residuals by subtracting the determined regional gravity values from the observed gravity values.

3.2.4 Vertical Gravity Data Processing

The observed value of the gravitational field of the earth is a function of the composition of the earth and the position vector of the measurement points. The values also obey the inverse square law such that the rock close to the observation point has greater effect than those further away. However, because of the enormous mass of the mantle and core, the structural features of the crust which are of interest in this work contributed little to the observed gravitational field of the earth. Therefore the enormous contribution of the mantle and core should be removed from the observed data in order to be left with the contribution due to the crust. The gravitational field of the mantle and core is removed using equation 3.41.The residual gravity anomaly left after the removal of the regional field (equation 3.41)

is then subjected to Fourier analysis so as to obtain the partial Fourier amplitude a_n and b_n by using discrete Fourier transform.

(A) **Discrete Fourier Transform**

The Fourier series expansion is given by:

$$f(x) = \frac{1}{2}a_0 + a_1\cos x + a_2\cos 2x + ... + a_n\cos nx + b_1\sin x + b_2\sin 2x + ... + b_n\sin nx \text{.....(3.75)}$$

Davis (2014) expressed the Fourier relationship (Equation 3.75) as a regression model in the form:

$$y_i = a_0 + \sum_{n=1}^{N-1}\left[a_n\cos\left(2\pi n\frac{x_i}{N}\right) + \sum_{n=1}^{N-1}b_n\sin\left(2\pi n\frac{x_i}{N}\right)\right] \text{.....(3.76)}$$

Where:

a_n and b_n = Partial amplitude of cosine and sine waves (or regression coefficients).

y_i = reading at x_i position vector

n = wave number (k) or frequency = 0,1,...,n

N = Number of data points

$2\pi x_i\frac{n}{N}$ = Instantaneous phase $\phi(t)$ for the harmonic wave in degree

y_i and x_i = two sets of vectors in ID plane

Note that 2π in equations 3.75 and 3.76 is in radians.

(B) Computation of a_n, b_n and A_n

$$\left.\begin{aligned} a_n &= \frac{2}{N}\left[\sum_{n=0}^{N-1} y_i \cos\left(2\pi n \frac{x_i}{N}\right)\right] \\ b_n &= \frac{2}{N}\left[\sum_{n=0}^{N-1} y_i \sin\left(2\pi n \frac{x_i}{N}\right)\right] \end{aligned}\right\} --(3.77)$$ Davis, 2014

Where:

a_n and b_n = partial amplitudes of cosine and sine waves.

The total amplitude A_n is given by the formular

$$A_n = \sqrt{a_n^2 + b_n^2} \text{ ----------(3.78)}$$

(C) Log Transformation

It is a transformation of arithmetic graph scale data to logarithmic graph scale data without a change in data value. However, there will be a change in the overall outlook of the data which enables better and clearer interpretation. In other words, it is only a transformation of arithmetic graph scale plot to log graph scale plot in the same domain (Predictor variable) and the same range. Hence we have Log-Log graph or semi Log graph.

- In gravity and magnetic data interpretation, log transformation is used for upwards and downwards continuation of data to any level of one's choice.
- It is also used in computing depth to the anomaly.

First, the gravity and magnetic data should be transformed to frequency domain through Fourier transform. If any of the attributes of the transformed gravity and magnetic data shows a linear relationship with the Predictor variable (frequency), then the log transformation can be used to do upwards and downwards continuation of the data to any level. It can also be used to calculate the depth to the causative body.

(D) Upwards and Downwards Continuation of Data

The upwards or downwards continuation of Potential Field data is achieved by multiplying the amplitude of the Partial wave by:

$$\exp\left[\left(\frac{2\pi}{L}\right)\times(z-z_0)\times f_{nm}\right] \text{----------(3.79)}$$

Hahn *et al.* (1970) showed that there is a linear relationship between the logarithm of the wave amplitude $Log_e A(f_{nm})$ and the frequency (f_{nm}) in a plane $Z = Z_0$.

Hence we obtain that:

$$Log_e A(f_{nm}, Z_0) = C \times f_{nm} + Log_e A_0 \text{----------(3.80)}$$

Where:

A = wave amplitude

f_{nm} = combined frequencies in x and y directions

C = gradient of the linear relations

A_0 = intercept on the amplitude Log Scale

Note that the amplitude is plotted on a Log Scale axis while frequency is plotted on arithmetic scale axis (i.e. Semi-log) graph paper. Rewrite equation (3.80) bearing in mind that the Log of a number is the power to which we raise the base to get that number.

Hence,

$$A(f, z_0) = \exp(C.f_{nm} + Log_e A_0) \text{----------} (3.81)$$

$$= \exp(C.f_{nm}) \times \exp Log_e A_0 \text{----------} (3.82)$$

But $$\exp(Log_e A_0) = e^{Log_e A_0} = A_0 \text{----------} (3.83)$$

Hence equation (3.81) becomes;

$$A(f, Z_0) = \exp(C.f_{nm}) A_0 \text{----------} (3.84)$$

At a different height Z, we multiply equation (3.84) by equation (3.79)

Thus:

$$A(f_{nm}, Z) = A_0 (C \times f) \times \exp\left[\left(\frac{2\pi}{L}\right) \times (Z - Z_0) \times f_{nm}\right] \text{-----} (3.85)$$

$$= A_0 \exp\left[C \times f_{nm} + \left(\left(\frac{2\pi}{L}\right)(Z - Z_0)\right) \times f_{nm}\right] \text{------} (3.86)$$

$$= A_0 \exp\left[\left[C + \left(\frac{2\pi}{L}\right)(Z - Z_0)\right] \times f_{nm}\right] \text{----------} (3.87)$$

Taking the Log of equation (3.87) to base e, we have:

$$Log_e A(f_{nm}, Z) = Log_e A_0 \exp\left[\left[C + \left(\frac{2\pi}{L}\right)(Z - Z_0)\right] \times f_{nm}\right] \text{------} (3.88)$$

Recall that the Log of a product is equals the sum of the Log of the individual entities of the product.

Hence equation (3.84) becomes:

$$Log_e A(f_{nm}, Z) = Log_e A_0 + \log_e \exp\left[\left[C + \left(\frac{2\pi}{L}\right)(Z - Z_0)\right] \times f_{nm}\right] --- (3.89)$$

Also recall that the Log of any base raised to any power is that number. Hence equation (3.89) becomes:

$$Log_e A(f_{nm}, Z) = Log_e A_0 + \left[C + \left(\frac{2\pi}{L}\right)(Z - Z_0)\right] \times f_{nm} -------- (3.90)$$

Equation (3.90) is another linear equation with gradient being equal to $\left[C + \left(\frac{2\pi}{L}\right)(Z - Z_0)\right]$ and intercept on the Log Scale axis being $Log_e A_0$.

Equation (3.90) shows that once we have linear relationship between Log_e of the Amplitude and frequency f_{nm} at a height Z_0, that we should also have it at another height Z. The slope of equation (3.90) is given by:

$$Slope = C + \left(\frac{2\pi}{L}\right)(Z - Z_0) ---------- (3.91)$$

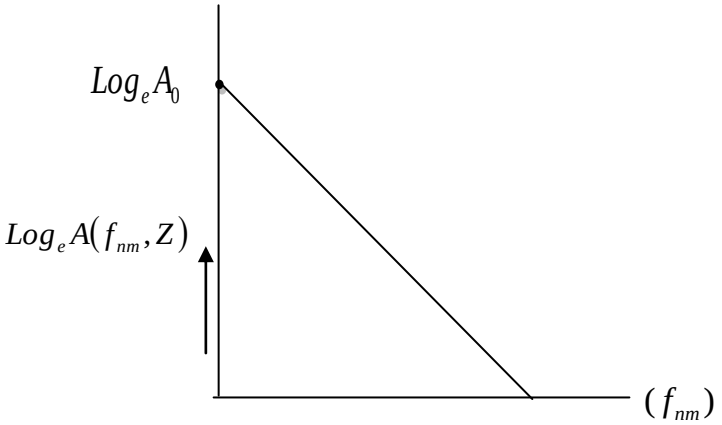

We can solve for $(Z - Z_0)$ in equation (3.91) by making linear curve horizontal, and hence the slope becomes zero.

$$0 = C + \left(\frac{2\pi}{L}\right)(Z - Z_0) \text{ ----------} \quad (3.92)$$

If Z_0 is ground surface which is zero, equation (3.92) becomes:

$$0 = C + \left(\frac{2\pi}{L}\right)Z \text{ ----------} \quad (3.93)$$

$$-C = \left(\frac{2\pi}{L}\right)Z \text{ ----------} \quad (3.94)$$

$$Z = \frac{-CL}{2\pi} \text{ ----------} \quad (3.95)$$ Onuba *et al.*, 2012

Note that C is the gradient of Amplitude Spectrum plot as given in equation (3.77) and L is the wavelength of the anomaly. Equation (3.95) was used to compute the depth to the causative gravity anomaly.

(E) Derivation of First Vertical Derivative Map of the Gravity Data

Using the usual conventions that depth, z, increases downward and that $\Delta z > 0$, the equation for the derivation of the vertical derivative of the first order is given by Blakely (1995) as shown below:

$$\frac{\partial}{\partial z}\phi(x,y,z) = \lim_{\Delta z \to 0} \frac{\phi(x,y,z) - \phi(x,y,z-\Delta z)}{\Delta z} \quad \text{.....(3.96)}$$

Transforming equation (3.96) to the Fourier domain, we have

$$F\left[\frac{\partial \phi}{\partial z}\right] = \lim_{\Delta z \to 0} \frac{F[\phi] - F[\phi]e^{-|k|\Delta z}}{\Delta z} \quad \text{.....(3.97)}$$

$$= \lim_{\Delta z \to 0} \frac{1 - e^{-|k|\Delta z}}{\Delta z} F[\phi] \quad \text{.....(3.98)}$$

$$= |k| F[\phi] \quad \text{.....(3.99)}$$

For the nth – order vertical gradient, the general equation is given by Blakely (1995) as

$$F\left[\frac{\partial^n \phi}{\partial z^n}\right] = |k|^n F[\phi] \quad \text{.....(3.100)}$$

3.2.5 Gravity Data Interpretation

The processed data were analyzed both qualitatively and quantitatively. Qualitative interpretation involved visual inspection of the colour band (spectrum) and contour maps. From these, inferences were drawn on both the geology of the area, lithologic boundaries and the possible types of the gravity anomalies. The quantitative interpretation involved the calculation of depth to anomaly sources across the study area. This was achieved by drawing profiles and carrying out both upward and downward continuations along such profiles.

3.2.6 Evaluation of Hydrocarbon Potentials

To evaluate the hydrocarbon potentials in the Anambra Basin, cross-correlation method (Davies, 2014) was applied. Hence, the downward continued residual gravity data was cross-correlated with well data, geothermal gradient data, and elevation data. From the observed relationships, inferences were made and conclusions subsequently drawn.

3.2.7 Presentation of Results

The results are presented as maps and tables. The maps include geologic, topographic, contour and road maps, as well as figures generated using some specialized filters.

CHAPTER FOUR

RESULTS AND DISCUSSION

4.1 Results

4.1.1 Gravity data

A plot of the field data generated by the Nigeria Geologic Survey Agency in about three (3) years field work in the study area gave rise to the bouguer gravity map (Fig. 4.1) of the Anambra basin

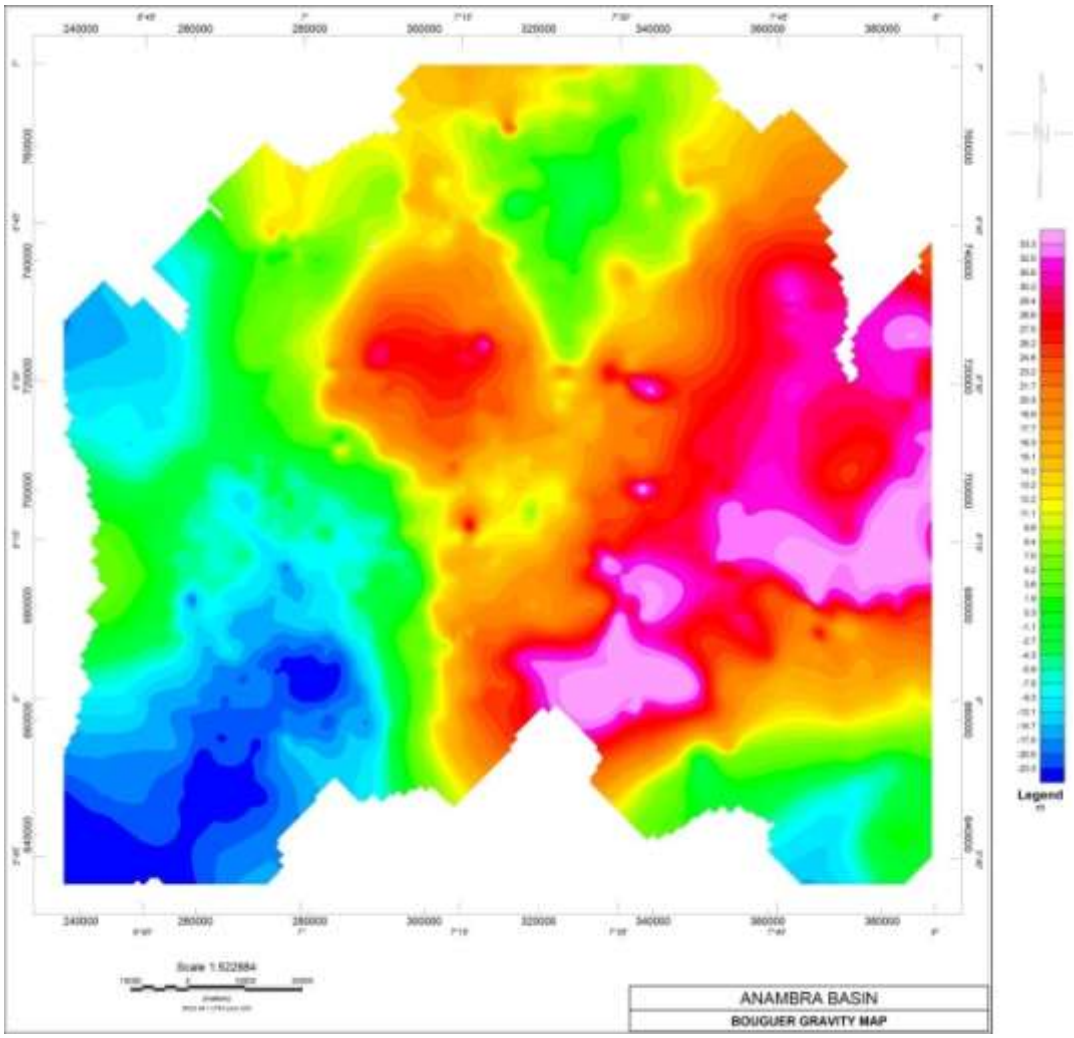

Fig. 4.1: Bouguer Gravity Map of the Anambra Basin

An application of the least square method of Polynomial fitting on the Bouguer gravity map of the study area gave rise to the residual gravity anomaly map (Fig. 4.2), which tried to display density variation locally.

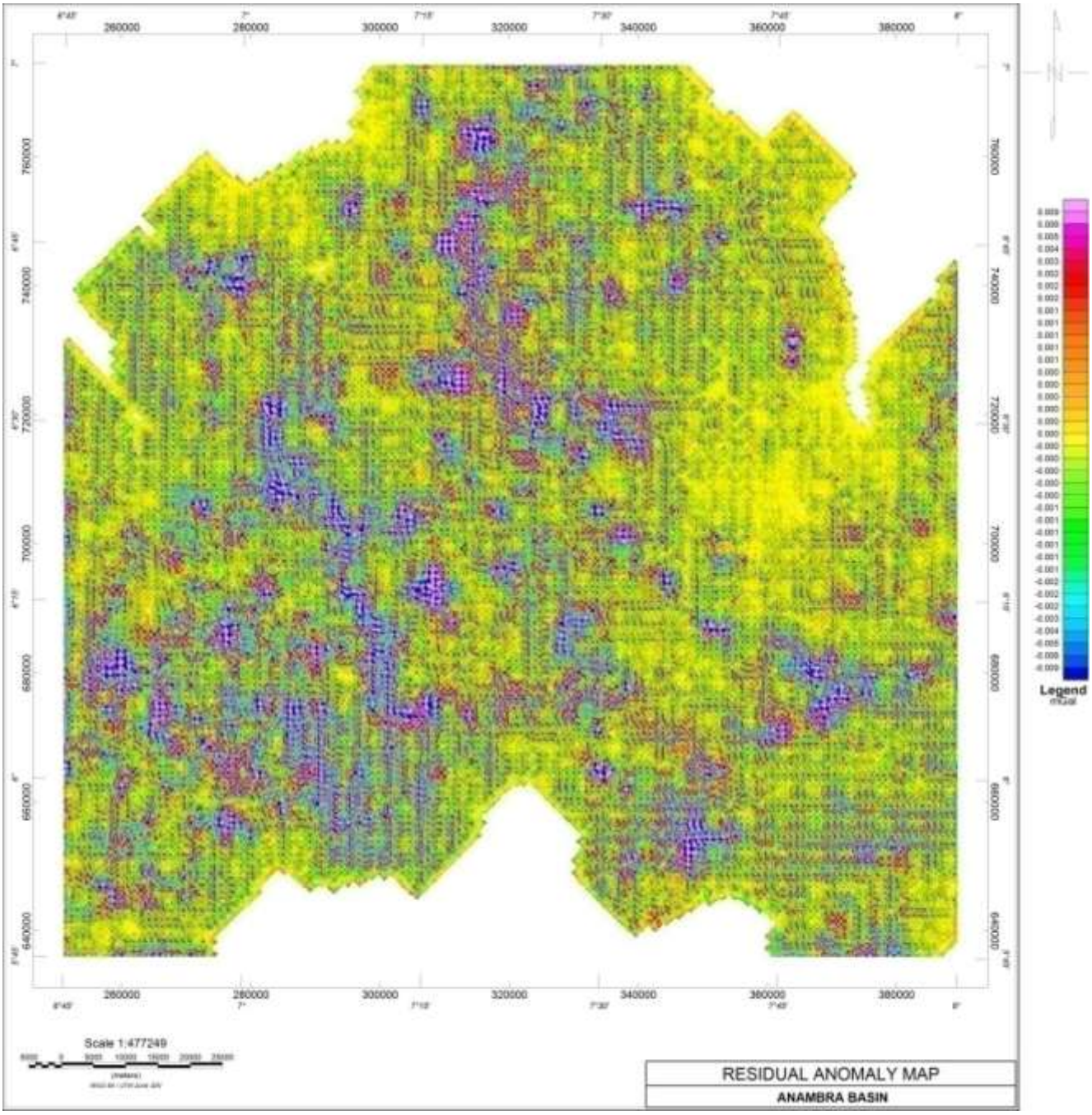

Fig. 4.2: Residual Gravity anomaly map of the Anambra Basin

Upward continuation of the residual gravity anomaly data to a height 200 m (Fig. 4.3) gave a noisy data which could not give any better information than the original map.

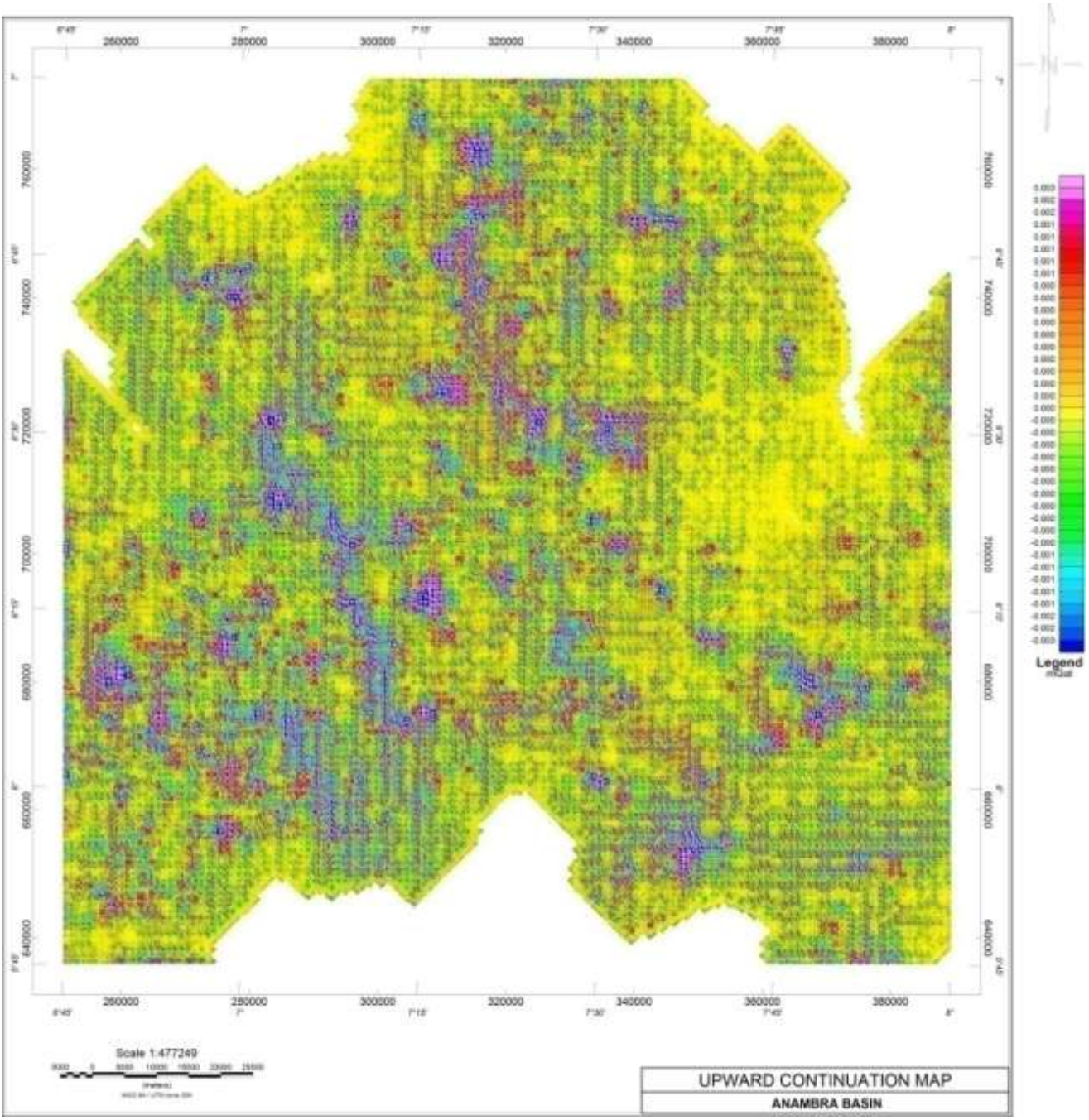

Fig. 4.3: The Residual gravity map upward continued to a height of 200 m.

The downward continuation of the residual anomaly to a depth of 1600 m (Fig. 4.4) gave a very clean view of the gravity anomalies within the study area.

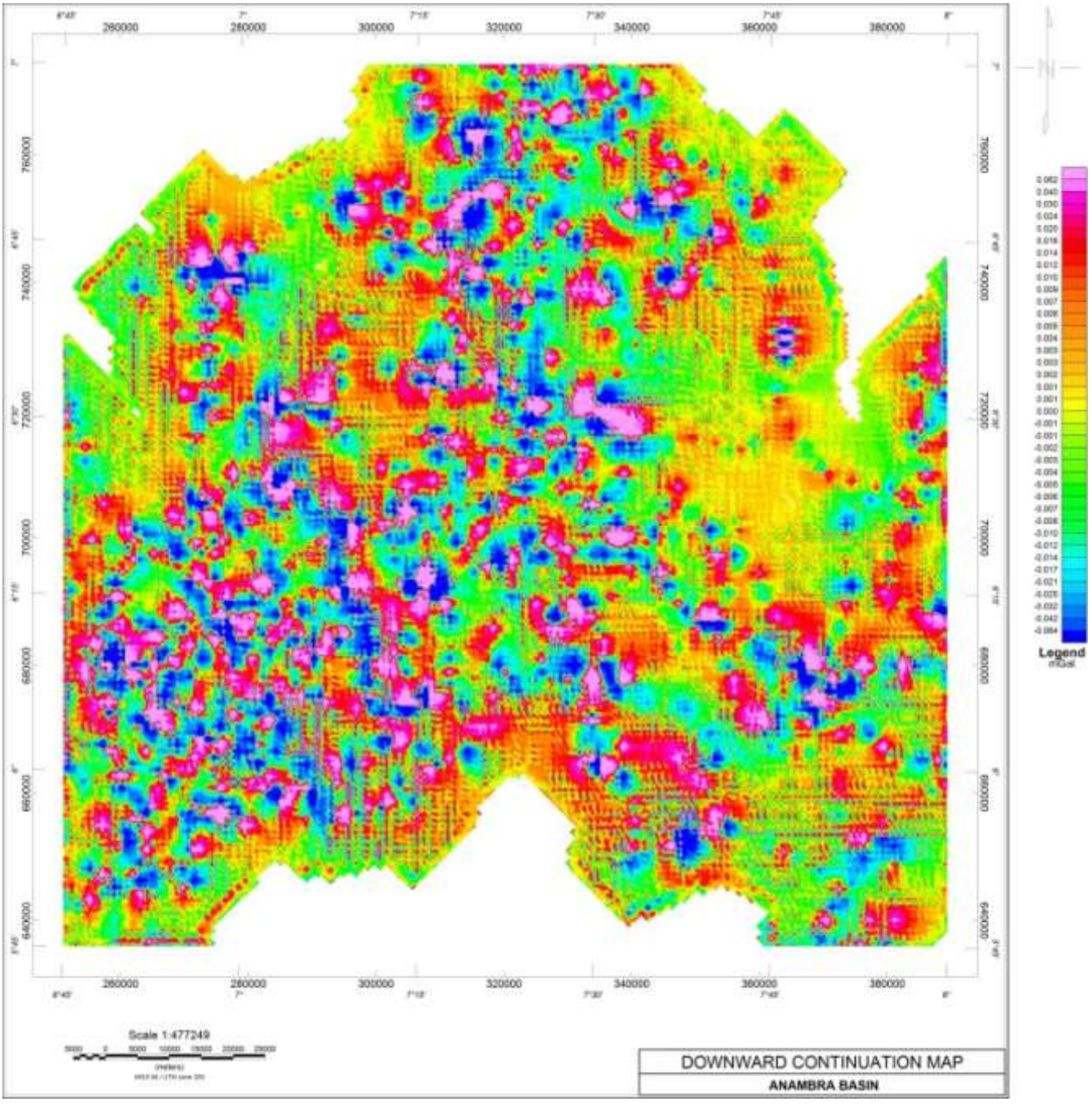

Fig. 4.4: Residual Gravity map downward continued to a depth of 1600 m.

The gravity data set was further subjected to first vertical derivative filter and the result is as shown in figure 4.5.

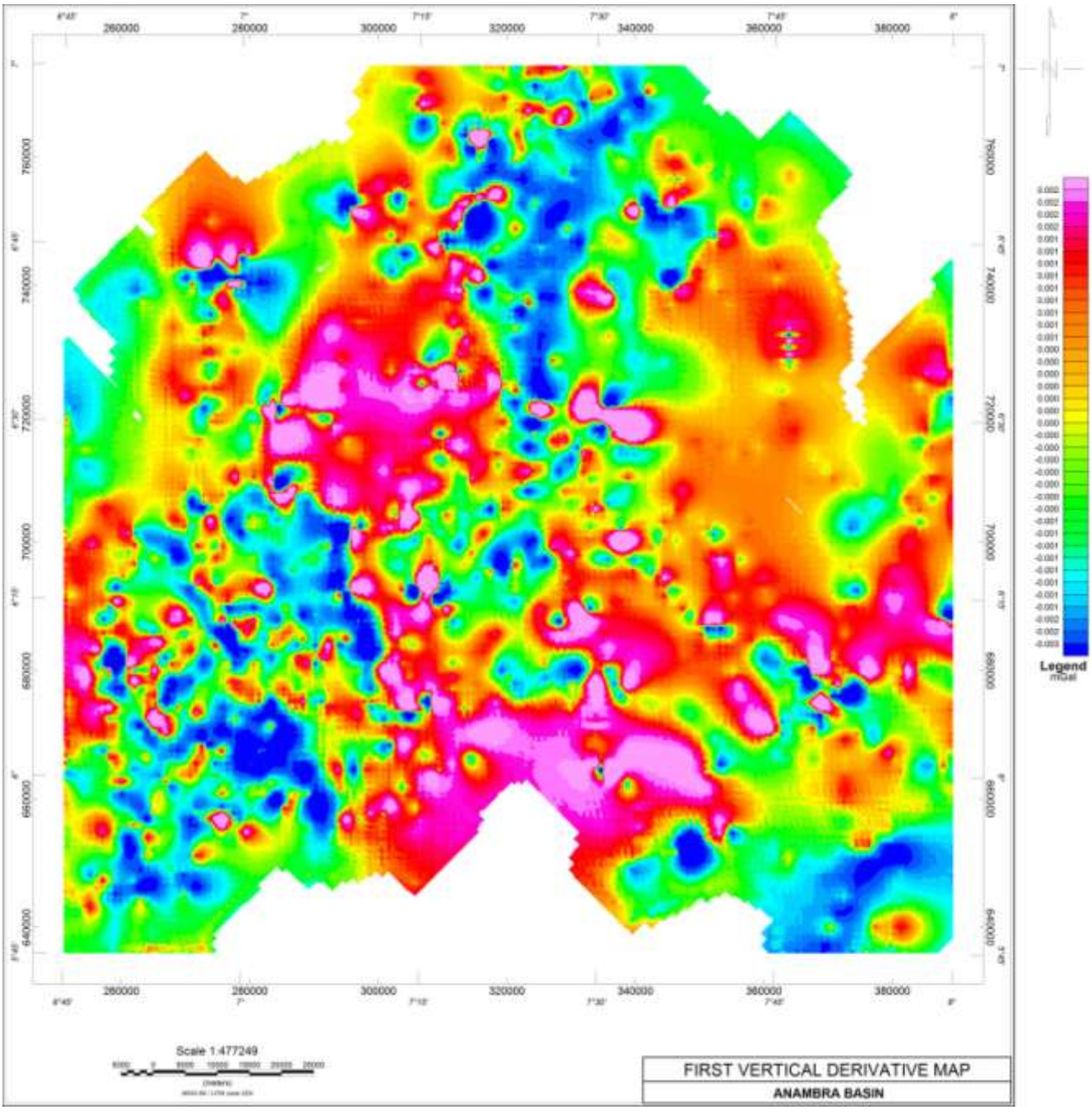

Fig. 4.5: First Vertical Derivative Map

4.1.2 Elevation Data (Shuttle Radar Topographic Mission Map)

A plot of the elevation data as was generated during the field work using altimeter and global positioning system (GPS) gave rise to the shuttle radar topographic mission (SRTM) map (Fig. 4.6) of the study area.

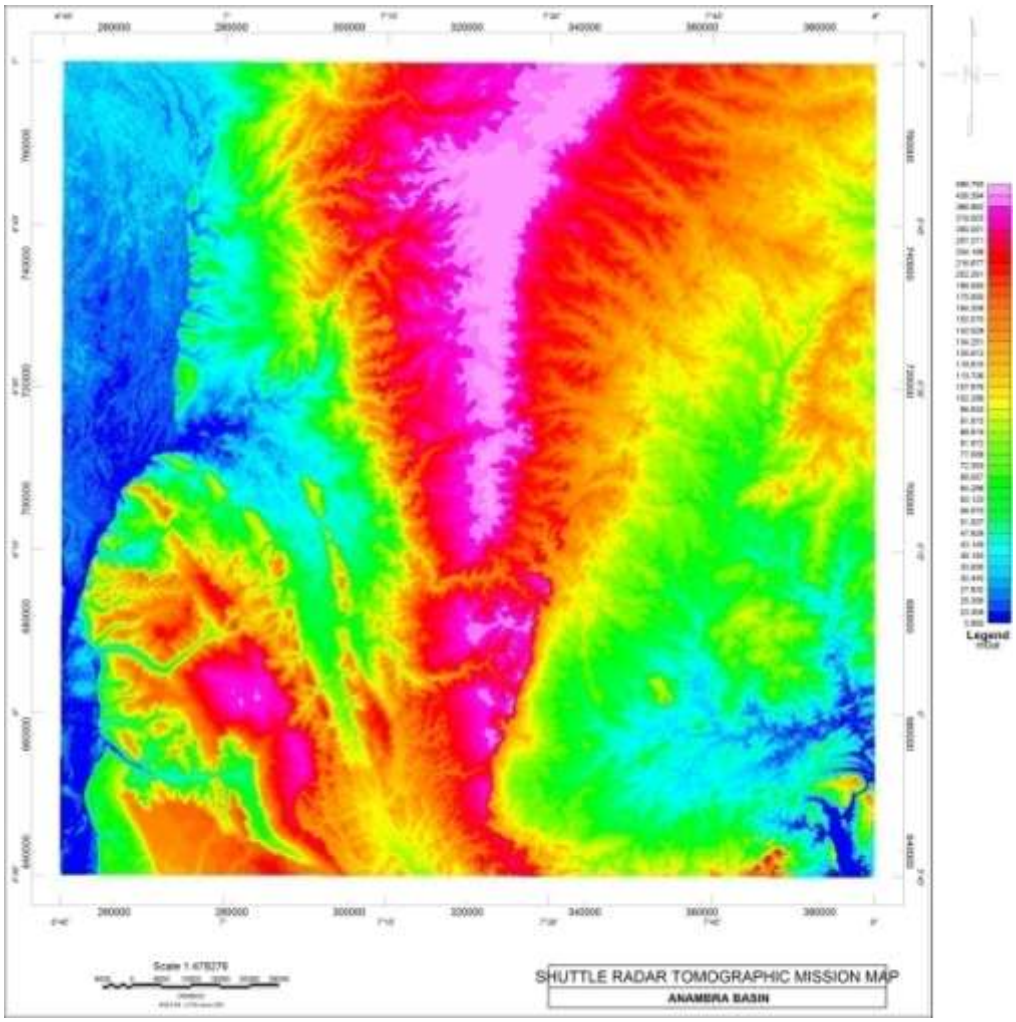

Fig. 4.6: Shuttle Radar Topographic Mission Map.

4.1.3 Well Data

A display of some exploration wells and their locations within the Anambra basin is as given in figure 4.7.

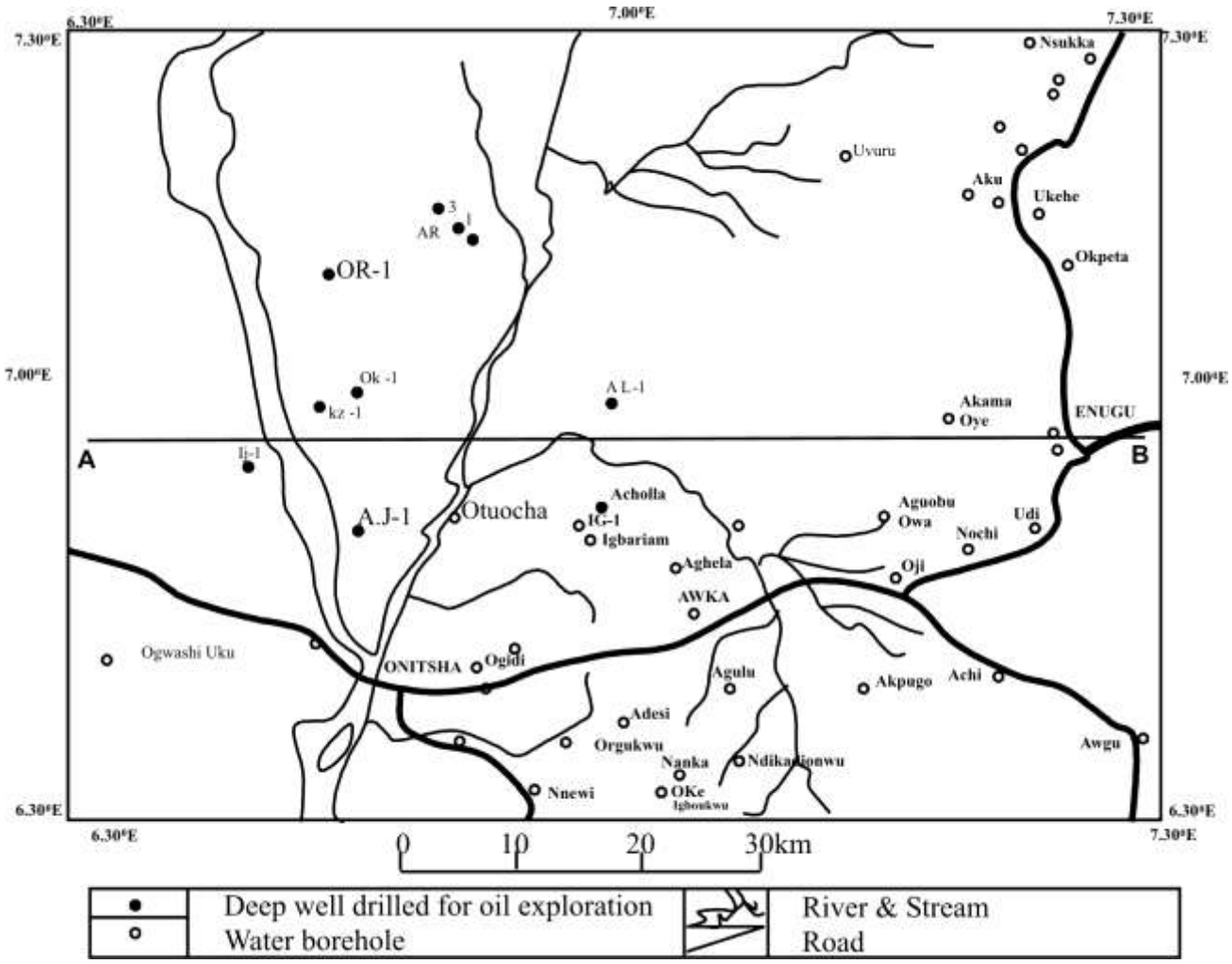

Fig. 4.7: Location of some wells drilled in the Anambra Basin

(After Avbovbo and Ayoola, 1981; Onuoha, 2005)

4.1.4 Geothermal Gradient Data

Figure 4.8 is a display of the geothermal gradient data from some drilled wells in the study area as given as measured by Onuoha and Ekine (1999).

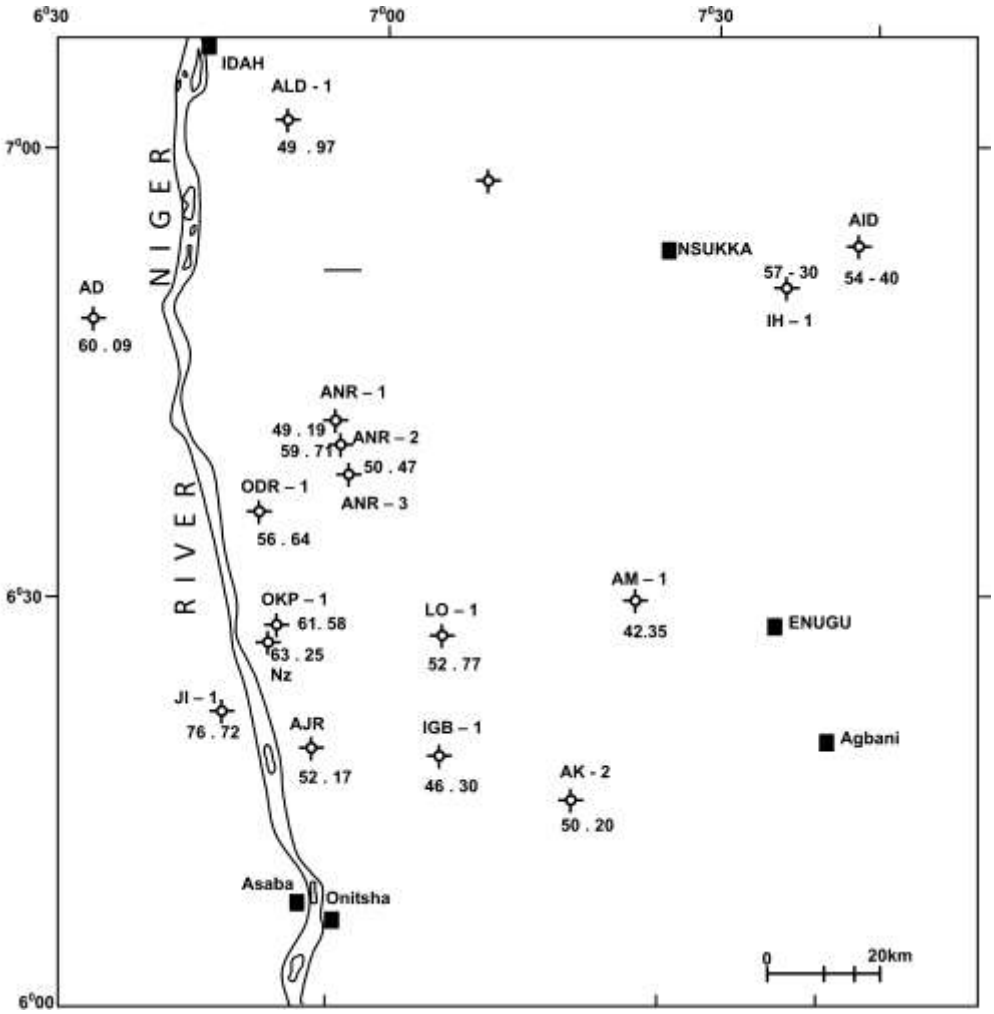

Fig. 4.8: Geothermal gradient variations across the Anambra Basin (in ^{0}C/Km)

(After Onuoha and Ekine, 1999).

4.2. Discussion

4.2.1 Visual Analysis of Gravity Maps.

The Bouguer gravity map of the study area (see fig. 4.1) indicates highest density values (≥ 30 mGal i.e. the area represented by pink colour) along the northeastern and southern part of the study area. The alignment occurs along the strike of the present Benue Trough and coincides with the igneous rocks of the Abakaliki - Ishiagu - Okigwe areas. The intermediate density values (11 – 29 mGal, the areas with red to yellow colours) represent the lower – middle Cretaceous sedimentary rocks which host the igneous rocks and also occupy the greater part of the study area. The least density values (< 11 mgal) as seen on the western and southeastern parts of Figure 4.1, represent sedimentary deposits of the uppermost Cretaceous – Tertiary ages and Alluvium.

The residual anomaly map (see fig. 4.2) shows that the highest density anomalies (areas that are pink colour on the map) are scattered all over the study area, in the form of intercalations, alongside the very low density anomalies (blue colours on the map), while the intermediate density anomalies (represented by light green to yellow colours) covered the entire map area. This suggests the occurrence of the Cretaceous sedimentary deposits in the entire area within the Cretaceous period.

Upward continuation of the residual gravity anomaly data to a height 200 m (see Fig. 4.3) gave a noisy data which could not give any better information than the original map. It means that we are moving away from the geologic bodies of interest and could not enhance the existing data, we reversed to downward continuation.

The downward continuation of the residual anomaly to a depth of 1600 m (see Fig. 4.4) gave a very clean view of the study area. The contact between geologic formations with varying density characteristics are distinct enough that they can be clearly mapped. This has further shown that the very high density anomalies are scattered randomly within the study

area. The highest density anomalies often lie interwoven with the very low density rocks. Considering the depth at which the features became very sharp (Fig. 4.4), it could be said that the causative body to the density anomalies are deep seated. Despite the fact that the downward continuation map was sharp enough to give the mappable contact between one point and another, it could not establish, in clear sense, the orientation of some of the anomalies. Figure 4.4 also support the original occupation of the entire area by the sediments of the Cretaceous age, with the later intrusion / extrusion of the highest density rocks.

The first vertical derivative map (see Fig. 4.5) show that the highest density anomalous bodies are oriented in the northwest – southeast directions, with very few in the Northeast- southwest direction, while the very low density rocks appear to be oriented almost north – south in the northern part of the study area and northwest – southeast in the southwestern and southeastern parts of the study area.

The shuttle radar topographic mission map (SRTM) (see Fig. 4.6) indicates that the zone of highest elevation (i.e. the area with pink colour on the map) runs almost through the centre of the study area, in the north – south direction. This zone of highest relief coincides with the cuesta described by Nwajide (2006; 2013). The zone of least topography (i.e. the areas with blue colour on the map) occurring majorly in the western part of the map (Fig. 4.6) but runs in the north – south direction, is area around the River Niger and it flows southwards into the Atlantic Ocean somewhere outside the study area. The drainage pattern in the area is dendritic. This is seen as some wave – like structures in figure 4.6. It shows flow pattern from the peak of the cuesta towards the east and west directions. From the SRTM map, the study area is generally drained to the south by the River Niger, with the help of its tributaries. From the ongoing discussion, origin of the major tributaries in the study area could be traced to the base of the Enugu cuesta.

4.2. 2 Structural Interpretation of Gravity Contour Map

Most of the contours are clustered and thereby suggests close source for the gravity values. Conversely, the downward continuation filter does not agree with this. The steep gravity gradient observed in the north-western corner of figure 4.9 (almost vertical) is interpreted as fault controlled contact between two lithologies. The contour value of 30 mgal forms a closure round the zones of highest density peaks in the study area. The gravity peaks occurring in closures are interpreted as areas associated with igneous rocks. The intermediate values of between 16 and 29 mGal are areas associated with the Cretaceous sedimentary rocks. In the southwestern part of the map, the contour lines are broken and occur in discrete patterns with very low gravity values. They are the alluvial deposits of the Tertiary - Recent age occurring at the alluvial planes around the River Niger.

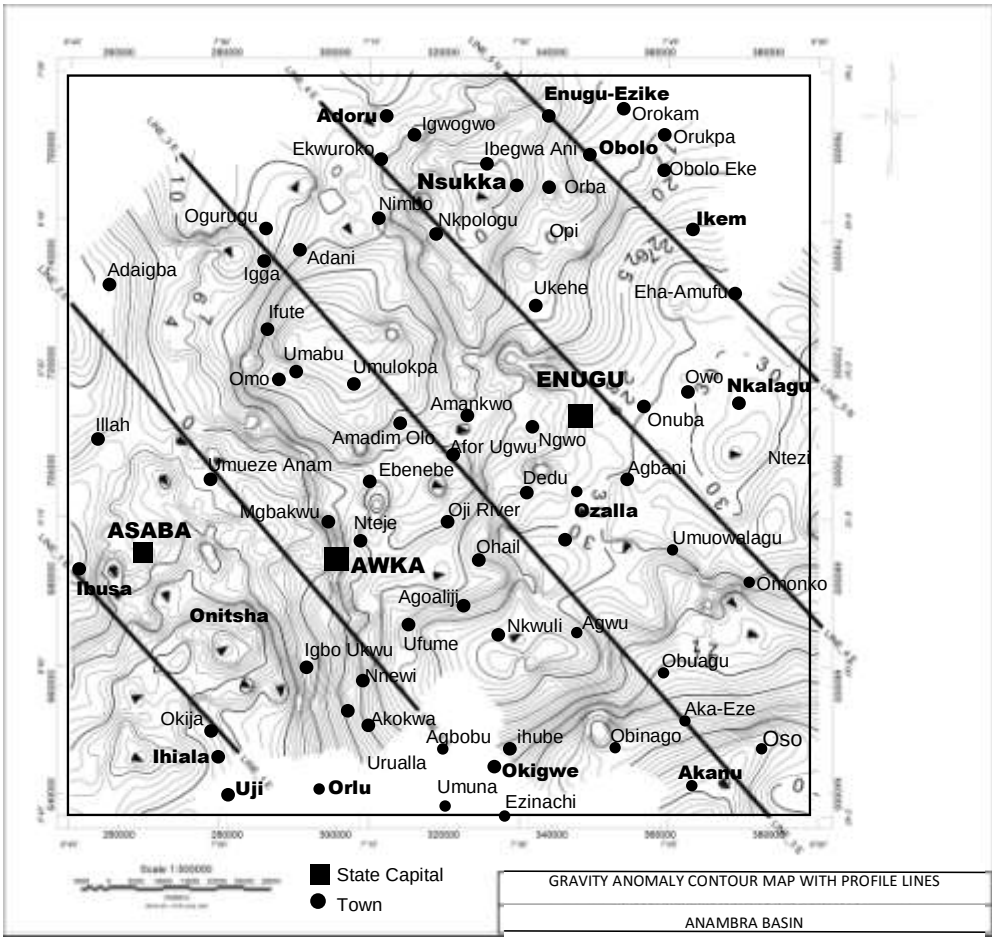

Fig. 4.9: Residual Gravity Contour map of the study area.

The contours trend northeast – southwest in the northeastern part of the map, almost east – west in the central to southern part, and north – south in the northern and southern part of the map. This suggests that the geologic materials which gave rise to the anomalies lay discordantly with each other and are not of the same geologic age.

4.2.3 Gravity Modelling of Profile Lines

Five profiles were selected within the study area. All the profiles were drawn in the northwest – southeast direction, parallel to each other (Fig. 4.9).

The cross section of profile line 1 (Fig. 4.10) shows a maximum sediment thickness of about 1 km, which is shallow when compared with other profiles below and suggests that the profile runs outside the basin in the southern part. The thin nature of the sediments in this area suggests that sediment deposition must have been in a short period of time, and so has not given any time for further subsidence due to load and possibly further sediment reworking. Hence, sediment deposition across profile 1 could be said to be of Tertiary age alone.

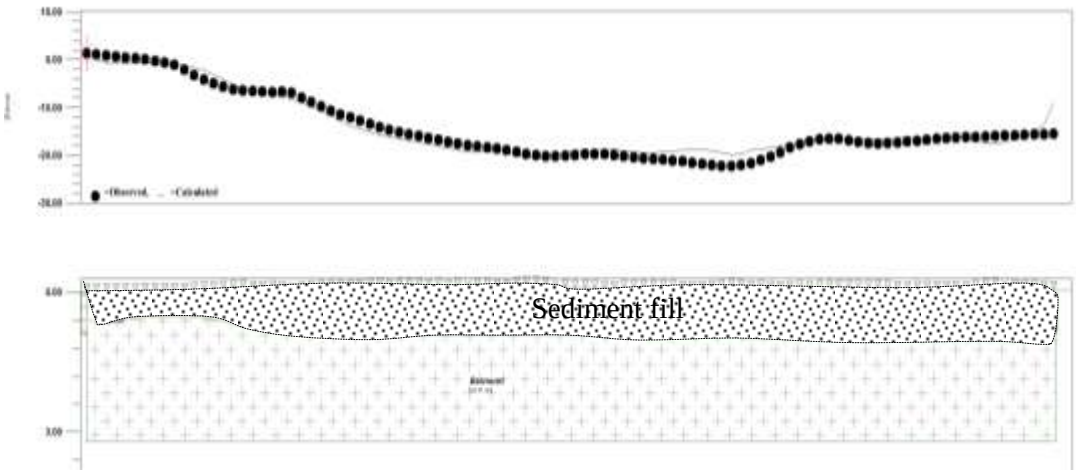

Fig. 4.10: Cross Section of Profile Line 1

The sediment thickness across the profile line 2 is quite irregular (Fig. 4.11), thus the basin floor here is irregular. The sediment thickness ranges from about 2.4 km on the northwestern end of the line to about 7 km on the southeastern end. This cross section is believed to pass through sediments of both tertiary and Cretaceous age respectively. The boundary of the Anambra Basin in the southern part could be inferred around this profile. However, an inclusion of geologic model into the basin would assist in drawing a conclusion on this matter.

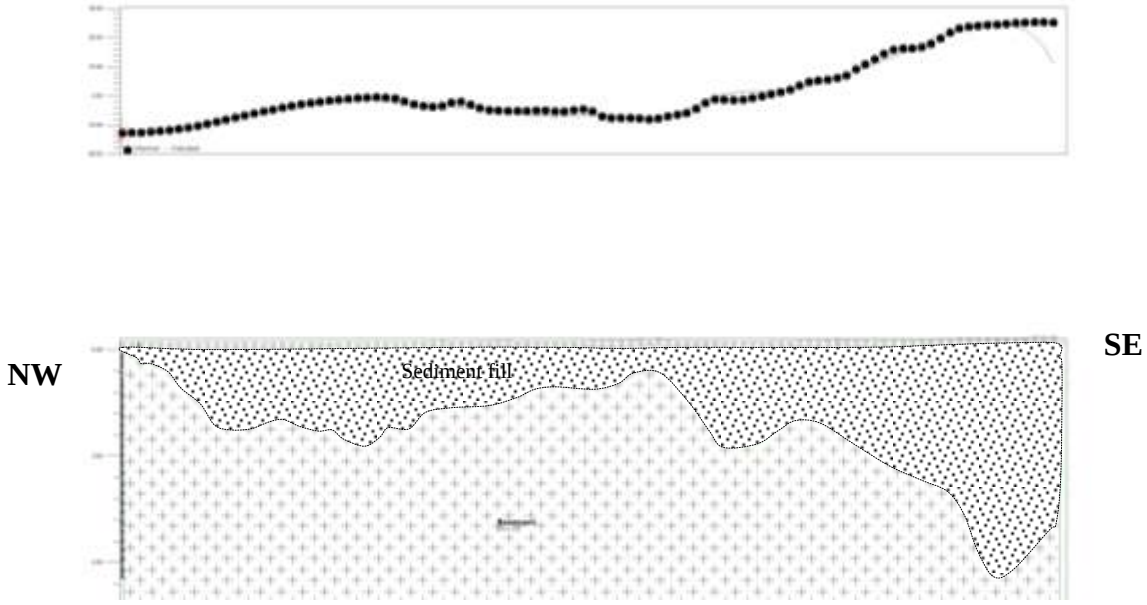

Fig. 4.11: Cross Section of Profile Line 2

The cross section drawn from profile line 3 shows a separation of four major basins (Fig. 4.12) within the area. Basin “A” is the extension of the Benue Trough across the study area, while Basin “B” is the Anambra Basin. Basins ‘C’ and ‘D’ are the Afikpo Basin and the Niger Delta respectively. Sediment thickness in this area is about 7 km.

The cross section of profile line 4 (Fig. 4.13) shows a maximum sediment thickness of about 7 km. It shows two models of a rectangular prism by the left and a partial sphere model at the

right hand side. It is a progression from the shallower part of a basin (possibly the basin margin) into a basin floor.

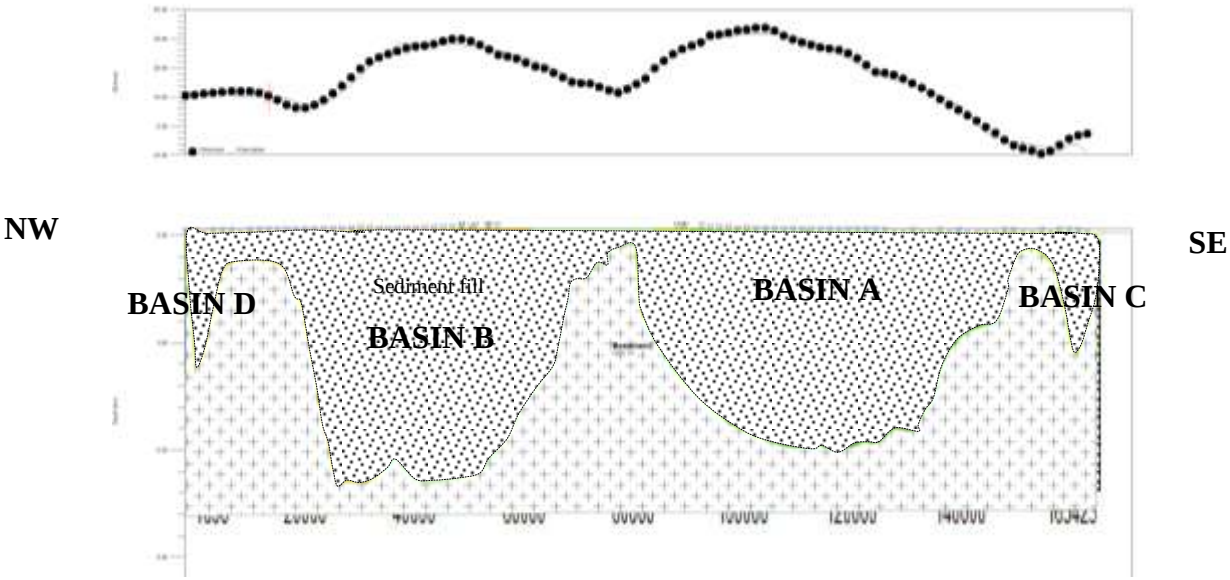

Fig. 4.12: Cross Section of Profile Line 3

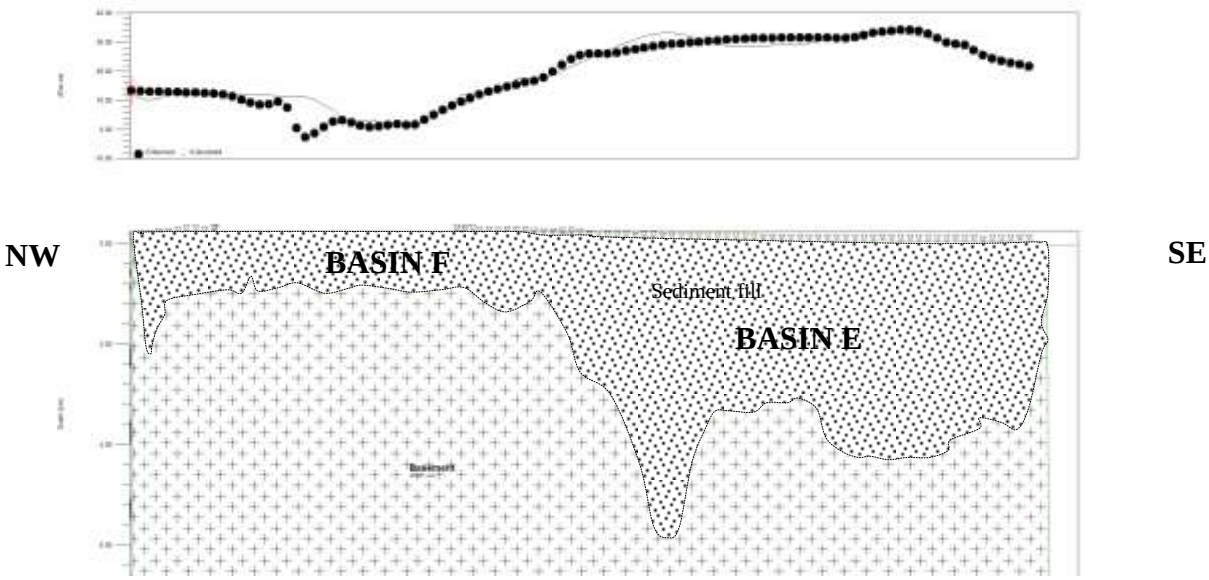

Fig. 4.13: Cross Section of Profile Line 4

Figure 4.14 is a cross section for profile line 5 in the study area. It as well displays irregularity in the floor architecture and variation in sediment thickness, with sediment

thickness of about 1.8 km - 2.5 km. The uplift between the arms G and H suggests again a separation between the present Anambra Basin (designated as H) and the Benue Trough (designated as G).

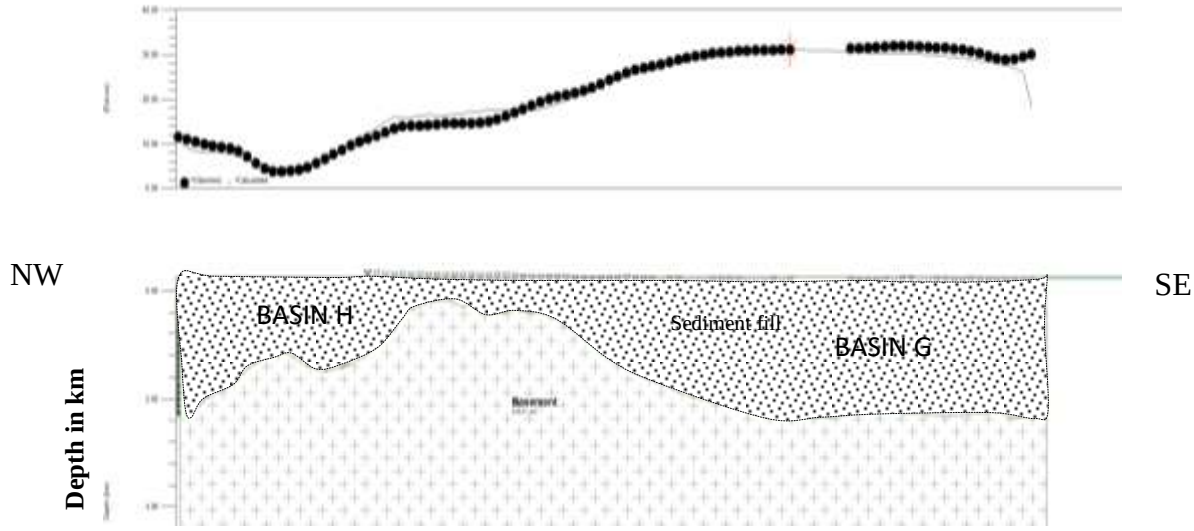

Fig. 4.14: Cross Section of Profile Line 5

4.2.4 Geologic Modelling of the Profile Lines

A further step was taken geologically in interpreting the gravity data of the study area. The sediment infill as seen in the cross sections 1 – 5 (i.e. Fig. 4.10 – 4.14) were modelled for their ideal geologic formations using the geologic map of the study area (Fig. 4.15) and having in mind the density variation across the basin. The lithological legends as used on the models are shown in table 2.

The geologic modelling of cross section one (Fig. 4.15) shows that it passed through a meander river belt (Mws), Ogwashi – Asaba Formation (Lsr) and Bende – Ameki Formation. Considering the works of Benkhelil (1988) and Nwajide (2013), it could be established that profile line one (1) did not pass through the Anambra Basin. If it did, it could have cut through the formations which the two authors have recognized to be deposited in the basin.

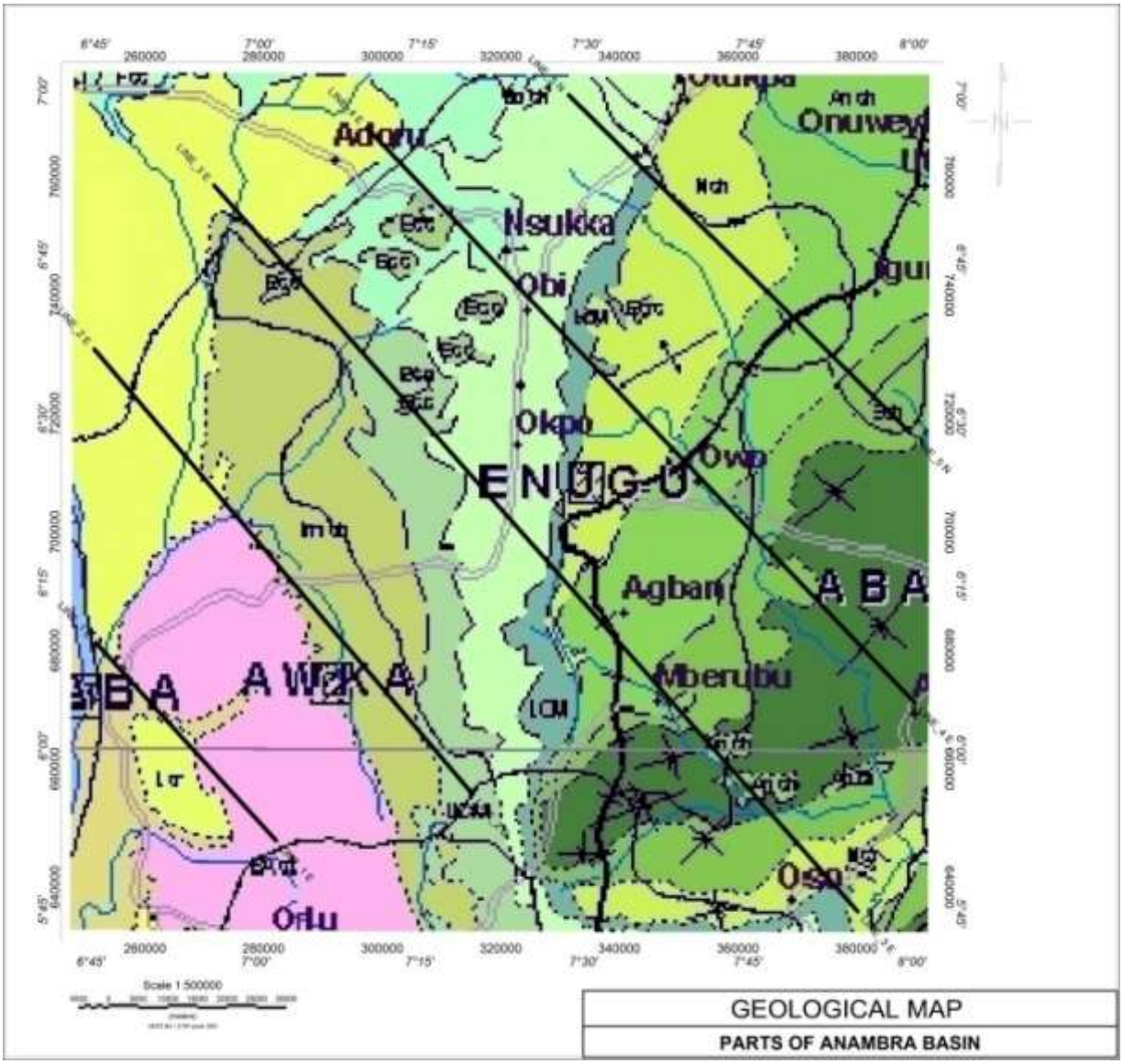

Fig. 4.15: Geological map of the study area

(**Source:** Nigeria Geologic Survey Agency, 2006)

Table 4.1: Lithological Codes and their descriptions (Source: Nigeria Geological Survey Agency).

S/N	Code	Lithostratigraphic Unit	Lithological Discription
1	Al	Sediment	Alluvium
2	Mws	Meander belt, back swamps, fresh water	Sand, gravel and clay
3	Lsr	Ogwashi-Asaba Formation	Lignite, claystone and shale
4	Bash	Bende-Ameki Group	
5	Imsh	Imo Formation	Clay and shale with limestone intercalation
6	Ncsh	Nsukka Formation	Coal, shale, sandstone and limestone
7	Ajst	Ajali Formation	False bedded sandstone
8	Mcst	Mamu Formation	Coal, sandstone and shale
9	Nsh	Nkporo Formation	
10	Ansh	Awgu Formation	
11	Esh	Eze Aku Group	Blackshale, siltstone and sandstone
12	Arish	Asu river group	Shale and limestone with sandstone intercalation

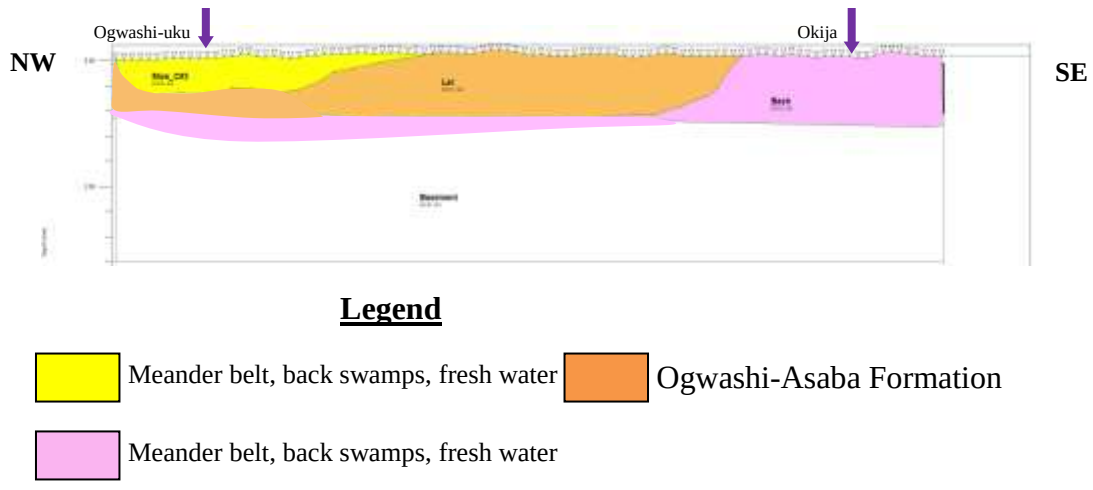

Fig. 4.16: Geologic model for Profile Line 1

The geologic model for profile line 2 (Fig. 4.17) shows that it cuts through alluvial deposits (sediments), Bende – Ameki Group, Imo Group and Nsukka Formation. Comparing the

profile again with the work of Nwajide (2013), it can be said that the profile started somewhere outside the Anambra Basin and then entered into the Basin. From this profile, the boundary of the Anambra Basin in the southern part is inferred around Umueze – Nteje - Agoaliji.

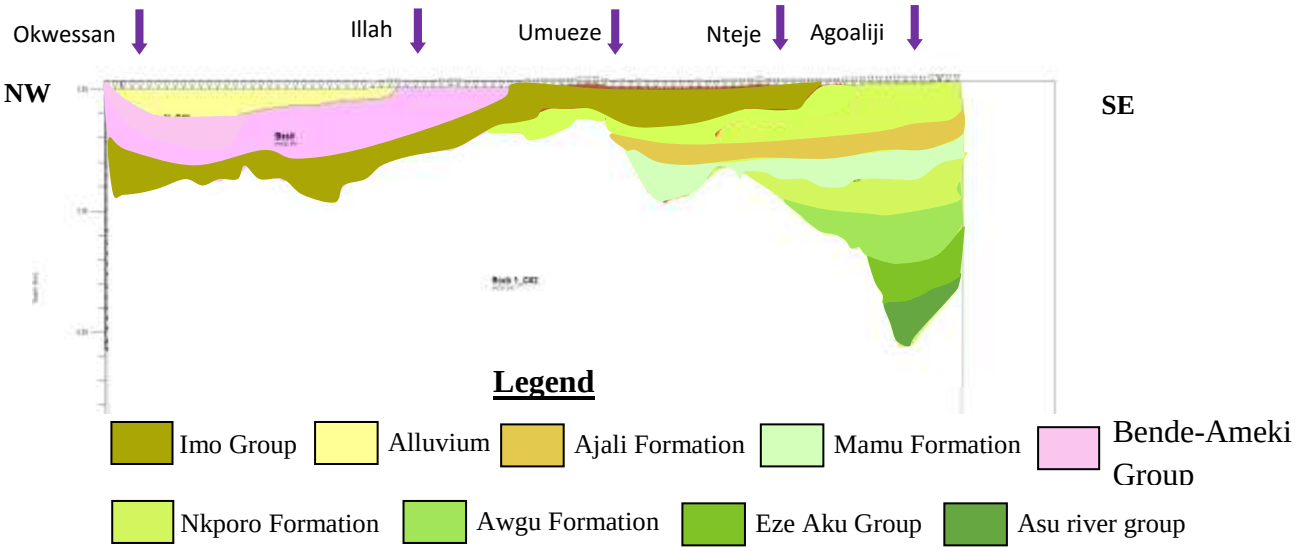

Fig. 4.17: Geologic model for Profile Line 2

The geologic model of the profile line 3 (Fig. 4.18) shows the presence of four sub-basins, with the basin "B" (i.e. the Anambra Basin) filled with sediments of Nkporo Group (Nsh), Mamu Formation (Mcst) and Ajali Formation (Ajst) with the Imo Formation capping it up. This is in line with the work of Nwajide (2013) which said that the Anambra basin is filled with the sediments of the Nkporo Group and the Coal Measures. The basin "A" contains the sediments of Nkporo Group (Nsh), Awgu Formation (Ansh), Ezeaku Group (ESh) and Asu River Group (Arish) respectively, while basin "C' contains sediments of Nkporo Group and Mamu Formation only. Based on the lithologic content of the sub – basins in this model and the position of the profile line 3 in figure 4.12, the basin B is ANAMBRA

BASIN, while basin A is a continuation of the Benue Trough, Basin C is the AFIKPO BASIN and Basin D is part of the Niger Delta.

Nwajide (2013) considered the Afikpo basin as part of the Anambra Basin considering the fact that they are both result of the same Santonian thermo-tectonic event; there is really no physical separation or barrier between the two areas and there does not appear to be any tectonic definition of that area into a depression separate from the area to the northwest. Conversely, Figure 4.18 shows that there is a distinct boundary between the two basins. The presence of the Benue in between them is enough boundaries. Again, the uplift of the basement in between Anambra Basin and the Benue Trough, and in between the Benue Trough and the Afikpo Basin is evidence of independence of each basin from another, although these boundaries did not extend to the surface. The non extension of the basin boundaries to the surface suggests that only geophysical approach (such as in this work) or well drilling can be used to establish their existence. The non continuation of the basement boundary to the surface could be as a result of further subsidence due to post depositional activities in the basin, which has pushed the boundary vertically downwards. The inferred basin boundaries are shown in red (Figure 4.18).

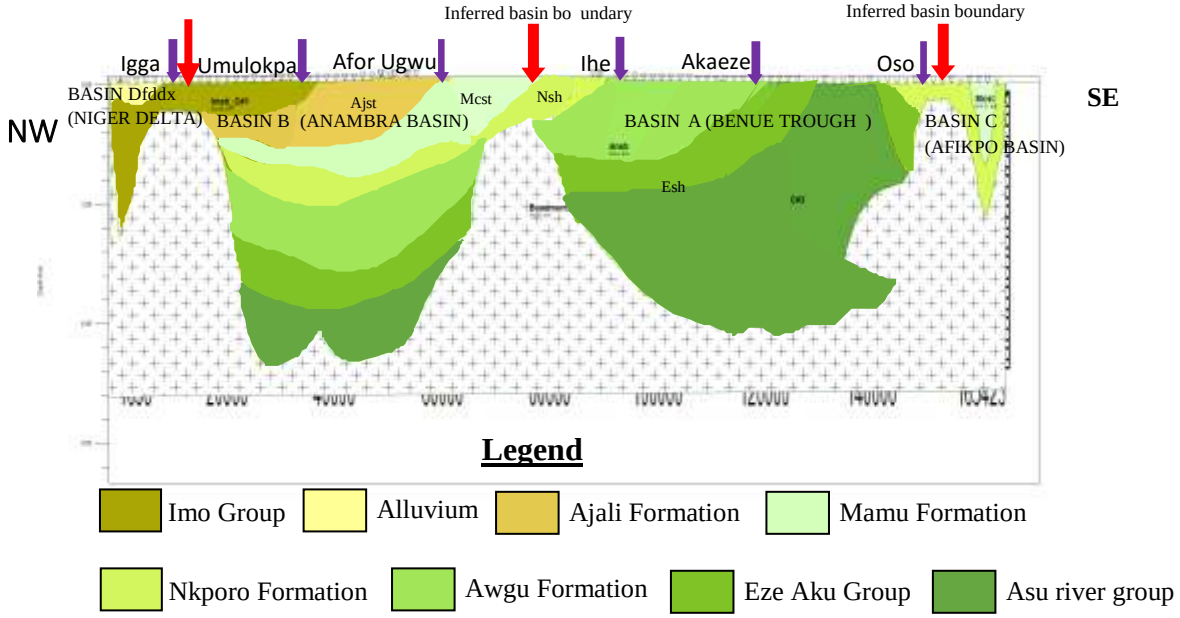

Fig. 4.18: Geologic Model for profile line 3.

The geologic model for the profile Line 4 (Fig. 4.19) shows again an intersection of two basins, with one of the basins shallower than the other. The shallower basin (Basin F) contains sediments of the Alluvial deposits (Al), Nsukka Formation (Ncsh), Ajali Formation (Ajst), Mamu Formation (Mcst) and Nkporo Formation. The deeper basin, which lies towards the right (Basin E) contains the Awgu Formation (Ansh), Ezeaku group (Esh) and the Asu River Group (Arish) sediments. Based on their lithological content, basin F is believed to be part of the Anambra Basin, while basin E is part of the Benue Trough. Hence, the Anambra Basin continues in the northern direction up to areas around Ekwuruko – Ukehe.

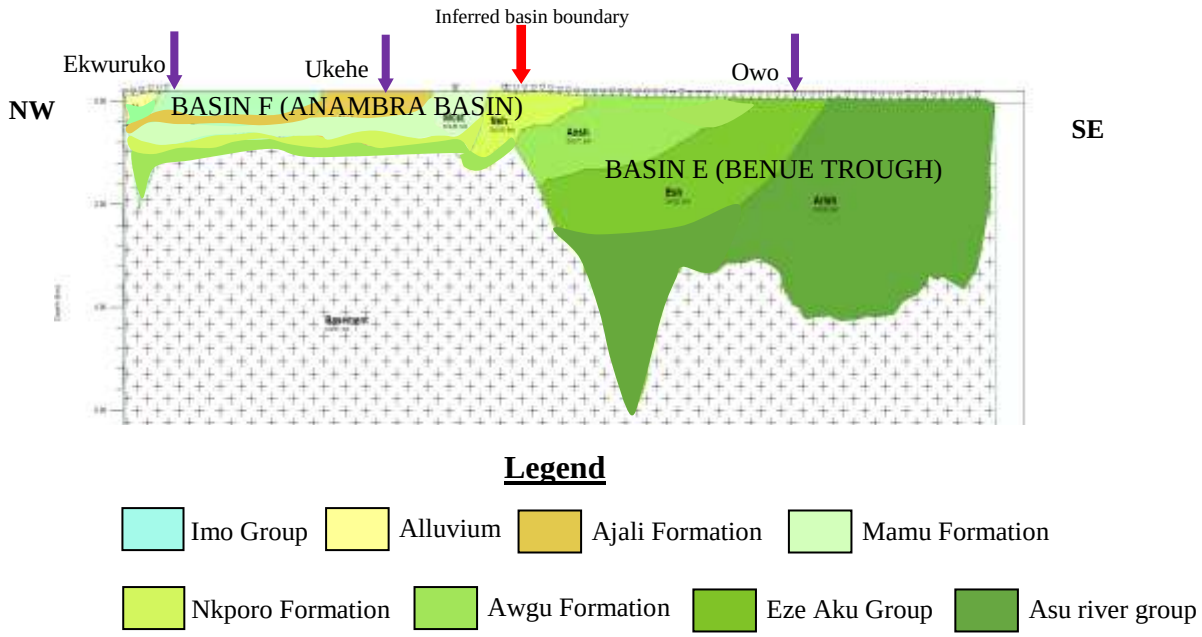

Fig. 4.19: Geologic Model for profile line 4.

The geologic model for profile line 5 (Fig. 4.20) has similarity with model 4 (Fig. 4.19) in that it also shows the interaction between the Anambra Basin with the Benue Trough in the Northeastern part of the study area. While the Benue Trough in this area contains the sediments of Ezeaku Group and Awgu Formation only, the Anambra Basin contains Nkporo Formation, Mamu Formation and Ajali Formation. It can however be observed that the sediments of the Nkporo group appears to have over flown into the top of the Awgu Formation, possibly due to erosion and subsidence. Hence, the Anambra Basin is inferred to have continued in the northeastern part up to areas around Obolo-Afor and Obolo Eke.

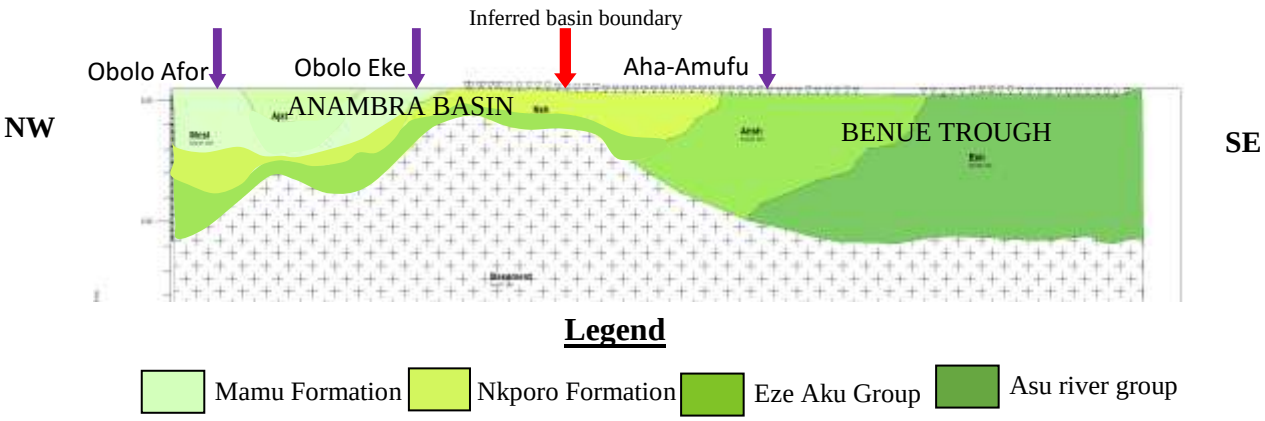

Fig. 4.20: Geologic Model for profile line 5

4.2.5 Correlation of Drilled wells with Gravity Data

A correlation of some of the deep wells drilled for hydrocarbon search in the basin with the gravity data (Fig. 4.21) has revealed that there is a relationship between the gravity contrast and the availability of hydrocarbon in the wells. Thus, wells that are drilled into points where we have very high gravity values (≥ 30 mgal i.e. areas with pink colour in figure 4.21) and those drilled into areas of gravity low (< 11 mgal i.e. areas with blue colour) were dry. Conversely, wells drilled in areas of intermediate gravity values (11 – 29 mgal, this includes the areas with light green, yellow and red colours) had hydrocarbons in them. This suggests that the major hydrocarbon reservoirs in the Anambra Basin occur within the middle - late Cretaceous sediments underlying the area. The works of Avbovbo and Ayoola (1981) and Whiteman (1982) support this.

Alade 1 (AL-1) and Anambra River 3 (AR - 3) wells are among the wells drilled into very high gravity value areas (Fig. 4.21) shaded pink colours on the map, and both are dry wells (Table 1). Ajire 1 (AJ - 1) and Oda River (OR - 1) wells were drilled into very low gravity areas shaded blue on the map, and wells were also dry. Anambra River 1 (AR - 1),

Anambra River 2 (AR - 2), Igbariam 1 (IG - 1), Iji 1 (JI - 1) and Okpo 1 (OK - 1) were drilled into an intermediate gravity zone with colour ranging from light green - yellow - red, of which all should have hydrocarbon in them. However, while AR – 1, AR – 2 and IG – 1 had hydrocarbon in them, it was observed that IJ – 1 and OK – 1 do not have. To explain the aforementioned anomaly, borehole data from some of the oil wells under discussion (Fig. 4.22) given by Nwajide (2013) was further evaluated.

From figure 26, it can be observed that sediment thickness in the basin and the depth of burial of different geologic formations gets higher as you move from the Northern part (i.e. from Aiddo – 1 well) towards the South (i.e. Iji – 1 well), hence, the beds dip in the southern direction. Consequently, the Turonian and Albian sediments were seen at shallower depths in the northern parts (see Aiddo-1 in Fig. 4.22), while they disappeared as you move towards the south/southwest (see Ijii-1 in Fig. 4.22), suggesting that they occur somewhere deeper in the crust.

Iji-1 is among the wells which failed into the intermediate zone but was dry. From figure 4.22, it can be seen at the depth of 1600 m that this well cuts through Paleocene age rocks (Ebenebe Sandstone member of the Imo Group) which neither were texturally mature (Agagu and Ekweozor, 1982; Obaje *et al.*, 1999) to generate its own hydrocarbon nor

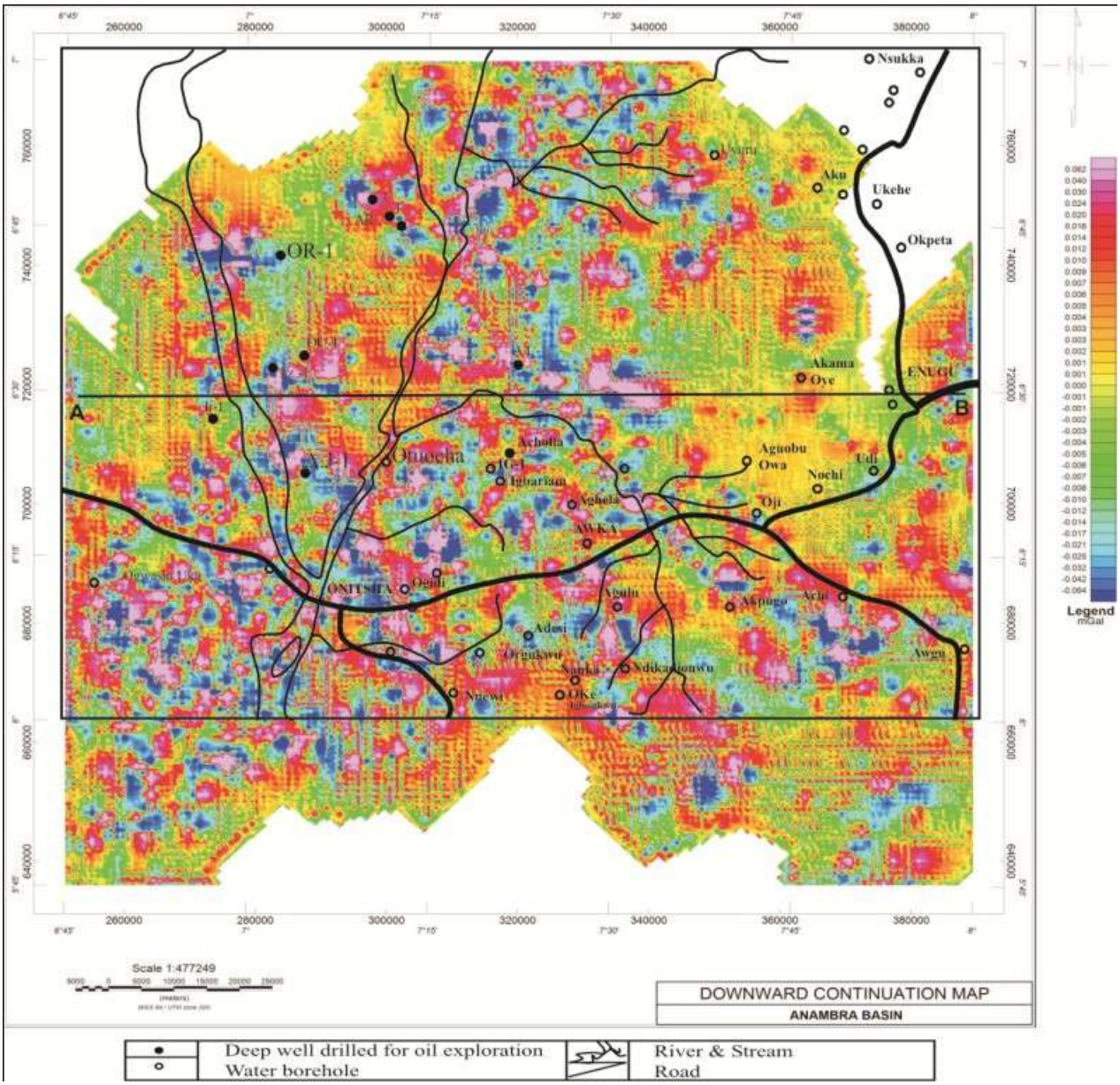

Fig. 4.21: Correlation of the map of drilled wells in the study area with the Gravity data.

stratigraphically positioned (Obaje *et al.,* 1999) to serve as reservoir in this basin. Iji-1 well showed little higher density in Fig. 4.21 (i.e. yellow colour surrounded by green). This is because it pierced through Ebenebe sandstone member of Imo Formation. The total drilling depth (TDD) is 2950 m (Fig. 4.22). The dryness of this well could be attributed to the fact

that it was not drilled to penetrate at least the Nkporo Group in the basin. Recall that it occurs in area of higher dip, which implies that the Nkporo Group, Awgu Formation, Ezeaku and Asu River Groups are below the total drilled depth. Nwajide (2005) argued that although the shales of the Nkporo Group is geo-thermally immature to serve as a source rock but they can attain maturity where deeply buried. It is therefore recommended that this well be drilled further as it could still yield hydrocarbon. Since it is down dip, the depth to reservoir at this point would be deeper. An enhanced understanding is got when looking at wells Igbariam-1, Amansiodo-1 and Ihandiagu-1, which all had hydrocarbon in them (Fig. 4.22). They all passed through the Nkporo Group. While the Igbariam-1 and Amansiodo-1 stopped at the Awgu Formation where the Agbani Sandstone member serves as the major reservoir, the Ihandiagu-1 went as far as the Ezeaku Group. Considering the stratigraphic position and depth of occurrence of the Agbani Sandstone member of the Awgu Formation, as can be seen from the well data, it is obvious that the Agbani sandstone is a major reservoir in this basin. Hence, well drilling in the basin should target this reservoir alongside other structural and stratigraphic reservoirs. Figure 4.23 is a geologic model of the subsurface layers.

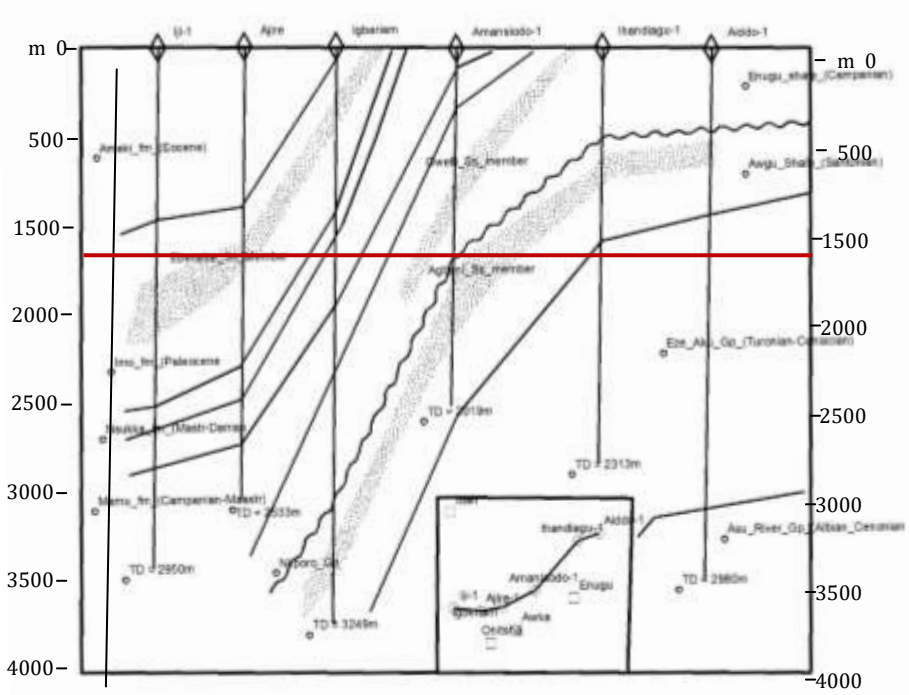

Fig. 4.22: Subsurface disposition of the stratigraphic units reconstructed using borehole data from the southern part of the Anambra Basin (After Nwajide, 2013).

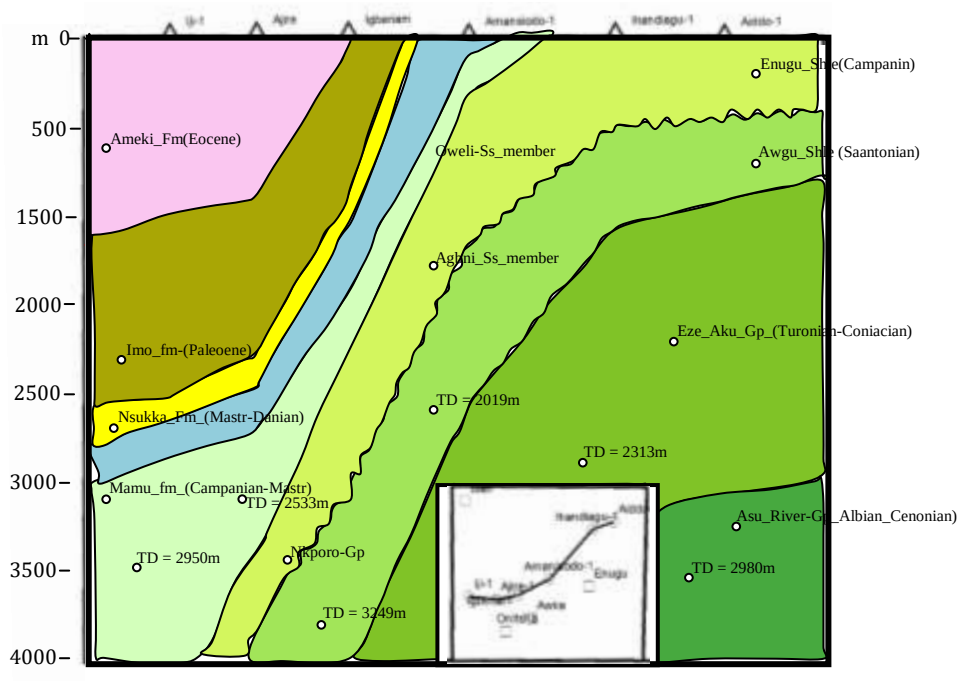

Fig. 4.23: Geologic model of the subsurface layers.

From the ongoing discussion, it can be seen that the earlier interpretation which suggested that hydrocarbon search in the basin be restricted to the intermediate gravity value zone is to a very large extent correct. The dryness of some of the wells drilled in the intermediate zone is as a result of not considering the regional dip while drilling, which in turn led to the stoppage of the wells before reaching depth to the major reservoirs, which majorly occur in the Nkporo Group sediments and the Awgu Formation.

On the basis of thermal studies (Onuoha and Ekine, 1999), Onuoha (2005) stated that The Maastrichtian – Paleocene sediments in the southwestern portion of the study area is more suitable for liquid hydrocarbon search, while the search for gas should be focused on the sediments of Senonian and older ages, with the northern part ignored for this purposes due to thermal immaturity. The present work agrees with the idea that hydrocarbon search in the northern portion of the basin be highly reduced while concentration is beefed up in the southern / southwestern portion. However, Maastrichtian – Paleocene sediments are not targets for major reservoirs. As evidenced from figure 4.22, the major reservoirs here (whether for liquid or gaseous hydrocarbon) occur within the sediments of the Nkporo Group and below, possibly, up to the Awgu Formation.

4.2.6 Correlation of Geothermal Gradient in Anambra Basin with Gravity Data

A comparison of the residual gravity data with geothermal gradient in the study area (Fig. 4.24 and Table 4.2) shows that the geothermal gradient for the wells which have yielded hydrocarbon ranges between 46 – 60 ^{0}C/Km. Agagu and Ekweozor (1982) was of the view that the geothermal gradient within the basin is lithologically controlled, hence, it varies between 9.2 and 24 ^{0}C/km in the Ajali and Mamu Formations, while it ranges between 29.4 to 70 ^{0}C/km in shaly sections. This supports the earlier submission that the major reservoirs

in the basin is located within the sediments not later than the Campanian age (i.e. the Nkporo Group and below). The high temperature gradient in the shales was attributed to lack of convection currents in the impermeable shales and possibly due to overpressure which is common in the reduction of thermal conductivity (Agagu and Ekweozor, 1982). Since the observed temperature gradient in this work is characteristic of the shale lithology in the study area, it implies that some of the shale members of the Nkporo Group and the older lithologies also serve as reservoirs in the study area. Consequently, they have some structural features which serve as reservoirs.

Heat and other fluids are transported across the basin by circulating meteoric waters (Onuoha and Ekine, 1999; Onuoha, 2005). Since increase in geothermal gradient enhances both hydrocarbon generation and migration (Onuoha and Ekine, 1999), areas of high heat flow coincide with areas of hydrocarbon generation and / or occurrence. This can partly explain why high geothermal gradients (46 – 60 ^{0}C/km) were recorded in the wells that yielded hydrocarbon. Within the aforementioned range of geothermal gradient, the above submissions hold. However, some local variations exist. An interval of Umuna – 1 well with a volcanic rock had a temperature gradient of 148^{0}C/km (Agagu and Ekweozor, 1982). Consequently, anomalously high temperatures of greater than 70^{0}C/km may no longer be attributed to the presence of hydrocarbon.

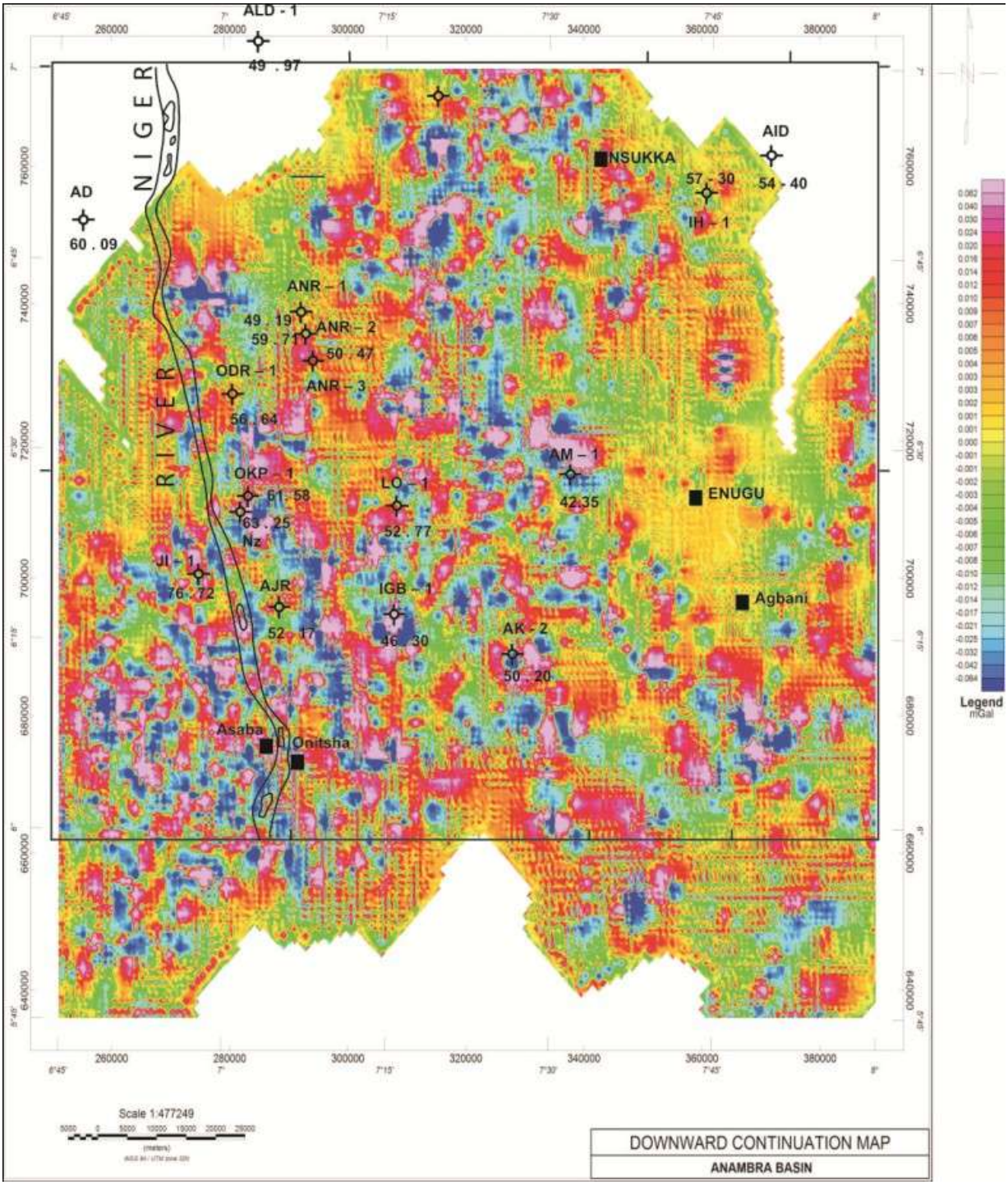

Fig. 4.24: Correlation of geothermal gradient data with Gravity data.

Table 4.2: Comparing Wells with Geothermal Gradient and Gravity Data.

S/N	Well Location	Total Depth (m)	Geothermal Gradient (^{0}c/km)	Gravity Colour	Gravity Range	Performance
1	Alade	3055	49.79	Pink	Very high	Dry
2	Anambra River – 3 (AL-1)	2430	50.47	Pink	Very high	Dry
3	Anambra River – 1 (AR-1)	3433	49.19	Red	Intermediate	Oil and Gas
4	Anambra River 2 (AR-2)	2179	59.71	Green	Intermediate	Gas only
5	Igbariam – 1 (IG-1)	3322	46.30	Yellow	Intermediate	Gas only
6	Iji – 1 (IJ-1)	3003	76.72	Yellow	Intermediate	Dry
7	Okpo – 1 (OK-1)	2431	61.58	Green	Intermediate	Dry
8	Ajire – 1 (AJ-1)	2257	52.00	Blue	Very low	Dry
9	Oda River (OR-1)	2400	56.00	Blue	Very low	dry

4.2.7 Correlation of Heat Flow in the Anambra Basin with Elevation Data

It has been observed that the heat flow variation in the study area is not directly proportional to relief (Fig. 4.26). This is why Aiddo well (AD) situated at a very low relief zone (area shaded blue on the map) has a heat flow value of 60.09 ^{0}C/Km, while Anambra River 1 (ANR – 1) well which is situated at a higher elevation (yellow – light green area on the map) has a heat flow of 49.19 ^{0}C/Km. The duo are not even inversely proportional to each other as it can be observed that JI – 1 well which is also at a higher elevation has a higher heat flow value of 76.72 ^{0}C/Km when compared with that of AD – 1 well. The distribution of the geothermal gradients and heat flow in the study area is rather dependent on the basin hydrodynamics (Onuoha and Ekine, 1999). All the groundwater flow systems in the area originated from the base of the Enugu cuesta (Fig. 4.25). Uma and Onuoha (1997) established three distinct hydraulic systems in the study area namely: an upper system made up of circulating meteoric water, a middle system in which pressure is moderately higher than hydrostatic, and a relatively deep system of abnormally high pressure. It is a combination of these flow systems that control heat flow instead of elevation. Onuoha and Ekine (1999) observed that areas of low ground surface elevation and low hydraulic head distribution in the southwest coincide with the areas of higher geothermal gradients and heat flow, while areas of higher elevation to the east (and water recharge zones) have lower gradients and heat flow values. They also observed a high geothermal gradient at the edge of the Abakaliki Anticlinorium in wells IH – 1 and AID – 1 situated at the eastern part of Nsukka (Fig. 4.25), which was attributed to the over pressured nature of the underlying formations. Table 3 is a correlation table for the geothermal gradient, sediment thickness, reservoir depth, gravity anomalies and well performances.

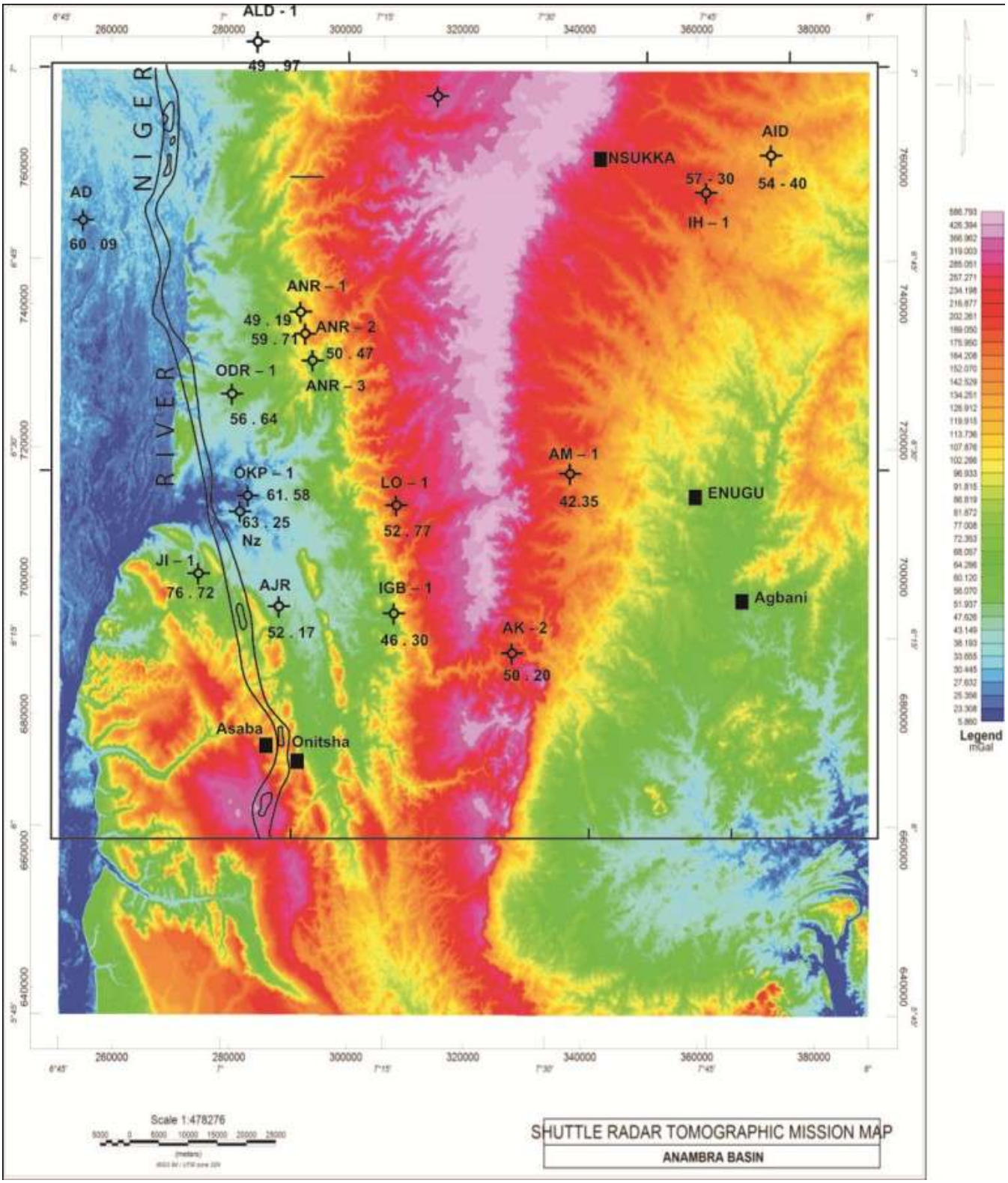

Fig. 4.25: Correlation of Geothermal Gradient Data with Elevation Data.

Table 3: Correlation table for all the measured parameters

S/N	Well Location	Geothermal Gradient (^{0}c/km)	Sediment thickness (m)	Reservoir Depth (m)	Gravity Range	Performance
1	Alade	49.79	3055	NN	Very high	Dry
2	Anambra River – 3 (AL-1)	50.47	2430	NN	Very high	Dry
3	Anambra River – 1 (AR-1)	49.19	3433	NN	Intermediate	Oil and Gas
4	Anambra River 2 (AR-2)	59.71	2179	NN	Intermediate	Gas only
5	Igbariam – 1 (IG-1)	46.30	3322	3000	Intermediate	Gas only
6	Iji – 1 (IJ-1)	76.72	3003	NN	Intermediate	Dry
7	Okpo – 1 (OK-1)	61.58	2431	NN	Intermediate	Dry
8	Ajire – 1 (AJ-1)	52.00	2257	NN	Very low	Dry
9	Oda River (OR-1)	56.00	2400	NN	Very low	Dry
10	Amansiodo 1	42.35	2019	1600	Intermediate	Gas only
11	Ihandiagu 1	57.30	2313	800	Intermediate	Gas only
12	Aido 1	54.40	2980	300	Very high	Dry

*NN = Not known

CHAPTER FIVE

SUMMARY, CONCLUSION AND RECOMMENDATION

5.1 Summary

This work analyzed the gravity data over the Anambra Basin with the intention to provide a better understanding of the subsurface geology of the study area and its petroleum potential. The interpretation of the Bouguer gravity anomalies ranged from visual inspection of the graphs and profiles for variations in the gravitational field to more complex methods that involved modelling of the subsurface layers. From this, bodies and structures were inferred which are of geologic interest. The primary aim of the present work is to infer the boundaries of the Anambra basin and re-evaluate its petroleum potentials using a combination of gravity data with well data and geothermal gradient data. The specific objectives included to produce a residual gravity map of the Anambra basin, delineate areas of gravity highs and lows as revealed by density contrasts caused by different rock types, generate geologic models of the causative bodies, determine sediment thickness in the basin, evaluate the relationship of the residual gravity data with hydrocarbon availability in the drilled wells, relate the gravity data to heat flow in the basin and infer basin boundaries.

The residual anomaly map shows that the highest density values are scattered all over the study area, in the form of intercalations, alongside the very low density rocks, while average density values covered the entire map area. Downward continuation of the residual anomaly to a depth of 1600 m gave a very clean view of the study area. The highest density anomalies often lie interwoven with the very low density rocks. Considering the depth at which the features became very sharp, it could be said that the causative body giving rise to the density anomalies are shallow seated (about 1.6 km). Despite the fact that the downward

continuation map was sharp enough to give the mappable contact between one point and another, it could not establish, in clear sense, the orientation of the anomalies.

The first vertical derivative map and the analytic signal map showed that the highest density anomalous bodies are oriented in the northwest – southeast directions, with very few in the Northeast- southwest direction, while the low density rocks appear to be oriented majorly in the northeast – southwest direction which suggests age difference between them.

The shuttle radar topographic mission (SRTM) map indicates that the zone of highest elevation runs almost through the centre of the study area, in the north – south direction. This zone of highest relief coincides with the cuesta described by Nwajide (2006; 2013). The zone of least topography occurring majorly in the western part of the map but runs in the north – south direction, is area around the River Niger and it flows southwards into the Atlantic Ocean. The drainage pattern in the area is dendritic. From the SRTM map, the study area is generally drained to the south by the River Niger, with the help of its tributaries. Most of the contours are clustered and thereby suggests close source for the gravity values. The highest contour value of 30 mgal forms a closure round the zones of highest density peaks in the study area. The gravity peaks occurring in closures are interpreted as areas associated with igneous rocks. The intermediate values of between 11 and 29 mgal are areas associated with the Cretaceous sedimentary rocks. In the south-western part of the map, the contour lines are broken and occur in discrete patterns with very low gravity values. They are the alluvial deposits of the Tertiary age occurring at the alluvial planes around the River Niger. The contours trend northeast – southwest in the north-eastern part of the map, almost east – west in the central to southern part, and north – south in the northern and southern part of the map. This suggests that the geologic materials which gave rise to the anomalies lay discordantly with each other.

The cross section of profile line 1 shows a maximum sediment thickness of about 1 km. This is shallow when compared with other profiles and suggests that the profile cut the basin towards the basin margin in the southern part. The thin nature of the sediments in this area suggests that sediment deposition must have been in a short period of time, and so has not given any time for further subsidence due to load and possibly further sediment reworking. Hence, sediment deposition across profile 1 is believed to be of Tertiary age alone. The sediment thickness across the profile line 2 is quite irregular, thus the basin floor here is irregular. The sediment thickness ranges from about 2.4 km on the north-western end of the line to about 7 km on the south-eastern end. This cross section is believed to pass through sediments of both tertiary and Cretaceous age respectively. The cross section drawn from profile line 3 shows a separation of three major basins within the area. Basin "A" is the extension of the Benue Trough across the study area, Basin "B" is the Anambra Basin, while basin C is the Afikpo Basin. Sediment thickness in this area is about 7 km as well.

The geologic modelling of cross section one shows that it passed through a meander river belt, Ogwashi – Asaba Formation and Bende – Ameki Formation. The geologic model for profile line 2 shows that it cuts through alluvial deposits (sediments) of Bende – Ameki Group, Imo Group and Nsukka Formation. Comparing the profile again with the work of Nwajide (2013), it can be said that the profile started somewhere outside the Anambra Basin and then entered into the Basin. The geologic model of the profile line 3 shows the presence of four sub-basins with the basin "B" filled with sediments of Imo group (Imsh), Ajali Formation (Ajst) and Mamu Formation respectively. The basin "A" contains the sediments Nkporo Formation (Nsh), Awgu Formation (Ansh), Ezeaku Group (ESh) and Asu River Group (Arish) respectively, while basin "C' contains sediments of Nkporo Group and Mamu Formation only. Basin 'D' contains the Alluvial deposits and the Ogwashi – Asaba Formation. Based on the lithologic content of the sub – basins in this model and the position

of the profile line 3, the basin B is ANAMBRA BASIN, while basin A is a continuation of the BENUE TROUGH, Basin C is the AFIKPO BASIN, and Basin D is a continuation of the Niger Delta. The geologic model for the profile Line 4 shows again an intersection of two basins, with one of the basins shallower than the other. The shallower basin contains sediments of the Alluvial deposits, Nsukka Formation, Ajali Formation, Mamu Formation and Nkporo Formation. The deeper basin contains the Awgu Formation, Ezeaku group and the Asu River Group sediments. Based on their lithological content, the shallower basin is believed to be part of the Anambra Basin, while basin E is part of the Benue Trough.

The geologic model 5 has similarity with model 4 in that it also shows the interaction between the Anambra Basin with the Benue Trough in the north-eastern part of the study area. While the Benue Trough in this area contains the sediments of Ezeaku Group and Awgu Formation only, the Anambra Basin contains Nkporo Formation, Mamu Formation and Ajali Formation.

A correlation of deep wells drilled for hydrocarbon search in the basin with the gravity data has revealed that there is a relationship between the gravity contrast and the availability of hydrocarbon in the wells. Thus, wells that are drilled into points where we have very high gravity values (≥ 30 mgal) and those drilled into areas of gravity low (< 11 mgal) were dry. Conversely, wells drilled in areas of intermediate gravity values (11 – 29 mgal) had hydrocarbons in them. The dryness of some of the wells drilled in the intermediate zone is as a result of not considering regional dip while drilling, which in turn led to stoppage of the wells before reaching depth to the major reservoirs, which majorly occur from the Nkporo Group sediments down to the Awgu Formation. The present work agrees with the idea that hydrocarbon search in the northern portion of the basin should be highly reduced while concentration is beefed up in the southern / southwestern portion. However,

Maastrichtian – Paleocene sediments are not targets for major reservoirs as they are not structurally mature for this purpose within the basin.

A comparison of the residual gravity data with geothermal gradient in the study area shows that the geothermal gradient for the wells which have yielded hydrocarbon ranges between 46 – 60 ^{0}C/Km. Since the observed temperature gradient in this work is characteristic of the shale lithology in the study area, it implies that some of the shale members of the Nkporo Group and the older lithologies also serve as reservoirs in the study area. Consequently, they have some structural features which serve as reservoirs. Heat and other fluids are transported across the basin by circulating meteoric waters. Due to some local variations, anomalously high temperatures of greater than 70^{0}C/km may no longer be attributed to the presence of hydrocarbon.

5.2 Conclusion

Having x-rayed the gravity data across the Anambra Basin and environs, in combination with geothermal gradient, elevation data and well data, the following conclusions have been made.

- Sediment thickness in the study area ranges from approximately 2.4 km – 7 km.
- The highest density value areas which are commonly enclosed by contour value of 30 mgal are areas associated with igneous rocks, the intermediate density values of between 11 and 29 mgal are areas associated with the Cretaceous sedimentary rocks, while the lower areas are associated with the Tertiary rocks.

  A modelling of five profile lines suggested the boundary of the Anambra Basin in the southwestern to the southern part be around Umueze – Nteje - Agoaliji. Its boundary

in the northeastern part is inferred around Obolo Afor – Obolo Eke. In the northern direction, the basin extends to around Adoru – Ekwuruko – Ukehe area.

- There is a distinct boundary between the Anambra and the Afikpo Basins and need not to be discussed as one basin. Each of the basins should be accorded its status as a full fledge inland basin. The non extension of the basin boundaries to the surface suggests that only geophysical approach can be used to establish their existence. The non continuation of the basement boundary to the surface has been attributed to further subsidence due to post depositional activities in the basin, which has pushed the boundary vertically downwards.
- Major hydrocarbon reservoirs within the basin occur in the sediments of the Awgu Formation up to the Nkporo Group. This work supports the earlier view that the northern portion of the basin is not promising in terms of hydrocarbon search, however, it disagrees with the Maastrichtian to Paleocene sediments being major reservoirs for whatever form of hydrocarbon (whether oil or gas) since they are texturally immature for this purpose within the basin. There exists a regional dip in the basin tilting southwards. Well drilling in the basin must target the depth of occurrence of at least the Nkporo Group sediments before they are terminated due to structural traps existing within the shale members of the Nkporo Group and the Awgu Formation.
- Geothermal gradient for the wells which have yielded hydrocarbon ranges between 49 – 60 mWm^{-1}. The geothermal gradient in the study area is not any way a function of relief. Hence, the present work supports the earlier view that temperature gradient in the basin is hydrodynamically controlled.

5.3. Recommendation

We recommend as follows:

1. That an enhancement of this work is done by further looking at the Anambra Basin from the perspective of 3D seismic data and relating the recently acquired aeromagnetic data from the study area to hydrocarbon search. This would go a long way in revealing the structural styles within the basin which are not clear in the gravity data.

2. That a detailed field geologic mapping be carried out around the communities where the boundaries of these basins have been inferred to really establish the contacts of this basin.

REFERENCES

Adeigbe, O.C and Salufu, A. E. (2009). Geology and Depositional Environment Of Campano-Maastrichtian Sediments In The Anambra Basin, Southeastern Nigeria: Evidence From Field Relationship And Sedimentological Study. Earth Sci. Res. J. vol.13 (2).

Adeleye, D.R. (19750). Nigerian late Cretaceous stratigraphy and paleogeography. AAPG Bull 59:2302–2313.

Adighije, C. I. (1981a). Gravity study of the Lower Benue Trough, Nigeria. Geol. Mag. Cambridge Univ. Press. 118(1). pp. 59-67.

Adighije, C. I., (1981b). A gravity interpretation of the Benue Trough, Nigeria. Tectonophysics, 79: 109 - 128.

Agagu, O. K. and Ekweozor, C. M. (1982). Source rock characteristics of the Senonian shales in the Anambra Syncline, southern Nigeria. Jour. Mining and Geology, v. 19, pp. 132 – 140.

Agagu, O. K., Fayose, E. A. and Petters, S. W. (1985). Stratigraphy and sedimentation in the Senonian Anambra Basinof eastern Nigeria. Jour. Min. and Geol. Vol. 22, p. 25 – 36.

Ajakaiye, D. E. and Burke, k. (1973). A Bouguer gravity map of Nigeria. Tectonophysics, 16, 103 – 115.

Akande S. O., Ojo O. J., Erdtmann B. D. (1998). Paleoenvironments, thermal history and source rock potentials of the Upper Benue Trough rift basins, Nigeria, and their implications for hydrocarbon exploration. NAPE Bull, Vol. 13, p. 20 – 30.

Alberts B. (2009). Regional gravity field modelling using airborne gravimetry data. NCG, Nederlandse Commissie voor Geodesie, Netherlands Geodetic Commission, Netherlands. 199p.

Avbovbo, A. A., and Ayoola, O. (1981). Petroleum prospects of southern Nigeria's Anambra Basin. Oil and Gas Jour. pp. 334 – 347.

Bell R. E, Anderson R, and Pratson L., (1997). Gravity gradiometry resurfaces. *The Leading Edge*, 16: 55–60.

Bell R.E., Childers V.A., Arko R.A., Blankenship D., and Brozena J. (1999). Airborne gravity and precise positioning for geologic applications. *Journal of Geophysical Research*, 104(B7): 15281–15292.

Benkhelil, J. (1988). Structure et evolution geodynamique du Basin intracontinental de la Benoue (Nigeria) Bull. Centres Rech. Explor. Prod. Elf Aquitaine 1207, 29-128.

Blakely R.J. (1995). Potential theory in gravity and magnetic applications: Cambridge Univ. Press, New York. 441p.

Brozena J. M. (1984). A preliminary analysis of the NRL airborne gravimetry system. Geophysics,49(7): 1060–1069.

Brozena J.M., (1992). The Greenland Aerogeophysics Project - Airborne gravity, topographic and magnetic mapping of an entire continent. In: *From Mars to Greenland: Charting gravity with space and airborne instruments - Fields, tides, methods, results*, pages 203–214.

Brozena J.M., Mader G.L., and Peters M.F. (1989). Interferometric Global Positioning System: three-dimensional positioning source for airborne gravimetry. *Journal of Geophysical Research*, 94(B9): 12153–12162.

Brozena J.M. and Peters M.F. (1994). Airborne gravity measurement at NRL. In: Cannon M. E. and Lachapelle G., (eds.), *Proceedings of the International Symposium on Kinematic Systems in Geodesy, Geomatics and Navigation (KIS94)*, pp. 495–506.

Brozena, J.M. and Peters, M. F. (1988). An airborne gravity study of eastern North Carolina. *Geophysics*, 53(2): 245–253.

Bruton A.M. (2000). *Improving the accuracy and resolution of SINS/DGPS airborne gravimetry*. Ucge report # 20145, Department of Geomatics Engineering, University of Calgary, Calgary, Canada.

Bruton A.M., Schwarz K.P., Ferguson S., Kern M., and Wei M. (2002). Deriving accelerations from DGPS: toward higher resolution applications of airborne gravimetry. *GPS Solutions*, 5(3): 1–14.

Cady J. W. (1980). Calculation of gravity and magnetic anomalies of finite-length right polygonal prisms: Geophysics, **45**, 1507-1512.

Czompo J (1994). Testing the rotation invariant scalar gravimeter concept. In: *Proceedings of the International Symposium on Kinematic Systems in Geodesy, Geomatics and Navigation (KIS94)*, pp. 483–493.

Davis, J. C. (2014). Statistics and Data Analysis in Geology. John Willey and Sons. New Delhi, India. Pages 638.

Eisfeller B. and Spietz P. (1989). Shaping filter design for the anomalous gravity field by means of spectral factorization. *Manuscripta Geodaetica*, 14: 183–192.

Ekine, A. S., and Onuoha, K. M., (2008). Burial History Analysis and Subsidence in the Anambra Basin, Nigera. Nigerian Journal of Physics,Vol. 20 (1), 145 – 154.

Ekine, A. S., and Onuoha, K. M. (2010). Seismic Geochemistry and Differential Interformational velocity analysis in the Anambra Basin, Nigeria. Earth sciences research journal, Vol. 14 (1), p88.

Evamy, B. D., Haremboure, J., Kamerling, P, Knaap, W. A., Molloy, F. A. and Rollands, P. H. (1978). Hydrocarbon habitat of Tertiary Niger Delta. AAPG Bull., v. 62, 1 – 39.

Forsberg R., Hehl K., Bastos L., Gidskehaug A., and Meyer U. (1997). Development of an Airborne Geoid Mapping System for Coastal Oceanography (AGMASCO). *Proceedings of the IAG International Symposium 'Gravity, Geoid and Marine Geodesy'*, volume 117 of *IAG Symposia*, pages 163–170.

Forsberg R. and Kenyon S. (1994). Evaluation and downward continuation of airborne gravity data - the Greenland example. *Proceedings of the International Symposium on Kinematic Systems in Geodesy, Geomatics and Navigation (KIS94)*, pages 531–538.

Forsberg R, Olesen AV, and Keller K (1999). Airborne gravity survey of the North Greenland continental shelf. Technical Report 10, National Survey and Cadastre (KMS), Copenhagen, Denmark.

Gabell A., Tuckett H., and Olson D. (2004). The GT-1A mobile gravimeter. In: Lane RJL, (ed.), *Airborne Gravity 2004 - Abstracts from the ASEG-PESA Airborne Gravity 2004 Workshop*, volume 2004/18 of *Geoscience Australia Record*, pages 55–61.

Glennie C.L. and Schwarz K.P. (1999). A comparison and analysis of airborne gravimetry results from two strapdown inertial/DGPS systems. *Journal of Geodesy*, 73: 311–321.

Gumert W.R. and Cobb G.E. (1970). Helicopter gravity measuring system. In: Kattner WT, (ed.), *Proceedings of the symposium on dynamic gravimetry "Advances in dynamic gravimetry"*. pp. 79–85.

Gumert, W. R., (1998). An historical review of airborne gravity. The Leading Edge, 17(1): 113–116.

Hammada Y. and Schwarz K.P., (1997). Airborne gravimetry model-based versus frequency-domain filtering approaches. *Proceedings of the International Symposium on Kinematic Systems in Geodesy, Geomatics and Navigation (KIS97).* pp. 581–595.

Hammer S (1983). Airborne gravity is here! *Geophysics*, 48(2): 213–223.

Hehl K., Bastos L., Cunha S., Forsberg R., Olesen A.V., Gidskehaug A., Meyer U., Boebel T., Timmen L., Xu G., and Nesemann M. (1997). Concepts and first results of the AGMASCO project. *Proceedings of the International Symposium on Kinematic Systems in Geodesy, Geomatics and Navigation (KIS97)*, pages 557–563.

Hoque, M. and Nwajide, C. S. (1984). Tectono-sedimentological evolution of an elongate intracratonic basin (aulacogen): the case of the Benue trough of Nigeria. Jour. Min. Geol., Vol. 21, p. 19 – 26.

Hwang C., Hsiao Y.S., Shih H.C., Yang M., Chen K.H., Forsberg R., and Olesen A.V. (2007). Geodetic and geophysical results from a Taiwan airborne gravity survey: Data reduction and accuracy assessment. *Journal of Geophysical Research*, 112(B4, B04407).

Jekeli C., (1994). Airborne vector gravimetry using precise, position-aided inertial measurement units. *Bulletin G´eod´esique*, 69: 1–11.

Jekeli C., and Kwon J.H. (1999). Results of airborne vector (3-D) gravimetry. *Geophysical Research Letters*, 26(23): 3533–3536.

Kearey, p., Brooks, M. and Hill, I. (2002). An Introduction to Geophysical Exploration. Blackwell Science Ltd, USA. Pages 262.

Kleusberg A., Peyton D., and Wells D. (1990). Airborne gravimetry and the Global Positioning System. *Proceedings of IEEE Plans '90" The 1990's - a decade of excellence in the navigation sciences"*, pp. 273 – 278.

Klingel´e E., Halliday M., Cocard M., and Kahle H.G. (1995). Airborne gravimetric survey of Switzerland. *Vermessung, Photogrammetrie, Kulturtechniek*, 4: 248–253.

LaCoste L, Clarkson N, and Hamilton G (1967). LaCoste and Romberg stabilized platform shipboard gravity meter. *Geophysics*, 32: 99–109.

Lee J.B. (2001). Falcon gravity gradiometer technology. *Exploration Geophysics*, 32: 247–250.

Lee J.B., Downey M.A., Turner R. J., Boggs D.B., Maddever R.A.M., and Dransfield M.H. (2006). First test survey results from the FALCON helicopter-borne airborne gravity gradiometer system. *Extended abstracts of the Australian Earth Sciences Convention* Melbourne, Australia.

Lines, L.R, and Newrick, R. T. (2004). Fundamentals of Geophysical Interpretation. Society of Exploration Geophysicists. 274p.

Lowrie, W. (2007). Fundamentals of Geophysics. Cambridge University Press, USA. 354p.

Lundberg, H. (1957). Airborne gravity surveys. Canadian Mining and Metallurgical Bulletin,Aug.: 465–473.

Mariita N. O. (2007). The Gravity Method. Presented at Short Course II on Surface Exploration for Geothermal Resources, organized by UNU-GTP and KenGen, at Lake Naivasha, Kenya.

Meyer U, Boedecker G, and Pflug H. (2003). Airborne Navigation and Gravimetry Ensemble & Laboratory (ANGEL). Introduction and first airborne tests. Scientific Technical Report STR03/06, GeoForschungs Zentrum Potsdam.

Milsom, J. (2003). Field geophysics. John Willey and Sons Limited, England. 232p.

Morelli, C., Gantor, C., Honkasalo, T., McConnell, R.K., Tanner, J.G., Szabo, B., Votila, V. & Whalen, C.T. (1971)**.** The International Gravity Standardisation Net. Pub. Spec. no. 4. International Association of Geodesy. Pp194.

Murat, R.C. (1972). Stratigraphy and Palaeogeography of Cretaceous and Lower Tertiary in S. Nigeria 1st Conference on African Geology, Ibadan 1970 Proceedings. Ibadan

University Press. pp. 251-266.

Murphy, C. A. (2004). The Air-FTG™ airborne gravity gradiometer sys-tem: Airborne Gravity 2004 — Abstracts from the ASEG-PESA Airborne Gravity Workshop: (Record) Geoscience Australia, 18, 7–14.

Ndefo, D., Aduroja, B., Unachukwu, O., Allix, P., Caileaux, P., Grugnola, M.T. (1987). Anambra Basin: A Synthetic Review of Exploration Activities by Elf Nigeria, pp. 1-68.

Nettleton LL, LaCoste L, and Harrison JC (1960). Tests of an airborne gravity meter. *Geophysics*, 25(1): 181–202.

Nigeria Geological Survey Agency (2006). The Geological map of Nigeria. A publication of the Nigeria Geological Survey Agency, Abuja, Nigeria.

Nwajide, C.S. (2005). Anambra Basin of Nigeria: Synoptic Basin Analysis as a Basis for Evaluating its Hydrocarbon Prospectivity. In: Hydrocarbon Potentials of the Anambra Basin by Okogbue C. O. (Ed), Proceedings of the First Seminar Organised by the Petroleum Technology Development Fund (PTDF) Chair in Geology, University of Nigeria, Nsukka. pp. 1- 46.

Nwajide, C.S. (2006). Training course in sedimentological techniques. Geological Survey of Nigeria Agency. 32p.

Nwajide, C.S. (2013). Geology of Nigeria's Sedimentary Basins. CSS bookshop limited. 15 broad street, Lagos, Nigeria. 565p.

Obaje, N. G., Ulu, O. K. and Petters, S. W. (1999) Biostratigraphic and geochemical controls of hydrocarbon prospects in the Benue Trough and Anambra Basin, Nigeria. *Nigerian Association of Petroleum Explorationists (NAPE) Bulletin* **14**, 18–54.

Obaje, N. G. (2009). Geology and Mineral Resources of Nigeria. Springer, Berlin, Germany. ISBN – 13: 9783540926849. 221p.

Odoh B.I. and Onwuemesi A.G. (2007). Using electrical wireline logs for aquifer characterization in parts of Anambra Basin, Southeastern Nigeria, Global Journal of Geological Sciences Vol. 6(1). pp. 33-39.

Odoh ,B.I., Onwuemesi, A.G. and Egboka, B.C.E. (2009). PETROLEUM EXPLORATION OF THE ANAMBRA BASIN: MISSING LINKS AND CHALLENGES. Natural and Applied Sciences Journal, Vol. 10 No. 2.

Ogala, J. E. (2011). HYDROCARBON POTENTIAL OF THE UPPER CRETACEOUS COAL AND SHALE UNITS IN THE ANAMBRA BASIN, SOUTHEASTERN NIGERIA. Petroleum & Coal 53 (1) 35-44.

Ojo, O. J, Kolawole, A. U. and Akande, S. O. (2009). Depositional Environments, Organic Richness and Petroleum Generating Potential of the Campanian to Maastrichtian Enugu Formation, Anambra Basin, Nigeria. Pacific Journal of Science and Technology. Vol 10 (1). pp. 614 – 627.

Okeke, H. C, Orajaka, I. P, Okoro, A. U. and Onuigbo, E. N. (2014). Biomarker evaluation of the oil generative potential of organic matter, in the upper Maastrichtian strata, Anambra Basin, southeastern Nigeria. Jour. Sci. Res. 2(1). pp. 016 – 025.

Olesen A.V. and Forsberg R. (2007b). Regional airborne scalar gravimetry for geoid determination.

Onuba, L. O., Anakwuba, E. K., Chinwuko, A. I., Nwokeabia, N. C.and Onwuemesi, A. G. (2012). Interpretation of Aeromagnetic Anomalies Over Parts of Upper Benue Trough and Southern Chad Basin, Nigeria. Advances in Applied Science Research, 3(3): 1757-1766.

Onuba L. N., Anudu G.K., Chiaghanam O.I. and Anakwuba E.K. (2011). Evaluation of Aeromagnetic Anomalies Over Okigwe Area, Southeastern Nigeria. Research Journal of Environmental and Earth Sciences 3(5): 498-507.

Onuoha, K. M. (1986). Basin Subsidence, sediment compaction and burial history modelling techniques: applicability to the Anambra Basin, Nigeria. NAPE proceedings, vol. 2, 6-17.

Onuoha K.M. and Ekine A.S. (1990). Pitfalls in the reconstruction of thermal histories and evolution of maturation stages of oil and gas bearing strata. NAPE Bull., vol. 5(1), 88 – 102.

Onuoha K.M. and Ekine A.S. (1999). Subsurface Temperature variations and heat flow in Anambra Basin Nigeria. J. African Earth Sciences, vol. 28 (3), 641-652.

Onuoha, K.M. (2005). A closer look at the Petroleum Potentials of the Anambra Basin: Inputs from Geophysics and Geohistory. In: Hydrocarbon Potentials of the Anambra Basin by Okogbue C. O. (Ed), Proceedings of the First Seminar Organised by the Petroleum Technology Development Fund (PTDF) Chair in Geology, University of Nigeria, Nsukka. Pp 47-82.

Onwuemesi A.G. and Egboka B.C.E. (2007). Petroleum Prospect of the Anambra Basin, Natural and Applied Sciences Journal vol. 8 No.1, pp.1-7.

Onwuemesi A.G. (1997). One-Dimensional Spectral Analysis of Aeromagnetic Anomalies and Curie Depth Isotherm in the Anambra Basin of Nigeria, J. Geodynamics Vol. 23, No.2, pp. 95-107.

Onwuemesi, A.G. (1995). Interpretation of Magnetic Anomalies from the Anambra Basin of Southeastern Nigeria. Ph.D. Thesis Nnamdi Azikiwe University, Awka, Nigeria

Onyewuchi R. A., Opara A.I., Ahiarakwem C.A., OKO F.U. (2012). Geological Interpretations Inferred From Airborne Magnetic and Landsat Data: Case Study of Nkalagu Area, Southeastern Nigeria. International Journal of Science and Technology, Vol. 2, pp. 178 – 191.

Osazuwa, I.B. (1985). The establishment of primary gravity network for Nigeria, unpublished ph.D Thesis. Ahmadu Bello University, Zaria, Nigeria.

Osazuwa, I.B., (1992a). The Nigerian standard gravimeter calibration line *survey review*, U.K., vol. 31, no. 245, pp. 397 - 408.

Petters S.W. (1978). Middle Cretaceous paleoenvironments and biostratigraphy of the Benue Trough, Nigeria. Geol Soc Am Bull 89:151–154.

Reijers T.J.A. and Nwajide C.S. (1998). Geology of the Southern Anambra Basin. Unpublished Report for Chevron Nigeria Limited. Field Course Note, 66p.

Reyment, R.A. (1965). Aspects of Geology of Nigeria, Ibadan University Press, Ibadan Nigeria. 106p.

Salychev O. S, Bykovsky A. V, Voronov V. V, Schwarz K, Liu Z, Wei M, and Panenka J. (1994). Determination of gravity and deflections of the vertical for geophysical applications using the ITC-2 platform. In: Proceedings of the International Symposium on Kinematic Systems in Geodesy, Geomatics and Navigation (KIS94), pp. 521–529.

Sander S., Argyle M., Elieff S., Ferguson S., Lavoie V., and Sander L. (2004). The AIRGrav airborne gravity system. In: Lane R.J.L., (ed.), *Airborne Gravity 2004 - Abstracts from the ASEG-PESA Airborne Gravity 2004 Workshop*, volume 2004/18 of *Geoscience Australia Record*. pp. 49–54.

Schwarz, K.P., Cannon, M.E. and Wong R.V.C. (1989). A comparison of GPS kinematic models for the determination of position and velocity along a trajectory. *Manuscripta Geodaetica*, 14: 345–353.

Schwarz, K. P.; Colombo, O; Hein, G, and Knickmeyer, E. T. (1991). Requirements for airborne vector gravimetry. In: *Proceedings of the IAG Symposium G3 'From Mars to Greenland: charting gravity with space and airborne instruments'*, Springer-Verlag, New York. pp 273–283.

.Schwarz, K. P. and Li, Z. (1997). An introduction to airborne gravimetry and its boundary value problems. In: Sanso F. and Rummel R., (eds.): *Geodetic boundary value problems in view of the one centimeter geoid*, volume 65 of *Lecture notes in earth sciences*, Springer-Verlag New York. Pp 312–358.

Talwani, M., Worzel, J.L, and Landisman, M. (1959). Rapid gravity computation for two dimensional bodies with application to the Mendocino submarine fracture zone. Journal of Geophysical Research, Vol. 64, pp 49-59.

Telford, W. M., Geldart, L. P. And Sheriff, R. E., (1990). Applied Geophysics, Cambridge Univ. Press, Cambridge.

Thompson L.G.D. and LaCoste L.J.B. (1960). Aerial gravity measurements. *Journal of Geophysical Research*, 65(1): 305–322.

Uma, K. O., and Onuoha, K. M. (1997). Hydrodynamic flow and formation pressures in the Anambra Basin, southern Nigeria. Hydrological Sciences Journal, 42 (2), 141 – 152.

Unwin, D. J. (1978). An Introduction to Trend Surface Analysis. Institute of British Geographers, Kingston Gore, London. p.40.

Whiteman, A. (1982). Nigeria: Its Petroleum Geology, Resources and Potential. Graham and Trotham, London.

Wei M. (1999). From airborne gravimetry to airborne geoid mapping - Report of SSG 3.164. In: Forsberg R, (ed.), *Determination of the gravity field. Report of IAG section III*, Danish National Survey and Cadastre (KMS), Copenhagen. pages 25–32.

Wei, M. and Schwarz, K.P., (1998). Flight test results from a strapdown airborne gravity system. *Journal of Geodesy*, 72: 323–332.

APPENDIX

DETERMINATION OF D, a, b, and c.

$$D=\sum_{i=1}^{N}x_i^2\left(N\sum_{j=1}^{N}y_j^2-\sum_{j=1}^{N}y_j\sum_{j=1}^{N}y_j\right)-\sum_{\substack{i=1\\j=1}}^{N}x_iy_j\left(N\sum_{\substack{i=1\\j=1}}^{N}x_iy_j-\sum_{i=1}^{N}x_i\sum_{j=1}^{N}y_j\right)+\sum_{i=1}^{N}x_i\left(\sum_{\substack{i=1\\j=1}}^{N}x_iy_j\sum_{j=1}^{N}y_j-\sum_{i=1}^{N}x_i\sum_{j=1}^{N}y_j^2\right)..(1)$$

Where:

122720	105706	189117	16,641	779527.4	907040.9	673155.1	1455105	1222040
x_i	y_j	Y_{ij}	N	x_iy_j	x_i^2	y_j^2	$Y_{ij}x_i$	$Y_{ij}y_j$

$$D=907040.9(16{,}641\times 673155.1-105{,}706\times 105{,}706)-779{,}527.4(16{,}641\times 779{,}527.4-122{,}720\times 105706)$$
$$+122{,}720(779527.4\times 105706-122720\times 673155.1).....(2)$$

$$D=907040.9(28{,}215{,}583.1)-779{,}527.4(-124{,}856.6)+122{,}720(-208{,}870{,}530).....(3)$$

$$D=2.559268508\times 10^{13}+9.733179116\times 10^{10}-2.563259144\times 10^{13}.....(4)$$

$$\therefore D=5.742543116\times 10^{10}.....(5)$$

Given that

$$a=\frac{\left(N\sum_{j=1}^{N}y_j^2-\sum_{j=1}^{N}y_j\sum_{j=1}^{N}y_j\right)\sum_{\substack{i=1\\j=1}}^{N}Y_{ij}x_i-\left(N\sum_{\substack{i=1\\j=1}}^{N}x_iy_j-\sum_{j=1}^{N}y_j\sum_{i=1}^{N}x_i\right)\sum_{\substack{i=1\\j=1}}^{N}Y_{ij}y_j+\left(\sum_{\substack{i=1\\j=1}}^{N}x_iy_j\sum_{j=1}^{N}y_j-\sum_{j=1}^{N}y_j^2\sum_{i=1}^{N}x_i\right)\sum_{\substack{i=1\\j=1}}^{N}Y_{ij}....(6)}{|D|}$$

$$\Rightarrow a = \frac{(16641\times 6731551 - 105706^2)1455105 - (16641\times 779527.4 - 122720\times 105706)1222040 + (779527.4\times 105706 - 6731551\times 122720)189117}{5.742543116\times 10^{10}} \ldots\ldots\ldots(7)$$

$$\Rightarrow a = \frac{4.105663605\times 10^{13} + 1.525797595\times 10^{11} - 3.949864672\times 10^{13}}{5.742543116\times 10^{10}} \ldots\ldots\ldots(8)$$

$$\Rightarrow a = \frac{1.71056909\times 10^{12}}{5.742543116\times 10^{10}} \ldots\ldots\ldots(9)$$

$$\therefore a = 29.78765775 \cong 30 \ldots\ldots\ldots(10)$$

Given that

$$b = \frac{-\left(N\sum_{\substack{i=1\\j=1}}^{N} x_i y_j - \sum_{i=1}^{N} x_i \sum_{j=1}^{N} y_j\right)\sum_{\substack{i=1\\j=1}}^{N} Y_{ij} x_i + \left(N\sum_{i=1}^{N} x_i^2 - \sum_{i=1}^{N} x_i \sum_{i=1}^{N} x_i\right)\sum_{\substack{i=1\\j=1}}^{N} Y_{ij} y_j - \left(\sum_{i=1}^{N} x_i^2 \sum_{j=1}^{N} y_j - \sum_{\substack{i=1\\j=1}}^{N} x_i y_j \sum_{i=1}^{N} x_i\right)\sum_{\substack{i=1\\j=1}}^{N} Y_{ij}}{|D|} \ldots\ldots(11)$$

$$b = \frac{(16641\times 779527.4 - 122720\times 105706) - 1,455105 + (16641\times 9070409 - 122720^2)1222040 - (9070409\times 105706 - 779527.4\times 122720)189117}{5.742543116\times 10^{10}} \ldots\ldots\ldots(12)$$

$$b = \frac{1.816794629\times 10^{11} + 4.138953782\times 10^{13} - 4.086115751\times 10^{13}}{5.742543116\times 10^{10}} \ldots\ldots\ldots(13)$$

$$b = \frac{7.100597729\times 10^{11}}{5.742543116\times 10^{10}} \ldots\ldots\ldots(14)$$

$$\therefore b = 12.36490103 \cong 12 \ldots\ldots\ldots(15)$$

Given that:

$$c=\frac{\left(\sum_{\substack{i=1\\j=1}}^{N}x_iy_j\sum_{j=1}^{N}y_j-\sum_{j=1}^{N}x_i\sum_{j=1}^{N}y_j^2\right)\sum_{\substack{i=1\\j=1}}^{N}Y_{ij}x_i-\left(\sum_{i=1}^{N}x_i^2\sum_{j=1}^{N}y_j-\sum_{i=1}^{N}x_i\sum_{\substack{i=1\\j=1}}^{N}x_iy_j\right)\sum_{\substack{i=1\\j=1}}^{N}Y_{ij}y_j+\left(\sum_{i=1}^{N}x_i^2\sum_{j=1}^{N}y_j^2-\sum_{\substack{i=1\\j=1}}^{N}x_iy_j\sum_{\substack{i=1\\j=1}}^{N}x_iy_j\right)\sum_{\substack{i=1\\j=1}}^{N}Y_{ij}}{|D|}\quad.....(16)$$

$$c=\frac{(779527.4\times105706-122720\times673155.1)1455105-(907040.9\times105706-122720\times779527.4)1222040}{+(907040.9\times673155.1-779527.4^2)189117}{5.742543116\times10^{10}}\quad.....(17)$$

$$\Rightarrow c=\frac{-3.039285491\times10^{14}-2.64037442\times10^{14}+5.515106344\times10^{14}}{5.742543116\times10^{10}}\quad.....(18)$$

$$\Rightarrow c=-\frac{1.64553567\times10^{13}}{5.742543116\times10^{10}}\quad.....(19)$$

$$\therefore c=-286.551731\cong-287.....(20)$$